NASA CONTRACTOR REPORT

NASA CR-1837

AN EXPERIMENTAL INVESTIGATION OF HIGH AMPLITUDE PANEL FLUTTER

by H. P. Kappus, C. E. Lemley, and N. H. Zimmerman

Prepared by
MCDONNELL DOUGLAS CORPORATION
St. Louis, Mo.
for George C. Marshall Space Flight Center

NATIONAL AERONAUTICS AND SPACE ADMINISTRATION • WASHINGTON, D. C. • MAY 1971

1. REPORT NO.	2. GOVERNMENT ACCESSION NO.	3. RECIPIENT'S CATALOG NO.
NASA CR-1837		

4. TITLE AND SUBTITLE	5. REPORT DATE
AN EXPERIMENTAL INVESTIGATION OF HIGH AMPLITUDE PANEL FLUTTER	May 1971
	6. PERFORMING ORGANIZATION CODE
7. AUTHOR(S)	8. PERFORMING ORGANIZATION REPORT #
H. P. Kappus, C. E. Lemley, and N. H. Zimmerman	
9. PERFORMING ORGANIZATION NAME AND ADDRESS	10. WORK UNIT NO.
McDonnell Douglas Corporation McDonnell Aircraft Co. St. Louis, Mo.	11. CONTRACT OR GRANT NO. NAS8-21250 - OMSF
	13. TYPE OF REPORT & PERIOD COVERED Contractor Report Low Series
12. SPONSORING AGENCY NAME AND ADDRESS NASA Washington, D. C. 25046	14. SPONSORING AGENCY CODE

15. SUPPLEMENTARY NOTES Technical Coordinator: W. W. Clever, Aerophysics Division, Aero-Astrodynamics Laboratory, Marshall Space Flight Center, Alabama 35812.

16. ABSTRACT

Panel flutter tests were conducted in the 1.1 to 1.4 Mach number range for flat, rectangular, aluminum panels clamped on four sides. All test panels were 30 inches long, 6.7 inches wide (L/W = 4.48) and .032 inch thick. The panel flutter boundary was defined as a function of the primary variables, Mach number, in-plane compression load, and pressure differential across the panel. Secondary variables, consisting of cavity volume, boundary layer thickness, and panel cross stiffening, were also investigated although they had a minor effect in the ranges tested. Panel stresses and motion were measured at flutter onset and during penetration beyond the flutter onset boundary.

Minimum flutter onset dynamic pressures occurred between Mach 1.3 and 1.4. Panel buckling lowered the flutter onset dynamic pressure by about a factor of four over the no-load condition. A pressure differential as little as 0.1 psi raised the flutter onset dynamic pressure by 50 percent. Maximum panel surface stresses of about 11,000 psi were measured at the panel trailing edge during a deep flutter penetration run (dynamic pressure set at 1000 psf - 3.33 times the onset value). The maximum stress conditions were maintained for over 300,000 panel oscillation cycles without panel failure.

17. KEY WORDS	18. DISTRIBUTION STATEMENT
Flutter, Panel Flutter, Aeroelasticity, Aeroelastic Instability, Structural Dynamics, Aerodynamics, Fluid Dynamics	Unclassified - Unlimited

19. SECURITY CLASSIF. (of this report)	20. SECURITY CLASSIF. (of this page)	21. NO. OF PAGES	22. PRICE*
UNCLASSIFIED	UNCLASSIFIED	129	$3.00

*For sale by the National Technical Information Service, Springfield, Virginia 22151

....NOTICE ....

Because of a waiver initiated and signed in compliance with NASA Policy Directive (NPD) 2220.4, para. 5-b, the International System of Units of measurement has not been used in this document.

TABLE OF CONTENTS

EXPLANATION OF SYMBOLS

Symbol	Explanation	Units
E	Young's Modulus	Pounds/Inch^2
$f(M)$	Mach number correction factor	----
f	Flutter frequency	Hz
L	Panel stream direction dimension	Inches
M	Freestream Mach number	-----
M_{CR}	Freestream Mach number at which minimum flutter onset dynamic pressure occurs	-----
N_x	Inplane compressive edge load	Pounds/Inch
$N_{x_{CRIT}}$	Still air buckling load	Pounds/Inch
$\bar{N}_x$	$= N_x/N_{x_{CRIT}}$, Normalized compressive edge load	-----
q	Freestream dynamic pressure	Pounds/Foot^2
q_{on}	Dynamic pressure at flutter onset	Pounds/Foot^2
q_{PENET}	$= q/q_{on}$, Flutter penetration factor	-----
t	Test panel thickness	Inches
U	Local stream velocity	Feet/Sec
U_∞	Freestream velocity	Feet/Sec
β	$=\sqrt{M^2 - 1}$, Compressibility factor	-----
ΔP	Differential pressure across panel	Pounds/Inch^2
δ	Boundary layer thickness	Inches
δ^*	Boundary layer displacement thickness	Inches
Φ	$= \left\{\frac{\beta E}{q_{on}}\right\}^{1/3} \frac{t}{L}$, Flutter Parameter	-----

INTRODUCTION

The possibility of encountering panel flutter on the forward skirt of the Saturn S-IVB stage of the Saturn V launch vehicle was indicated by analysis, and subsequent wind tunnel testing (References 1 and 2) verified that panel flutter could occur within the trajectory dynamic pressure envelope. Both the analyses and test, however, were inconclusive as to whether or not the amplitudes of the panel flutter could result in panel failure.

Although extensive studies have been carried out to define the effects of various parameters on flutter onset boundaries(see bibliographies in References 3, 4, 5, 6) relatively little has been done to define the post flutter behavior of panels. Several analytical investigations of post flutter behavior have been conducted recently (References 7, 8, 9, 10) and a non-linear analysis computer program for determining the time history of a disturbed panel in a supersonic flow has been included in Reference 8. However, experimental investigations in this area have been essentially non-existent.

The purpose of the program described here was to provide a carefully controlled experimental study of several factors affecting high amplitude panel flutter. The test program was designed primarily to assess the severity of panel flutter (relative severity being measured by panel stress and displacement amplitudes) as a function of dynamic pressure deficiency (i.e., penetration into the flutter region).

The following parameters were varied to investigate their influence on the severity of flutter:

- Flow Mach number
- Static pressure differential across the panel
- Compressive edge load
- Boundary layer thickness
- In-plane edge rigidity
- Cavity volume

These parameters were selected for study because of their relevance to the launch vehicle panel flutter problem. The Saturn S-IVB must be qualified to fly in the subsonic, supersonic, and hypersonic flight regimes. From the panel flutter standpoint the low supersonic Mach regime ($1<M<\sqrt{2}$) is most critical; the flutter onset dynamic pressure in this area is usually at a minimum while the trajectory dynamic pressure is at a maximum. A positive (bursting) pressure differential generally exists across the skin panels of a launch vehicle because the internal static pressure is greater than the ambient pressure outside as the vehicle gains altitude. During pitch and yaw maneuvers, a negative (crushing) differential pressure can also occur as local angles of attack become large. Pitch and yaw maneuvers may also cause panel in-plane stresses which are compressive on one side of the vehicle and tensile on the other. The compressive panel loads during maneuver can actually exceed the panel buckling load. The effect of boundary layer thickness on panel flutter has not been resolved. Although the boundary layer thickness on the S-IVB stage in flight is estimated to be on the order of six inches, it was not feasible to attain a comparable thickness in the wind tunnels under consideration for this test program. It was decided, therefore, to study boundary layer by testing at two values of boundary layer thickness, and comparing their effects.

A single bay panel configuration with smooth adjacent areas was selected for these tests. This single bay test concept has been used extensively in panel flutter test programs (see Reference 11, for example). Provision was made for changing the edge restraint stiffness during the test program; this parameter could therefore be investigated as a possible cause for differences in flutter characteristics between single and multi-bay panels.

The test panel configuration used in this program was a representative Saturn S-IVB skin panel - .032 inch thick aluminum, 6.7 inches wide, and 30 inches long. The test panels were flat even though the S-IVB

panels have a very slight curvature (Radius - 130"). It was not expected that the flutter boundaries for the curved vehicle panels would be significantly different from the flat test panels.

The wind tunnel tests were conducted in the NASA/Ames 2' by 2' Transonic Tunnel in a Mach number range of 1.1 to 1.4 and a dynamic pressure range of 200 to 1200 psf.

The results of this report are employed in Reference 12 to assess the fatigue life of Saturn V panels.

TEST APPARATUS

Test Fixture-General

The parameters to be varied during these tests required the incorporation of the following features into the wind tunnel test fixture:

1. A compressive edge load device capable of exerting in-plane stresses on the test panels ranging from zero to twice the panel buckling stress.
2. A pressurization system capable of producing up to a 1 psi pressure differential across the test panels.
3. The capability of thickening the boundary layer over the test panels.
4. The capability of varying in-plane edge restraint of the test panels in the cross-stream direction.

The test fixture is shown in Figure 1. The panel flutter test fixture consisted of a 5 foot by 2 foot wind tunnel wall replacement section to which two box-like units, the equipment mounting platform and the cavity enclosure, were fastened, one above the other. The test panels were attached to the panel support and loading frame which was in turn fitted flush into a cutout in the wall replacement section. A hand pump actuated hydraulic cylinder mounted on the equipment platform provided the compressive edge load capability. The entire unit was covered on the underside with a cavity enclosure to permit pressurization of the interior. Sealing was accomplished by means of "O" rings and a teflon impregnated fiberglass cloth which was fastened all around the panel frame. The boundary layer over the test panels could be thickened by inserting cylindrical proturberances (spring pins) into predrilled holes ahead of the test panel in the wall replacement. The in-

plane edge fixity in the cross-stream direction could be increased by inserting removable cross stiffeners between the panel support longerons. The features of the test fixture are described below in more detail.

Test Panels

Twelve geometrically identical test panels were fabricated for these tests to provide an adequate replacement supply in case of flutter damage. To insure consistency of the test results from panel to panel, all panels were fabricated from the same sheet stock. The more significant panel data is summarized below:

Overall Length (measured in stream direction)	40 inches
Active Length	30 inches
Overall Width	10.7 inches
Active Width	6.7 inches
Nominal Thickness	.032 Sheet
Actual Thickness	.033 inches $^{+.001}_{-.000}$
Material	7075-T6 Aluminum
Young's Modulus	
Compression	10.5×10^6 psi
Tension	10.3×10^6 psi
Poisson's Ratio	.33
Density	.101 pound/inch^3

The panels were attached to the mounting frame with a double row of button head screws spaced at 1-1/2 inch intervals along the edge of the panel. Once mounted the test panel had an active, or fluttering, portion 30 inches long and 6.7 inches wide (L/W = 4.48). The edge attachments were designed to simulate clamped-edge boundary conditions.

Panel Frame

The panel frame was constructed of two parallel aluminum I-beam longerons with transverse spacer blocks. A photograph of the frame in

position on the equipment platform is shown in Figure 2. The "active" panel dimensions were assumed to be the spacing between the inside edges of the longeron flanges and the spacer blocks. The fiberglass cloth seal all around the frame can be seen in the photograph. The loading and butt block rigidities, and distance of the "active" portion of the panel from the point of load application was designed to minimize shear distortion in the panel under compressive load. Furthermore, the load from the hydraulic cylinder was applied through a ball at a point on the loading block corresponding to the cross sectional centroid of the panel and support longerons. This would help assure equal load division between the longerons with no tendency to bend them. Since slight load asymmetries might occur between the side longerons, tests were conducted with a much simplified fixture to investigate the effects of a compressive load imbalance on panel dynamics (see Appendix A).

Seven removable cross-stiffeners which fitted from web to web of the support longerons were intended to increase the panel in-plane edge restraint in the cross stream direction. The purpose was to investigate the effect of this edge restraint on limiting the amplitude of panel flutter.

Equipment Platform

The equipment platform served as the mounting base for the Wayne-Kerr displacement pickups, the electromagnetic shaker, and the hydraulic cylinder. The frame fitted into grooves on the top surface of the platform. In addition, the frame was held in the grooves by rails which ran along the outside edges of the lower longeron flange as shown in Figure 3. The rails made contact along their entire length with the equipment platform but contacted the longeron flanges only for short lengths to minimize load distortions due to friction and to allow local realignment. Friction was further reduced by coating the longeron flanges with a Teflon spray.

Electromagnetic Shaker

A Goodmans V-47 electromagnetic shaker was used to excite the panels during the wind off conditions. The shaker was attached to the panel near the leading edge as shown in Figure 4 to minimize mode shape and frequency distortion due to the mass of the exciter spindle. An analytical study was performed to determine the effect of the shaker mass loading on panel vibration. This study, discussed in more detail in Appendix B, showed a negligible effect on panel frequencies and mode shapes.

Wall Replacement

The wind tunnel wall replacement section was sized to fit the Ames 2' x 2' transonic tunnel and was sufficiently massive (steel: 60" x 24" x 1.5") that negligible deformation would result in reacting hydraulic cylinder loads. Spring pins could be inserted ahead of the panel cutout to increase the boundary layer thickness over its smooth wall value. This boundary layer thickening technique is similar to a "short angle" method described by Schlichting in Reference 13. Spring pins have the advantages of being self-fastening and height adjustable. The spring pin thickening technique was checked out in the NASA/Marshall 14 x 14-inch trisonic wind tunnel and showed up to a 58% thickening for a .25 inch pin height (see Reference 14). This thickening was accomplished while still retaining the basic smooth wall characteristics.

Five static pressure taps were located in the wall replacement as indicated in Figure 5. The #4 port, located near the mid-chord of the active portion of the panel, was used as the cavity pressure reference. The figure also locates a Bytrex fluctuating pressure transducer which was used to search out tunnel resonances that might cause spurious panel excitation.

Cavity Enclosure

The cavity enclosure created a cavity with a depth of 17 inches behind the test panel and was sized to minimize the cavity effect on panel dynamics and flutter. The total enclosed volume was approximately 8000 in^3. An 8" x 12" rectangular opening was cut out of the back of the cavity enclosure so that an "infinite" cavity depth could be simulated with the cover plate removed. The cutout also permitted easy access to the interior instrumentation.

Cavity Pressurization System

A schematic of the cavity pressurization system is shown in Figure 6. The system was operated according to the following procedure:

1. The valves at the vacuum source were cracked open to permit a very slow air bleed rate.
2. The two valves upstream of valve C were adjusted such that the available pressure at C was on the order of the desired pressure differential across the panel.
3. Valve C was adjusted so that the air flow rate through C roughly matched the air flow rate into the vacuum source.
4. The power switch was then closed. This opened Valve B and closed Valve A permitting pressurization of the cavity.
5. Valve C was then further adjusted to obtain the desired pressure differential across the panel.

The ΔP limit switch limited the pressure differential across the panel by venting the cavity to the tunnel plenum when ΔP exceeded 1.0 psi. The ΔP system could be operated with the tunnel closed.

Compressive Load System

A hydraulic cylinder (Carter Controls, Inc. NNS style MS-7, working pressure 5,000 psi, Bore: 2 inches) was used to load the panel. A schematic of the load system is shown in Figure 7. The panels were

loaded by pumping up to the desired hydraulic pressure and closing the hand valve.

The accumulator was added to the high pressure line to minimize pressure drift due to leakage. The compressive load system was remotely controlled so that the compressive load in the panel could be raised while the tunnel was in operation.

INSTRUMENTATION

The test fixture instrumentation consisted of strain gauges, displacement pickups, and thermocouples. A schematic of the data gathering network is shown in Figure 8. Figure 8 also summarizes pertinent strain gauge, displacement pickup, and tape recorder data.

Strain Gauging

All of the test panels were instrumented with strain gauges measuring axial and bending strains. Table I presents a tabulation of the strain gauges on each of the test panels. The gauge location designations are explained in Figure 9.

The primary gauges for measuring panel flutter stresses were those denoted as A_1, B_1, A_3, and B_2 in Figure 9. Gauges A_1 and B_1 were located about mid-span at the trailing edge where maximum panel flutter stresses in the streamwise direction were expected. Likewise gauges A_3 and B_2 were located where the maximum panel flutter stresses in the cross stream direction were expected.

Since the initial test runs did not show the cross stream stresses to be more critical than streamwise stresses, gauges A_3 and B_2 were not incorporated on the other panels with the exception of Panel 5. They were included on Panel 5 to record cross stream stiffening effects which were investigated with this panel.

The gauges A_2, Λ_1, and Λ_2 were used primarily in connection with the loading system for applying compressive loads to the panel. They served as a functional check on the overall operation of the loading system, and as an indicator of the compressive stress applied to the panel. The longeron mounted gauges Λ_1 and Λ_2 were indicators of load imbalance, if any, between the longerons. Any such imbalance would infer unsymmetrical panel shear which could confuse interpretation of the test results. Furthermore, any imbalance between Λ_1 and A_2 (near the panel

edge) would indicate an incomplete transfer of compressive load to the panel which also could distort test results. The readings from gauges A_1 and B_1 rounded out the information required to assess panel behavior under applied compressive load, particularly the buckling load. From panel theory, buckling would be accompanied by (a) a sudden reduction in incremental strain in A_1 with increased load and (b) a sudden change from no strain to finite strain in B_1 with increased load. Although these ideal situations did not prevail, they were close enough for accurate, repeatable detection of buckling, particularly the gauge B_1 behavior (see section on Buckling Tests).

Displacement Pickups

Panel displacement was measured with Wayne-Kerr capacitance type displacement sensors located, as shown in Figure 4, at the expected flutter mode anti-nodes. The sensors were mounted off-center so that the panel displacement would be within the sensor operating range during pressurization of the cavity. The sensors were held in place by clamping them onto aluminum blocks (see Figure 2) which were cut out to receive the probe holder assembly. The cylindrical metal sleeves surrounding the sensor heads were wrapped with a Teflon insulation tape to prevent them from grounding to the aluminum blocks.

The spacing between the probe heads and the panel surface had to be adjusted daily during testing to maintain the optimum .05 inches. This spacing changed from day to day because of slight local deformations in the panel. The daily spacing adjustment proved to be quite a time consuming procedure because of the difficulty in adjusting dimensions on the order of several mils.

The displacement accuracy of the probes was advertised at ± 2 mils for the full range of 100 mils. Errors in the measurement of panel displacement can also be introduced by a non-parallel alignment of

sensing surface with the reference object, reaching 1% of indicated at an 8 degree misalignment. Such a misalignment will not cause any errors in peak-to-peak readings since the maximum and minimum displacements are affected equally.

Thermocouples

Two iron constantan thermocouples were mounted on the test fixture, one on the panel underside and the other on the longeron web, to determine the panel stresses induced by thermal gradients between the panel and support longerons. During the early runs the tunnel was exercised throughout its supersonic Mach number and dynamic pressure ranges and a maximum differential of 2°F was recorded. This temperature differential corresponds to a maximum compressive edge load on the panel equivalent to 17% of buckling. The thermocouples were removed after the first 14 flutter test points since they were suspected of being a source of electrical noise in the other instrumentation.

CHECKOUT TESTS

Particular care was exercised in the design and fabrication of the test hardware to minimize scatter in the test results. This was followed up, at the completion of fabrication, by a series of checkout tests designed to assess the degree of reliability and repeatability built into the test hardware. These tests provided for uncovering and correcting gross deficiencies, if any existed. In addition these tests provided basic information on the static and dynamic characteristics of the panels when mounted to the test fixture. Any changes in these characteristics would affect panel flutter behavior.

Functional Tests

The functional tests were conducted to insure the proper operation of the test fixture and instrumentation. The fixture was completely assembled and the following tests were performed:

1. Checkout of cavity pressurization system (ΔP system)
2. Checkout of compressive load system
3. Checkout of strain gauges and Wayne-Kerr pickups

Cavity Pressurization System Checkout

The ΔP system was checked out to a ΔP of 1.0 psi. There was no tendency for the test panel and frame to lift away from the wall replacement upon cavity pressurization. It was necessary to fasten additional sealing cloth at the loading block to permit pressurization to 1 psi.

Compressive Load System Checkout

The compressive load system was checked out to hydraulic pressures of 2,000 psi, which corresponds to approximately 170% of buckling. The load balance between the two I-beam longerons was determined by monitoring the output of the longeron mounted strain gauges while increasing the hydraulic pressure. (The panel was mounted on the frame during these tests.) Longeron strain imbalances as high as 20% were initially recorded (see Figure 10). It was found that the imbalance could be lowered to a maximum of about 5% (see Figure 11) by adjusting the tightness of the screws holding the rails

against the I-beam flanges (Figure 3). Once the optimum balance between longerons was obtained the rail screws were wired in place.

Checks were also conducted to see if the fixture would unload itself evenly when the hydraulic pressure was reduced. A large hysteresis effect was noted (Figure 10) prior to rail adjustment as the frame tended to hang-up as the pressure was reduced. After adjustment the hysteresis was significantly reduced (Figure 11). (The imbalance between longerons was about the same during loading and unloading.) The effect of the remaining slight hysteresis on control of compressive load was avoided by applying load via increasing hydraulic pressure (rather than backing down from a high pressure).

Additional checkout of this system was conducted during the buckling tests.

Instrumentation Checkout

The operation of the strain gauges and Wayne-Kerr pickups was confirmed by monitoring their outputs while exercising the cavity pressurization and compressive edge load systems.

Buckling Tests

Panel buckling loads were determined by incrementally loading the panels with the hand pump and then plotting indicated strains versus the hydraulic pressure in the loading cylinder. A typical plot is shown in Figure 12. While gauges A_2 and A_1 vary at a nearly linear rate, gauges A_1 and B_1 deviate markedly from this linear behavior especially beyond the buckling load. Bending strain output B_1 exhibits two examples of predictable behavior. The first is the slight strain buildup with load indicating that the panel is not ideally flat but has small initial eccentricity; and the second is the abrupt change in slope indicating that the panel has assumed its buckled mode shape. Gauge A_1 demonstrates that the panel strain (and stress) at the center will not exceed the buckling value even though the load is increased beyond buckling. Buckling was defined by the intersection of the extensions of the linear portions of the B_1 curve. Projection of this intersection to the A_1 output yielded the buckling strain from which the buckling stress was obtained. Using this method the buckling stresses were surprisingly repeatable ($\pm 8\%$). The table below lists buckling

stresses for the panels used in this program. For consistency of results from panel to panel, only the latter four were used in this wind tunnel test.

Panel Number	Experimental Buckling Stress (psi)
11	1564
1	1533
10	1347
5	1248
4	1289
6	1370

The theoretical buckling stress of the test panels is listed below for several boundary conditions:

Buckling Stress	Boundary Conditions
1590	Clamped All Around
1543	Long Sides Clamped Short Sides Pinned
929	Long Sides Pinned Short Sides Clamped
906	Pinned All Around

The predicted buckling mode for a fully clamped panel with L/W = 4.48 is the 7-2 mode (7 node lines parallel to the short sides, including the panel edges, and 2 node lines parallel to the long sides) while the actual measured mode was found to be 8-2. In theory, the 8-2 mode requires about a 3% higher load than the 7-2 mode. The measured mode is shown in Figure 13.

Vibration Tests

Test Procedure

These tests provided information on the operation of the vibration excitation and measurement systems and on the panel dynamic characteristics (frequencies and mode shapes) including the effects (if any) of compressive edge load, differential pressure, and the size of the cavity behind the panel. Acoustic and electromagnetic (fixture mounted Goodmans V-47) excitation was used to excite panel resonances in the 100 to 1000 Hz frequency range. Panel response was measured by the Wayne-Kerr displacement pickups. Acoustic excitation, independent of the shaker, was used to examine the effect of the fixture mounted Goodmans shaker on panel frequencies. The Wayne-Kerr pickups inside the test fixture were used along with an externally mounted Wayne-Kerr probe to make the response measurements so that non-panel resonances (fixture resonances) could be identified. Fixture resonances would show up as extra frequency spikes on the response plots of the output from the internally mounted pickups. The first ten panel modes were mapped with a Wayne-Kerr probe mounted on a traversing assembly which was fitted above the active portion of the panel as shown in the photograph on Figure 14. The traverse assembly permitted the measurement of panel displacement at 30 stream direction locations and any desired cross stream location. The probe support detail is shown in Figure 15. The internal probes were used as phase references for the external mapping probe.

Test Results

Panel Frequencies - The panel resonant frequencies excited by the fixture mounted Goodmans V-47 shaker are listed in Table II. The table also shows theoretically predicted test panel frequencies for a variety of boundary conditions. The first mode was virtually undetectable because the shaker location made excitation of this mode difficult.

The panel frequencies were also measured using acoustic excitation. The Goodmans shaker was left attached during the acoustic excitation. The shaker and horn excited frequencies are compared below:

Frequencies in Hz

Mode	2	3	4	5	6	7	8
Shaker	136-141	154-161	175-180	198-206	216-228	262-275	310-324
Horn	142	153	173	197	215	262	309

The horn excited frequencies show the slight effects of the "dead" shaker mass and shaker spring. This data is of interest because the shaker was left attached throughout the wind tunnel test. The first nine vibration mode shapes for the $\Delta P = 0$, $\bar{N}_x = 0$ case are shown in Figure 16.

Effect of Compressive Edge Load - Compressive edge load-frequency data for the test panel are given in Figure 17 for the recognizable vibration modes. Frequency resonances did occur in the 100 to 300 Hz range when $\bar{N}_x$ exceeded .5 but the modes were not recognizable. The recognizable modes 9, 10, and 11 showed decreasing frequency to near buckling; thereafter frequencies increased.

Mode identification with no compressive load is relatively easy since the number of node lines defines a unique mode. When a panel is under compressive edge load, however, mode identification is complicated because different modes can have the same number of node lines and the mode frequency no longer necessarily increases with mode number.

Figures 18 through 20 show modes mapped for resonances between 100 and 450 Hz with edge loads varying from 1/2 to 1-1/2 times buckling. For the 1-1/2 buckling load case resonances in the 200 to 350 Hz frequency

range could not be detected. Frequency response plots for the no load and 1-1/2 buckling cases are given on Figure 21. The plots verify the disappearance of four modes in the frequency range analyzed. The missing frequencies may have disappeared entirely or they could have shifted outside of the 100-450 Hz range. Disappearance of a first mode and drastic frequency shifts have been theoretically predicted in Reference 16 for panels subjected to edge load. The figure also shows that the compressive edge load resulted in a considerable reduction of panel response to excitation (excitation force was identical for both plots).

Effect of Differential Pressure - An increasing pressure differential across the test panels tended to increase panel frequencies. As in the case of high compressive load, multiple frequencies were recorded for identical modes at the higher differential pressures. Figure 22, summarizing ΔP effects, also shows the good repeatability in dynamic behavior from panel to panel.

Effect of Combining Compressive Load and Differential Pressure - Figure 23 shows the effects of subjecting the test panels to a combination of compressive load and ΔP. The .3 psi pressure differential across the panels accounted not only for frequency increases but also for the flattening of the frequency versus edge load plots.

Effect of the Cavity - The cavity had a negligible effect on panel dynamics. Table III lists frequency data for Panels 1 and 10 with the cavity enclosure access cover on and off (closed and open cavity). These results were encouraging because it was desirable to minimize cavity effect in the test fixture since the S-IVB stage with its 260 inch section diameter has what is essentially an infinite cavity behind its skin panels.

AERODYNAMIC FLOW SURVEY TESTS

Test Procedure

Boundary layer profile and surface static pressure surveys were conducted within a Mach number range of 1.05 to 1.40 and a dynamic pressure range of 200 to 1200 psf. This was done for both the natural and modified (1/8" spring pin height) tunnel boundary layers.

An instrumented rigid panel (1/4 inch steel) was flush mounted in place of the flutter panel and was used to conduct a static pressure and boundary layer survey in the tunnel prior to testing the flutter panels. The purpose of the static pressure survey was to determine the variation of static pressure over the panel and the adjacent tunnel wall replacement. Thirteen static pressure taps, shown in Figure 24 were used on this panel to measure static wall pressures. A Bytrex (Model HFO-SB) transducer was used to measure fluctuations in the static pressure so that frequency peaks in the pressure spectrum could be later correlated with test panel behavior if unexplained peculiarities in panel response were observed. Five static pressure taps and one Bytrex transducer located in the adjacent areas on the replacement section (see Figure 5) were used during both the flow survey and panel flutter phases of the test program. A 20 probe boundary layer rake (Figure 25) was used at each of the three locations shown in Figure 26 during the survey to measure the boundary layer profile. The purpose of the boundary layer survey was to determine the natural boundary layer profile of the tunnel at the panel location as well as to determine the changes in profile brought about by the spring pins. The Ames scanivalve system was used to record static and rake dynamic pressures. Bytrex transducer output was recorded on magnetic tape for subsequent spectral analysis.

Results of Aerodynamic Flow Survey

Static Pressure Distribution

Representative static pressure distributions are shown in Figures 27 and 28 for Mach numbers of 1.3 and 1.4, the values at which minimum flutter onset dynamic pressure was detected. All of these plots are characterized by a sharp static pressure rise five inches downstream of the panel leading edge. This static pressure peak is attributed to the presence of two rows of 1/8" high screw heads oriented transverse to the flow and located directly in front of the pressure reference port.

Static pressure tap #4 (19.5 inches aft of panel leading edge and 10 inches off centerline) was used as the reference static pressure source in monitoring and controlling the differential pressure ΔP across the panel. The variation in static pressure over the face of the panel was about the same order of magnitude as the differential pressure range covered in the panel flutter tests (zero to 0.15 psi). As a consequence, the difference between the monitored differential pressure (referenced to tap #4) and the average differential pressure could be significant. The approach taken to circumvent this problem is discussed under Panel Flutter Tests.

Boundary Layer

Typical boundary layer profiles are presented in Figures 29 and 30 for both the rough and smooth wall configurations at the Mach 1.4 condition. Profiles at several rake positions are shown on each plot to show the shape of the normalized boundary layer profiles as a function of streamwise location. A constant normalized profile would indicate that the boundary layer over the panel is "fully developed". Except for minor deviations the figures show that this was, indeed, the case (boundary layer thickness increases with distance from the wall replacement leading edge). The lack of "smoothness" in some of the profiles (such as the RP2 profiles for q = 1200 psf on Figure 30 is due

in part to obstructions in the rake pressure probes and also to erratic tunnel behavior while running at its operating limits (M = 1.4, q = 200 psf and M = 1.4, q = 1200 psf).

The boundary layer thickness increased with the distance from the leading edge of the wall replacement. Figures 31 and 32 show the thickening as a function of stream direction location for the Mach 1.4, q = 200 and 1200 psf conditions. Both smooth tunnel wall replacement and rough wall (spring pins inserted) replacement data are shown. Inserting the spring pins into the wall replacement caused boundary layer thickening ranging anywhere from negligible to 56% depending on flow conditions and streamwise position. Boundary layer thickness at the aft rake position is given in Figure 33 as a function of Mach number.

Fluctuating Pressure

Power spectral density plots of the Bytrex transducer data recorded for tunnel dynamic pressures of 200 and 1200 psf are given in Figures 34 and 35. The spikes at 60, 120, 180, and 300 Hz appear to be multiples of 60 cycle noise. Whether or not these data spikes represent true pressure fluctuations is important because the flutter frequency for most of the test cases was in the vicinity of 120 Hz. It seems reasonable that the spikes are electrical noise both because previously reported fluctuating pressure data for the 2' x 2' transonic tunnel has not exhibited such characteristics (see Reference 17) and because the spike frequencies shown are independent of the wind tunnel drive motor RPM, which varies with dynamic pressure.

PANEL FLUTTER TESTS

Test Procedures

The panel flutter tests were conducted in the NASA/Ames 2 ft. by 2 ft. transonic wind tunnel that has the Mach number and dynamic pressure ranges shown in Figure 36. A photograph of the installation, viewed from the side of the tunnel opposite the wall replacement section, is shown in Figure 26. The test panels were .032 inch thick, had active surface dimensions of 30 inches streamwise by 6.7 inches cross stream, and were mounted in a vertical plane. Except for installing and inspecting the panels, all work on the fixture was done from the reverse side of the assembly which was accessible from the plenum chamber. The test plan, formulated in Reference 18, was designed to:

(1) Determine the critical Mach number (M_{CR}) for which panel flutter occurs at the lowest dynamic pressure.

(2) Define the dynamic pressure flutter boundaries at M_{CR} as a function of inplane compressive load (N_x) and differential pressure (ΔP) as well as of the secondary parameters boundary layer thickness, cavity volume, and cross stream restraint stiffness.

(3) Determine the magnitude of panel flutter as a function of dynamic pressure deficiency, i.e., dynamic pressure penetration beyond onset, including the influence of the parameters in (2) above.

The compressive load system (see Figure 7) that was used to apply inplane compression stress was pressurized by a hand pump located in the wind tunnel control room. The cavity pressurization system (Figure 6) used for ΔP control was operated from a console located near the

visual display equipment. Changes in boundary layer thickness, cavity volume, and cross stream restraint stiffness were made with the wind off and the tunnel open.

Setting the Differential Pressure

Differential pressure was measured by a transducer comparing pressure in the cavity with tunnel wall static pressure. Pressure port #4 (see Figure 5) was located on the wall replacement section near the center of the flutter panel and was used as the reference pressure for ΔP measurement and control. Since the static pressure distribution over the surface of the panel varied somewhat with tunnel flow conditions, a zero indicated ΔP was not necessarily equivalent to a true zero ΔP averaged across the entire panel. A zero reference for the average ΔP was determined by varying the indicated cavity pressure through a range of values, both positive and negative, in order to locate the pressure setting which resulted in maximum panel response. This pressure setting defined the zero reference for the average ΔP setting since a non-zero ΔP is known to reduce the response amplitudes of flat panels. Once the ΔP for maximum panel response was found, the indicated cavity pressure was adjusted by this amount to obtain true ΔP.

The unsteady flow conditions made ΔP a difficult variable to control precisely, especially at high tunnel q. However, the operators became skillful at establishing a mean value of ΔP even though fluctuations were present in the meter readings.

Determination of Flutter Boundary

A flutter onset condition (flutter point) was determined as a function of M, q, N_x, ΔP and the secondary parameters. Since N_x was a primary variable and had a strong influence on flutter, the boundary could be approached by increasing either N_x or q, while holding the remaining parameters fixed. For the case of $N_x = 0$ (point A on sketch) and for large values of N_x

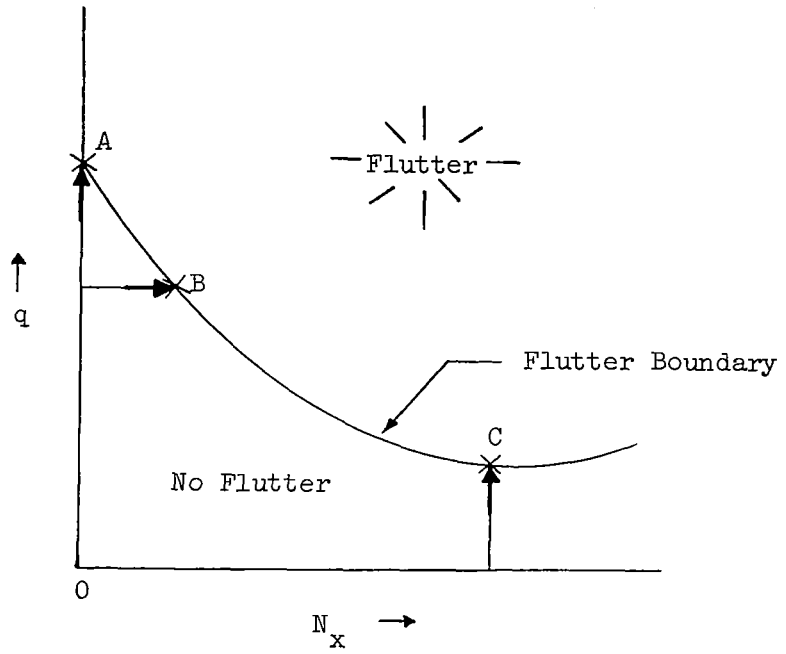

(such as point C) where the slope is shallow it was expedient to define flutter points by varying the tunnel q. The flutter boundary was identified by the changing nature of the output of bending strain gauge B_1. The transition from stability to instability (flutter) may be best described as a change from random to periodic motion accompanied by a substantial increase in strain amplitude. The random motion is induced by turbulence in the tunnel flow (aerodynamic noise). By using on-line oscillograph strip charts of displacement and strain outputs and the visual displays from oscilloscopes, the uncertainty in flutter point location was reduced to less than 25 psf dynamic pressure. The output of the bending strain gauge B_1 was an excellent indicator of the transition to flutter onset and was used throughout the runs defining the flutter boundary.

Figure 37 shows records of strain amplitude and waveform that were obtained for a typical flutter point. The upper sequence of records shows a gradual increase in strain amplitude as dynamic pressure

is increased from 200 to 600 psf. The strain amplitude increase is roughly in proportion to dynamic pressure and is caused by increasing wall turbulence in the tunnel. At q = 650 psf, the strain has increased sharply indicating that the panel has become aeroelastically unstable. The plot of bending stress amplitude versus dynamic pressure shows the magnitude of increase involved and indicates a flutter boundary of about 625 psf. The lower sequence of records shows how the strain waveforms also indicate the transition between stability and instability. A randomness of gauge output is observed at q values well below flutter (notably at 200 and 400 psf). At 500 and 600 psf the output begins to show the emergence of a dominant frequency component and also begins to exhibit a beating characteristic. Just above the flutter boundary, the randomness disappears and the wave becomes periodic.

The flutter onset points found by this method were remarkably repeatable due mainly to the fact that transition of gauge waveform characteristics occurred abruptly in a very small range of dynamic pressure.

Flutter Penetration

After establishing the flutter onset dynamic pressure (q_{on}) as a function of the test parameters, the panels were subjected to q levels exceeding the flutter onset values. The primary purpose of the flutter penetration was to collect information that will aid in predicting panel fatigue life. The quantitites primarily sought therefore were stress amplitude and flutter frequency. As in the flutter boundary determination, it was found that N_x made a very convenient variable for locating a flutter penetration point once M and q were established. The usual procedure was first to define the flutter boundary (line A-C on next page). Usually four data points were sufficient for this purpose. Once the flutter boundary was defined, lines of constant penetration - the 17, 33, and 50% penetration lines on the sketch - could be constructed by multiplying the q_{on} values at each N_x by the desired penetration percentage. Thus, a 50% penetration would mean that

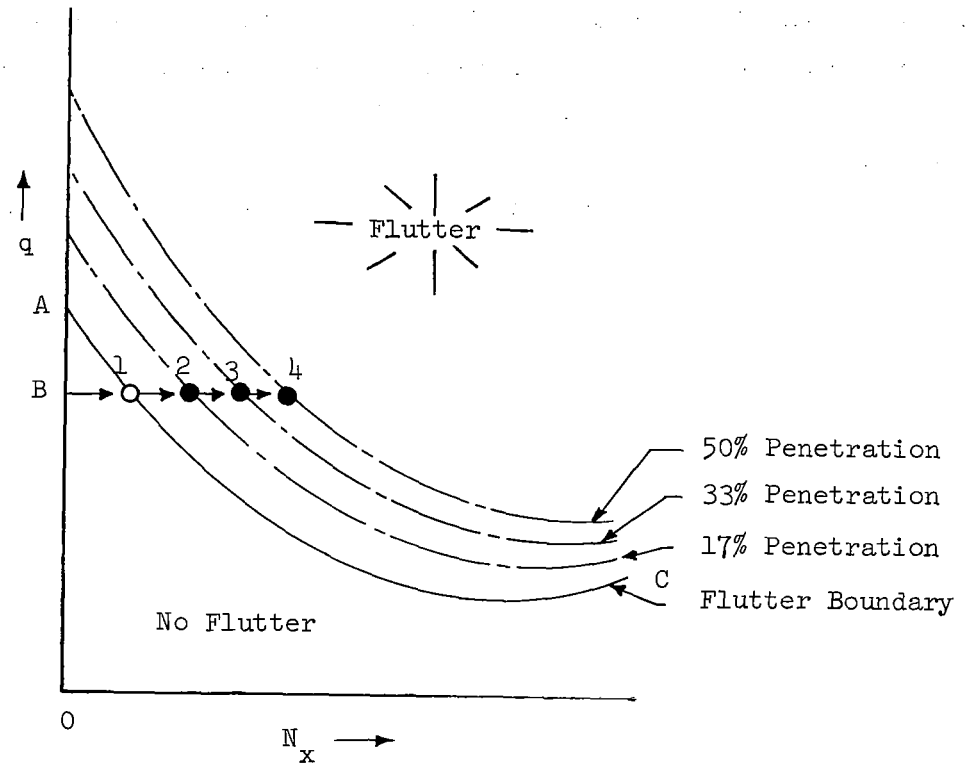

the dynamic pressure was 50% higher than the onset value. Data points were taken by setting q at B, for example, increasing N_x to flutter onset point 1, taking data, increasing N_x to penetration point 2, taking data, and so on. When ΔP variation was to be investigated, M, q, and N_x were fixed and ΔP was varied to obtain a flutter point.

Panel Inspection

Once a panel had experienced flutter, constant surveillance was maintained on the condition of the panel. In addition to the possibility that a panel could sustain damage during flutter (due to fatigue or yielding), it was also possible that the panel could slip under its attaching screws and thereby attain characteristics different from those of the original installation. The periodic checks were both visual and by means of instrumentation outputs. Visual checks were made from the tunnel side of the panel and consisted of inspecting for evidence of fatigue cracks as well as for deviations from flatness, the latter including qualitative indications from reflected light patterns. Though no fatigue cracks were ever indicated, several panels

exhibited deviations from flatness indicating either material yielding or edge restraint slippage. Two additional checks were made at longer intervals, or whenever visual inspection indicated the need. These were a vibration sweep survey and a check of buckling load. The vibration survey consisted of sweeping with the Goodmans shaker through a frequency range of approximately 100 to 700 Hz, and comparing the response plot with previously obtained plots. Significant changes in resonant peaks indicated a change in panel dynamic characteristics. A further check on static characteristics was made by measuring the buckling stress and comparing against earlier measurements. If deviations in dynamics and/or buckling were indicated, the attaching screws were loosened and the panel was reseated on the frame. Checks were then repeated. If the panel had not regained its original static and dynamic characteristics, it was assumed the panel had sustained permanent damage and it was replaced. Four panels were used during the wind tunnel tests.

To further enhance the validity of experimental data obtained for either the reseated panels or replacement panels, a flutter onset check run (usually for $N_x = 0$ and $\Delta P = 0$) was made before continuing with the panel flutter test schedule. If flutter onset did not compare favorably with prior valid results, the panel was replaced even if it had passed the frequency and buckling checks.

A typical history of the modal resonant frequencies obtained for Panel 5 is shown in Table IV. This panel was flutter tested and the succeeding vibration survey indicated changes in dynamics. These changes in part consisted of shifts in modal resonant frequencies accompanied by differences in response amplitude. In addition, however, some modes having the same number of cross stream node lines were found to resonate at more than one frequency; these are designated in the table as multiple modes. The panel was reseated and the dynamics then agreed satisfactorily with the original configuration. The same panel was subsequently flutter tested, reseated, and flutter tested again before it was decided that the panel should be replaced.

Flutter Test Results

The test program covered 33 tunnel occupancy days during which 4 panels were flutter tested. The scope of the test program is summarized below:

Summary of Test Program

Wind Tunnel	NASA/Ames 2' by 2' transonic
Panels Tested	4
Range of M	1.1 - 1.4
Range of $\bar{N}_x$	0 - 1.7
Range of ΔP	0 - .20 psi
Cavity	Closed and Open
Cross Stream Stiffening	Stiffened and Unstiffened
Boundary Layer	Smooth and Rough Wall
Flutter Penetration (Nominal)	1.17, 1.33, and 1.5 times q_{on}
Flutter Penetration (Panel 6)	Up to 3.3 times q_{on}

A complete record of the test points, both subflutter and flutter, is given in Appendix C.

Determination of Flutter Onset Boundary

The dynamic pressure deficiency (q penetration) can only be established when flutter onset boundaries are accurately determined. Therefore, a proper assessment of panel behavior in flutter must be preceded by experimental definition of flutter onset boundaries. This section describes the effects of the parameters that were varied and distinguishes between the secondary parameters (those that caused relatively small change in flutter onset) and the primary parameters (those that caused large changes in the flutter boundaries). The secondary parameters are discussed first and it is shown that their effects are either insignificant or inconclusive and do not warrant further treatment in this report. The primary parameters (Mach number, compressive edge load, and differential pressure) are then presented individually, their effects noted, and a brief discussion is made of the effects on flutter due to their interaction.

Secondary Effects - The secondary parameters in this investigation are defined as cavity volume, boundary layer thickness and cross stream stiffening.

The cavity enclosure portion of the test fixture was sized to minimize the effect of the cavity volume on panel flutter. Design dimensions were adapted from data given in Reference 3 and two cavity conditions were simulated: a finite cavity volume obtained with the cavity closed, and an infinite cavity volume obtained by opening the rear of the panel to the plenum chamber.

The flow rougheners that could be added forward of the panel were designed to increase the thickness of the natural boundary layer along the tunnel wall. The protuberances were sized and spaced according to flow data given in Reference 13. While a large increase in boundary layer thickness was desired, it was also considered necessary that the modified boundary layer be established over the entire length of the panel. The ensuing compromise, based on theory and on tests conducted at NASA/MSFC (Reference 14), resulted in average boundary layer increases over the panel that varied between 6 and 45%.

Cross stiffeners were inserted between the side longerons (see Figure 2) to provide a more realistic simulation of the inplane edge restraint experienced by the S-IVB panel. In order to assess the effect of lateral stiffening, the cross pieces were removed for a portion of the test.

Test data for evaluating the effects of these parameters was obtained from Panel 5, and Table V presents the resulting composite of values of flutter onset dynamic pressure. For $\bar{N}_x = \Delta P = 0$, and the indicated Mach variation the table shows (within the normal repeatability range of q_{on}) essentially no change in flutter boundary for the open or closed cavity and a slight increase for the rough wall over the smooth wall. The removal of the cross stiffeners (see the M = 1.2 and 1.3 cases in Table V) resulted in a small increase in q_{on} (about 100 psf). Whether this increase in q_{on} is really due to the stiffness decrease, or is simply within the normal range of variation in the experimental data, is not clear. The indicated trend is contrary to expectation;

although high amplitude (flutter) motion should be affected by the additional restraint, flutter onset should not. In any event its effect is small in comparison to the primary variables.

Mach Number Effect - The effect of Mach number on panel flutter boundaries, especially in the low supersonic regime has not been well defined. This section presents Mach effect data for the panels tested (length-to-width ratios of 4.48). Figures 38 and 39 show the variation in q_{on} with M that was obtained in this test. Although maximum wind tunnel Mach number was restricted to 1.4, these plots clearly indicate that the critical Mach number (where q_{on} is a minimum) for a panel of L/W = 4.48 lies between 1.3 and 1.4. This result is consistent with previous panel flutter experience which indicates that the majority of panel flutter problems occur in the low supersonic flight regime. As noted in Figure 38, the flutter boundary then increases rapidly as Mach number decreases toward 1.0. This contrasts with the frequently employed theoretical parameter which predicts a rapid decrease toward zero at M = 1.0. A detailed discussion of the Mach effect on the panel flutter parameter is given in Reference 3. In addition, pertinent Mach effect data from this test program appears in Appendix D.

Effect of Compressive Edge Load - The flutter onset dynamic pressure of the test panels decreased with increasing compressive edge load, and then leveled off in the vicinity of $\overline{N}_x = 1.0$. This effect is shown in Figures 40 and 41. Figure 40, which is a plot of q_{on} versus $\overline{N}_x$ for one Mach number (M = 1.3), shows 72% reduction in onset dynamic pressure between $\overline{N}_x = 0$ and 1.0. Figure 41 presents a comparison of the data obtained at M = 1.1, 1.2, 1.3, and 1.4. The trend of decreasing q_{on} with increasing $\overline{N}_x$ is evident in all cases as well as the tendency for minimum q_{on} to occur near $\overline{N}_x = 1.0$ (the still air buckling load).

Effect of Differential Pressure - Static differential pressure has a strongly stabilizing effect on flat panels. Differential pressure was remotely controlled in a manner that is discussed earlier in this section. During wind tunnel tests, the static pressure distribution over the panel face varied, and also fluctuated with time. Values of ΔP shown on the data therefore, represent an average in both space and time.

Figure 42 shows how ΔP increases the basic level of q_{on} versus $\overline{N}_x$. The higher curves ($\Delta P > 0$) show that the general shape of the flutter boundary

remains the same as the base curve for $\Delta P = 0$. Figure 43 is a cross plot of the curves in Figure 42 and shows how ΔP increases flutter boundaries at fixed values of $\overline{N}_x$.

Test data for Panel 5, for $\Delta P = 0$ and 0.1 psi is given in Figure 44. To better visualize just how significant this effect is, a 0.1 psi change in ΔP can nullify the effect of a compressive load of about 40% buckling.

Panel Behavior During Flutter

The panel dynamic response features of primary interest were bending and axial stress, flutter frequency, and flutter mode shape. The strain and displacement sensors, in addition to defining onset, were used to measure the dynamic parameters during flutter. On the basis of preliminary design information, strain gauges A_1 and B_1 were located as near as possible to the point that would experience maximum bending stress during flutter, and the Wayne-Kerr displacement pickups were located to define the flutter mode shape. In the event that the point of maximum stress occurred elsewhere on the panel, a reasonably accurate description of the mode shape could then be used to calculate the maximum stress by extrapolating from the measured value. With knowledge of the flutter frequency and maximum stress, existing fatigue criteria can then be used to estimate the panel fatigue life in a given flutter environment. This section describes the stresses (both static and dynamic) that were measured during flutter, the frequencies, and the displacements.

Panel Stresses - The panel stresses measured during the wind tunnel program were obtained from strain gauges that were located downstream and near the panel edges (see Figure 9). Strain gauge elements at each location were mounted on both sides of the panel and each gauge could measure either bending or axial (membrane) strain depending on the electrical hookup. The bridges were temperature compensated up to 130°F which was well above the tunnel wall temperature. Strains were converted to stress by use of the generalized Hooke's law. Both the bending and axial stresses consisted of static and dynamic components. The static stress component in bending resulted from static panel deformation induced either by N_x (buckling) or by ΔP. The static part of the axial stress was due to compression caused by N_x and stretching caused by ΔP. The dynamic part of the bending stress was caused by unsteady panel motion induced by panel flutter or by response to turbulence, and the dynamic part of the axial stress was caused by stretching as the panel underwent large amplitude flutter motion.

The dynamic part of the axial stress plays a major role in distinguishing large amplitude plate theory from small deflection theory (Reference 19). Furthermore, this dynamic axial stress limits amplitude buildup when a panel is subjected to deep flutter.

Figures 45 through 54 summarize the stress measurements obtained from two panels (4 and 6) that provided extensive test data. Figure 45 is a typical plot of the static component of measured axial stress at flutter onset versus applied compression load. The static component of the bending stress was erratic and unrepeatable due again to slight initial curvature of unknown magnitude. The measurements showed however, that the largest static bending stress was about the same magnitude as the static axial stress.

Oscillatory axial stresses are shown in Figures 46 and 47 as plots of peak-to-peak stress versus $\overline{N}_x$. These data are given for the flutter onset condition and for flutter penetration at 1.17, 1.33, and 1.5 times flutter onset dynamic pressure. Deeper penetration is indicated by the dark symbols located higher along the lines of constant q.

Figure 48, a plot of the peak-to-peak oscillatory bending stress at flutter onset versus $\overline{N}_x$, indicates that the oscillatory amplitude remains bounded below buckling (when $\overline{N}_x < 1$) but rises rather sharply when $\overline{N}_x$ exceeds 1. This same trend was also clearly indicated by Panel 4 onset data, as shown in Figures 49 and 50. Also, to be noted in these two figures is the indicated effect of ΔP which apparently increases the amplitude of the oscillatory bending stress at flutter onset. This trend is demonstrated in the following table (for $\overline{N}_x < 1.0$):

ΔP (psi	Max. Osc. Bending Stress p-p, psi
0	1800
.1	2250
.15	2600

The effect of flutter boundary penetration on oscillatory bending stress is shown in Figures 51 and 52. The general trends are very similar to those of the oscillatory axial stresses (Figures 46 and 47) although the peak-to-peak bending stresses are larger by about 5 to 1 in one case (comparing Figure 51 with Figure 46) and about 3 to 1 in the other (comparing Figure 52 with Figure 47). In addition, the bending stresses at higher levels of penetration show a fairly well defined tendency to level out; this is more evident in Figure 52.

Figure 53 is a cross-plot of Figure 52 showing how the oscillatory bending stress amplitude varies with dynamic pressure for parametric variations in compression loading $\overline{N}_x$. Figure 54 shows how the oscillatory bending stress changed with q up to a penetration (q/q_{on}) of almost 3 to 1 and clearly shows the leveling off tendency at the higher penetration. This sequence of test points (Appendix C, log 50) was made at the termination of the program to test the endurance of a typical test panel. The most severe penetration occurred during the log 51 run (q = 1000 psf, q/q_{on} = 3.33, $\overline{N}_x$ = 1.7). The panel did not fail, even after dwelling at q = 1000 psf for twenty minutes.

Flutter Frequencies - The flutter frequencies listed in Appendix C were measured by a pulse counter which works very well for waveforms that do not have multiple peaks during one period of the fundamental frequency. Since the strain gauge and Wayne-Kerr waveforms often contained higher frequency harmonics, a more detailed study of the frequency content of these waves was performed on 25 wind tunnel data logs. Visual inspection and Fourier transform analyses of the wave shapes were employed in the study.

The fundamental flutter onset frequencies obtained from Fourier transform analyses of the data logs are shown in Figure 55 as a function of Mach number and compressive edge load. The figure shows a general lowering of onset frequency with increasing compressive edge load and decreasing Mach number, the effect being most pronounced at M = 1.1 and 113% of buckling. The differential pressures that were employed in the tests (zero to .15 psi) had a negligible effect on the flutter frequency.

As dynamic pressure was increased beyond flutter onset the fundamental flutter frequency increased slightly. This is shown in the table below for Panel 6 deep penetration sequence (Appendix C, log 50) at 96% buckling load:

Deep Penetration Sequence for $\overline{N}_x = 0.96$ (Panel 6, M = 1.3, ΔP = 0)

Dynamic Pressure (psf)	Fund. Flutter Freq. (Hz)	Condition
300	114	Flutter Onset
400	117	Penetration
600	121	Penetration
800	127	Penetration

In addition to the above fundamental frequency trend, the signal waveforms exhibited increasing first overtone content (twice the fundamental frequency) with increasing penetration. This increasing harmonic content first became evident in the outputs from the transducer located at the trailing edge of the panel (probe F and bending gauge B_1) and moved forward with increasing penetration (to probes C and A). Figure 56 shows the changing waveform trends with increasing penetration. The first overtone content at the rear part of the panel very quickly dominated the fundamental, giving the impression that the rear of the panel was fluttering at twice the frequency of the forward part. The waveforms at the far right of the figure are for the greatest penetration run during these tests.

In summary, the following frequency characteristics were observed:

(a) Flutter onset frequencies generally decreased with increasing compressive load and decreasing Mach number.

(b) Flutter frequency increased somewhat with increasing dynamic pressure penetration beyond flutter onset.

(c) In deep flutter penetration, the predominant frequency component of the rear portion of the panel was twice that of the forward portion.

Panel Motion During Flutter - The total panel deformation was measured with Wayne-Kerr non-contacting displacement gauges at six streamwise panel locations (described in Instrumentation section). At the beginning of the tests the gauges were located along the panel centerline. However, non-uniform static pressure along the tunnel wall caused panel static deformations that could either short the panel to the probes (inward pressure) or cause a head spacing too large for linear operation of the sensors (outward pressure). The Wayne-Kerr pickups were then moved to a line 2.5

inches off the centerline where panel motion was smaller, but where the transducers remained within their linear operating ranges. The displacement amplitude data presented in this section were measured at this off centerline location where the panel is estimated to move through 1/3 to 1/5 of the displacement at the centerline. On this basis, the peak oscillatory panel motion during flutter was estimated to be of the order of one panel thickness which caused a significant buildup of membrane stress, about 20 to 33% of the bending stress. The displacement pickup at position B (See Figure 4) did not function properly during tunnel tests.

Figures 57(a) through 57(d) show a series of flutter mode shapes that were obtained with increasing values of $\overline{N}_x$. The presence of both Co (in-phase) and Quad (90° phase shift) components indicates that flutter was of the traveling wave variety. These mode shapes show that panel deformation is generally larger toward the trailing edge although not to a significant degree. Additionally, the component mode shapes tend to take on additional cross stream nodal lines with increasing $\overline{N}_x$. This trend suggests that as $\overline{N}_x$ approaches 1, the flutter mode shape takes on more of the character of the buckling mode shape (a minimum energy configuration under static inplane loading).

Figures 58 through 61 present peak-to-peak panel displacements measured during flutter as functions of $\overline{N}_x$, q and sensor location. Figures 58 and 59, for zero ΔP, show oscillatory displacements for an upstream and downstream panel location as a function of $\overline{N}_x$ for both flutter onset and penetration. These figures show (a) sharp increases in flutter onset amplitude when the panel buckling load is exceeded ($\overline{N}_x > 1$), (b) linear increases in amplitude with flutter penetration (up to 50% dynamic pressure penetration), and (c) generally larger amplitudes downstream.

The effect of differential pressure on panel displacement is shown in Figure 60. The most obvious effect of ΔP is the leveling-off behavior at the higher displacements in contrast to the nearly linear behavior for the zero ΔP cases.

Figure 61 shows panel displacement behavior for a deep flutter penetration run. Specifically, the displacements at the forward, middle, and aft portions of the panel are presented as a function of dynamic pressure. These displacements all increase linearly with q until q = 500 psf (167% q_{on}). Thereafter the middle and aft displacements generally continue to grow, but at a slower rate, while the forward displacement tends to drop somewhat. The reason for the slight kink at about q = 550 psf (183% q_{on}) is not known but may be indicating a shift in flutter mode.

CONCLUSIONS

Flutter Onset

1. The minimum flutter onset dynamic pressure for the panels tested occurred between Mach 1.3 and 1.4.

2. In-plane compressive edge loads have a marked destabilizing effect on onset dynamic pressure. Maximum effect occurred near the panel buckling load where the onset dynamic pressure was reduced to about one fourth of the zero load value.

3. An average pressure differential across the panel as little as 0.10 psi raised the onset dynamic pressure by about 50%. This pressure differential is very small, of the same order as the variation in static pressure over the panel surface. A differential pressure of this size has about the same effect on flutter onset as a decrease in compressive load of about 40 to 50% of buckling.

4. Boundary layer, cavity volume, and cross stream stiffness had minor effects on flutter onset. The average boundary layer thickness was varied from approximately 1.0 to 1.3 inches and the equivalent cavity depths were 40 inches and infinity.

Flutter Penetration

1. During flutter penetration, the induced bending stresses were approximately 3 to 5 times the induced in-plane (membrane) stresses.

2. The total surface stresses induced by flutter start from a finite level at onset, increase linearly with dynamic pressure, then appear to flatten out with further increase in dynamic pressure.

3. The maximum penetration run (170% buckling, dynamic pressure 3.3 times onset) resulted in no panel failure or evidence of fatigue cracks. Maximum stress measured at the surface of the panel trailing edge was 11,000 psi and this was maintained for more than twenty minutes, corresponding to about 360,000 cycles.

Table I - Summary of Test Panel Strain Gauges

Panel Number	B_1	B_2	A_1	A_2	A_3	When Panel Was Tested
11	x	-	x	-	-	CT
1	x	x	x	x	x	CT
10	x	x	x	x	x	CT & WTT
4	x	-	x	-	-	WTT
5	x	x	x	-	x	WTT
6	x	-	x	-	-	WTT
3	x	-	x	-	-	WTT*
2,7,8,9,12	x	-	x	-	-	Untested

* Panel 3 had a buckling load and frequency response characteristics which were incompatible with the other test panels. It was rejected before flutter testing.

Notes

A ∿ gauge measuring axial strain

B ∿ gauge measuring bending strain

Subscripts denote gauge locations - see Figure 9

CT ∿ Checkout Test

WTT ∿ Wind Tunnel Test

Table II - Frequency Comparison Data, Experiment and Theory

Mode	Experimental Data (Hz)	Theoretical Resonant Frequencies (Hz)			
		Pinned All Around	Long Sides Pinned Short Sides Clamped	Long Sides Clamped Short Sides Pinned	Clamped All Around
1	128	72	73	157	158
2	136-142	82	86	164	165
3	152-161	99	106	174	178
4	173-180	123	133	191	198
5	197-206	154	167	215	225
6	215-228	192	209	246	260
7	262-275	236	256	285	302
8	309-324	288	312	331	352

Experimental Data is for Panel 1 $\bar{N}_x = 0$, $\Delta P = 0$, cross stiffeners IN

Theoretical Data was obtained from a single mode approximation, $\bar{N}_x = 0$, $\Delta P = 0$. See Reference 15.

Table III - Comparison of Frequency Data for Cavity Access Cover On and Off

Mode	Experimental Resonant Frequencies - Hz							
	$\bar{N}_x = 0$				$\bar{N}_x = 0.5$			
	Panel 1		Panel 10		Panel 1		Panel 10	
	ON	OFF	ON	OFF	ON	OFF	ON	OFF
f_1	128	-	-	-	-	-		-
f_2	136-142	141	134-135	135	120-128	-		-
f_3	152-161	153-154	153-155	152	127-135	132		-
f_4	173-180	175-177	178-180	178-179	142-153	153	Not Avail-	143
f_5	197-206	197-202	205-206	205	152-169	168	able	156-158
f_6	215-228	217-218	234-235	233-234	172-180	182		178
f_7	262-275	263-268	275-277	273-274	203-208	207		207-208
f_8	309-324	311-315	322-323	320-322	242-262	260		248
f_9	358-372	363-367	376-378	375-376	293-304	303		293-294
f_{10}	417-434	427-425	431	435	345-360	354		355

$\Delta P = 0$ for all data

Table IV - Chronological History of Panel 5 Frequencies
Showing the Effect of Flutter Testing

Panel Resonant Frequencies - Hz						
f_3	f_4	f_5	f_6	f_7	f_8	Comment
145	156	179	204	234	272	New Panel
Flutter Testing*						
150	161	170	193*,209	216,224*	242,260*	After Flutter Tests. Multiple 6,7,8th modes. Low panel response amplitudes.
142	154	176	201	230	268	Reseated Panel. Panel OK.
Flutter Testing*						
NP	156	172	191*,200	234	276	After Flutter Testing. Multiple 6th mode. Low panel response amplitudes.
142	155	170	198	228	265	Panel Reseated. Panel OK.
Flutter Testing						
NP	155	172,179*	195,209*	225,243*	283	After Flutter Testing. Multiple 5,6,7th modes.

NP - No Resonant Peak Observed
* - Dominant Mode

Table V - Data Showing Effect of Secondary Parameters on Flutter Onset

	Range of q_{on} (psf)			
	Cross Stiffeners			No Cross Stiffness
	Smooth Wall		Rough Wall	
Mach Number	Cavity Open	Cavity Closed		
1.2	850	750	795	915
1.3	645-675	625-720	670-740	790
1.4	690	650-720	755	*

*Not Measured

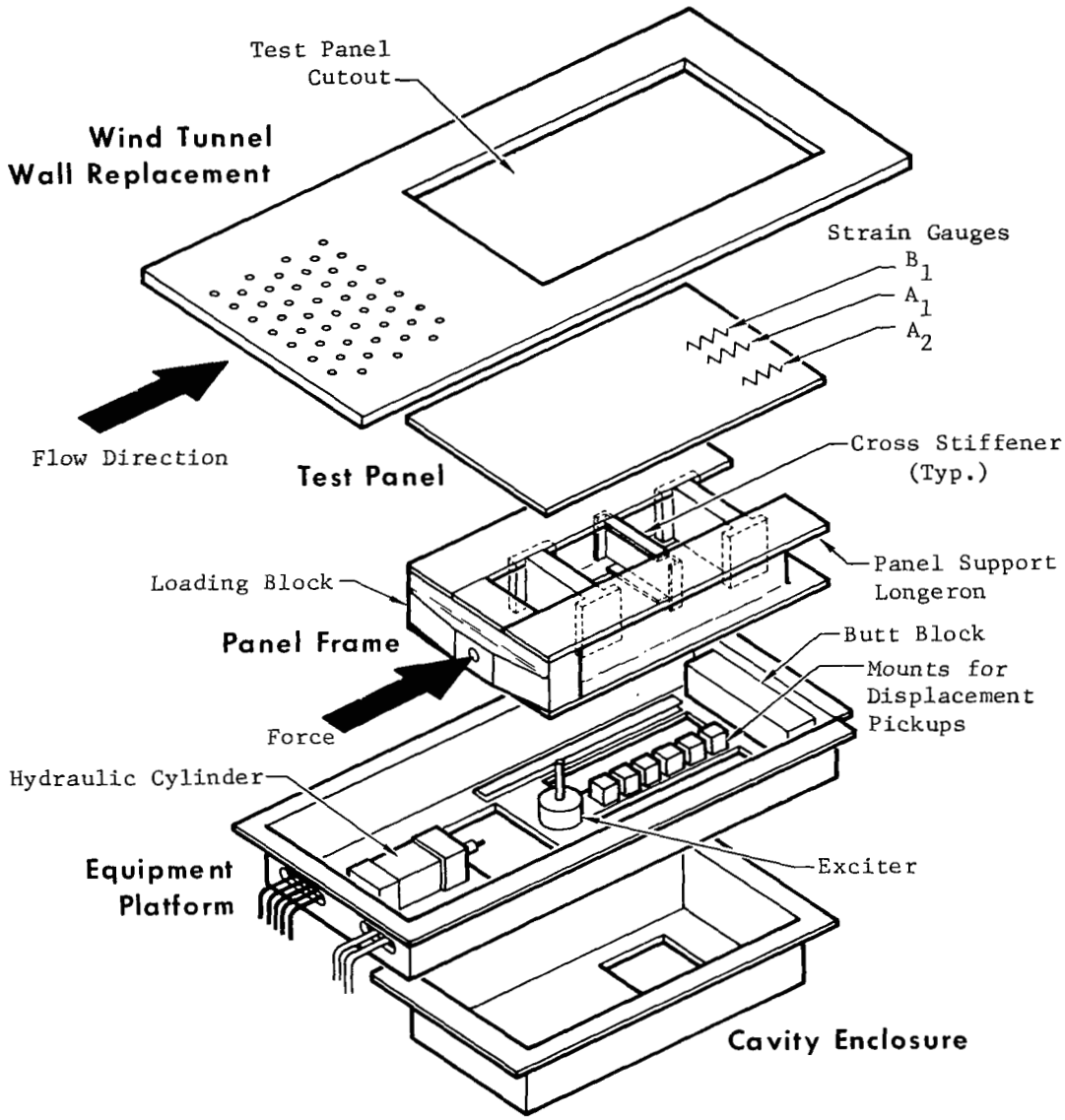

Figure 1 Panel Flutter Test Fixture

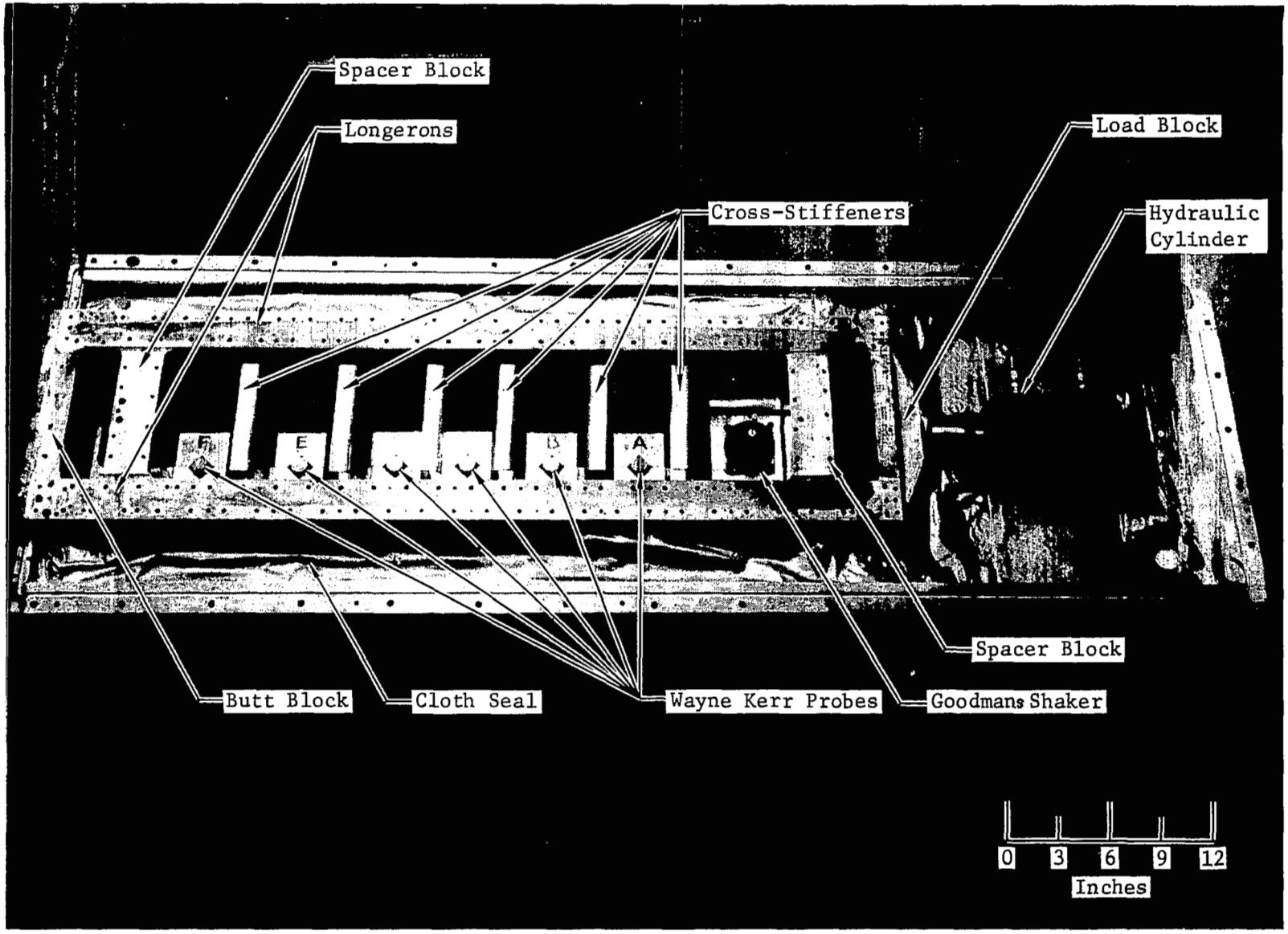

Figure 2 Panel Holder Assembly

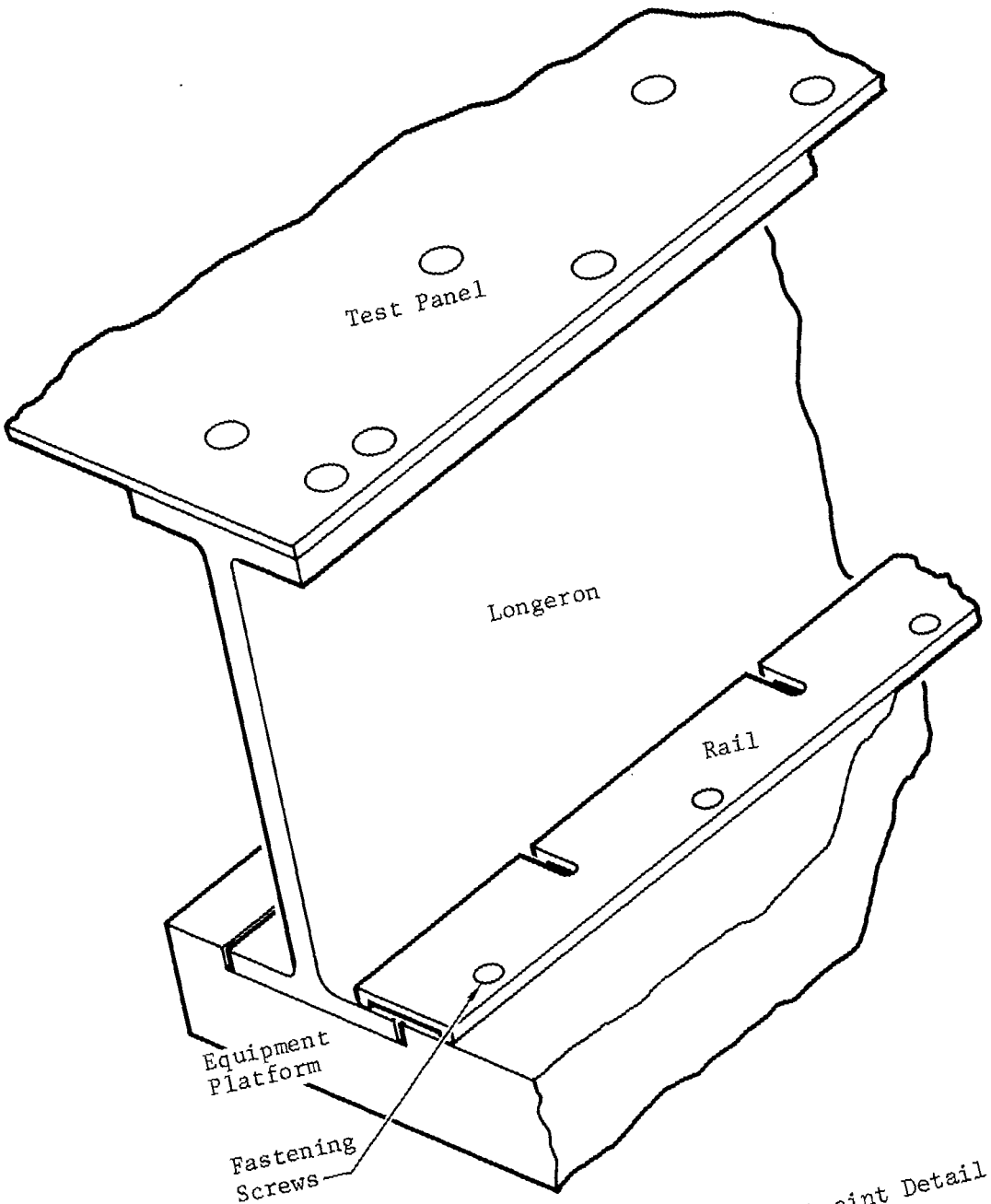

Figure 3 Sketch of Longeron Restraint Detail

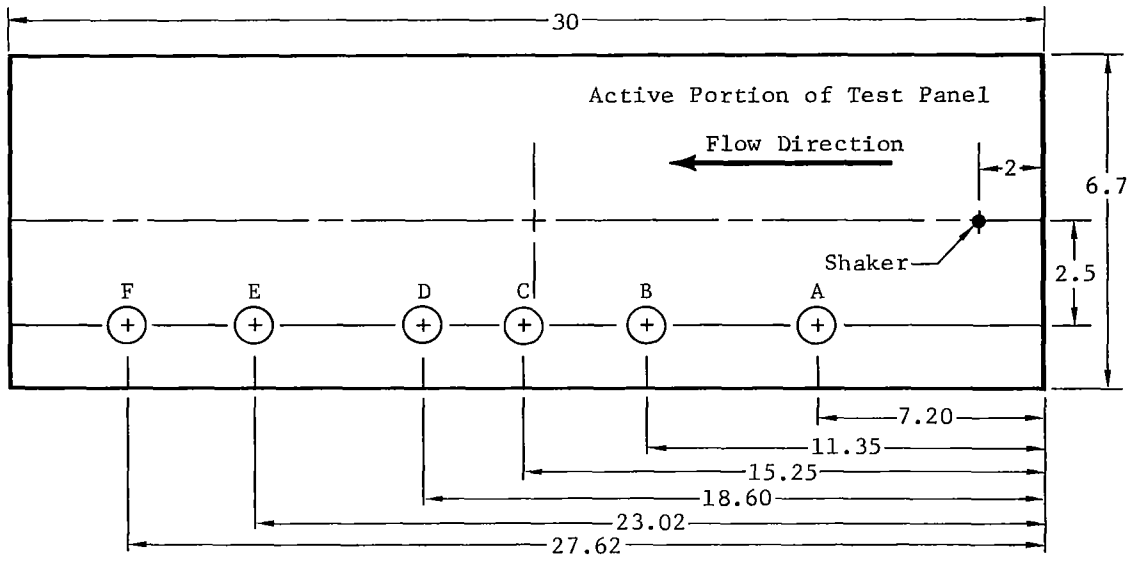

⊕ Wayne-Kerr Non-Contacting Displacement Probe, Type ME-1

Measurements in inches

Figure 4 Wayne-Kerr Probe and Shaker Locations

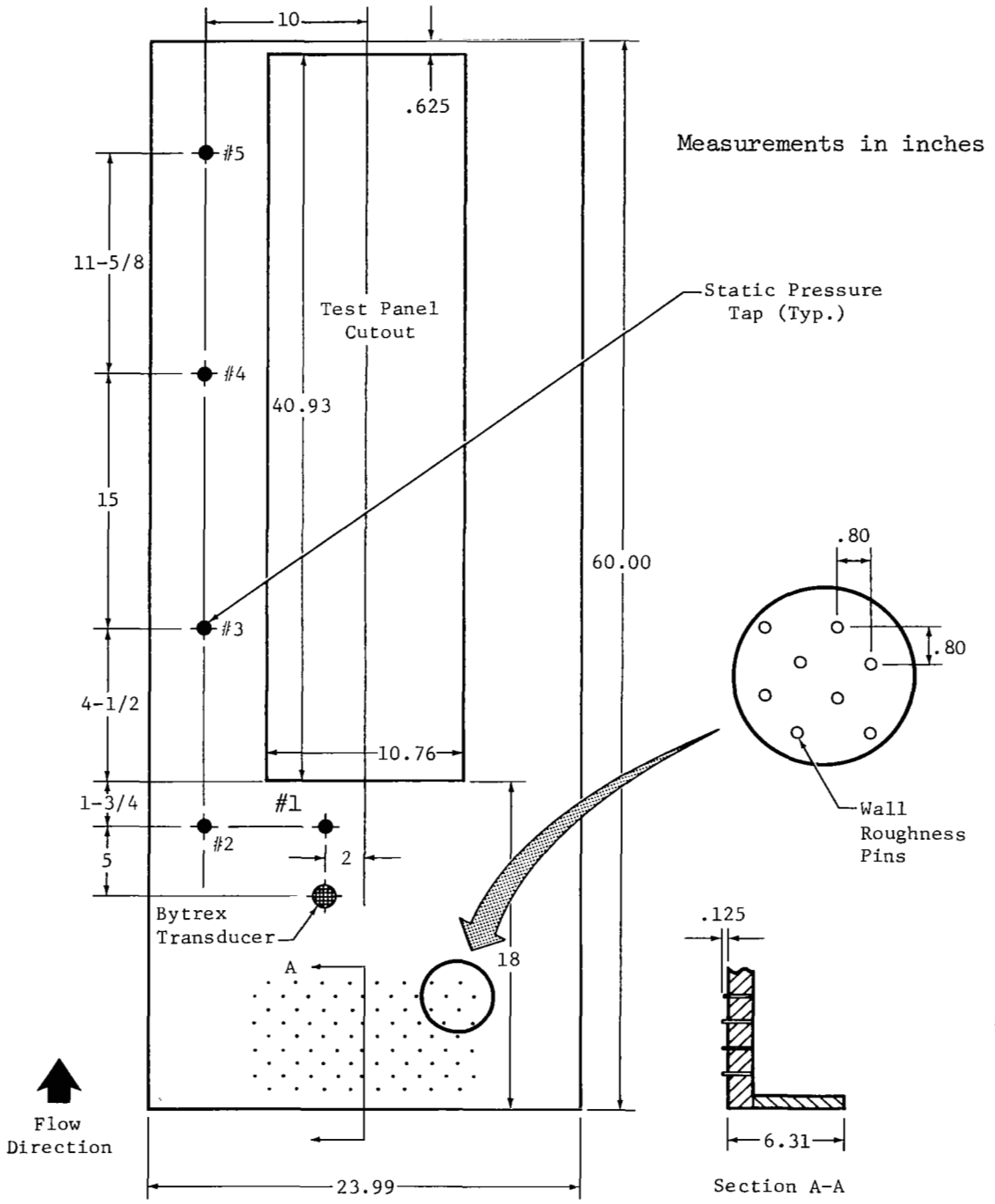

Figure 5 Wall Replacement

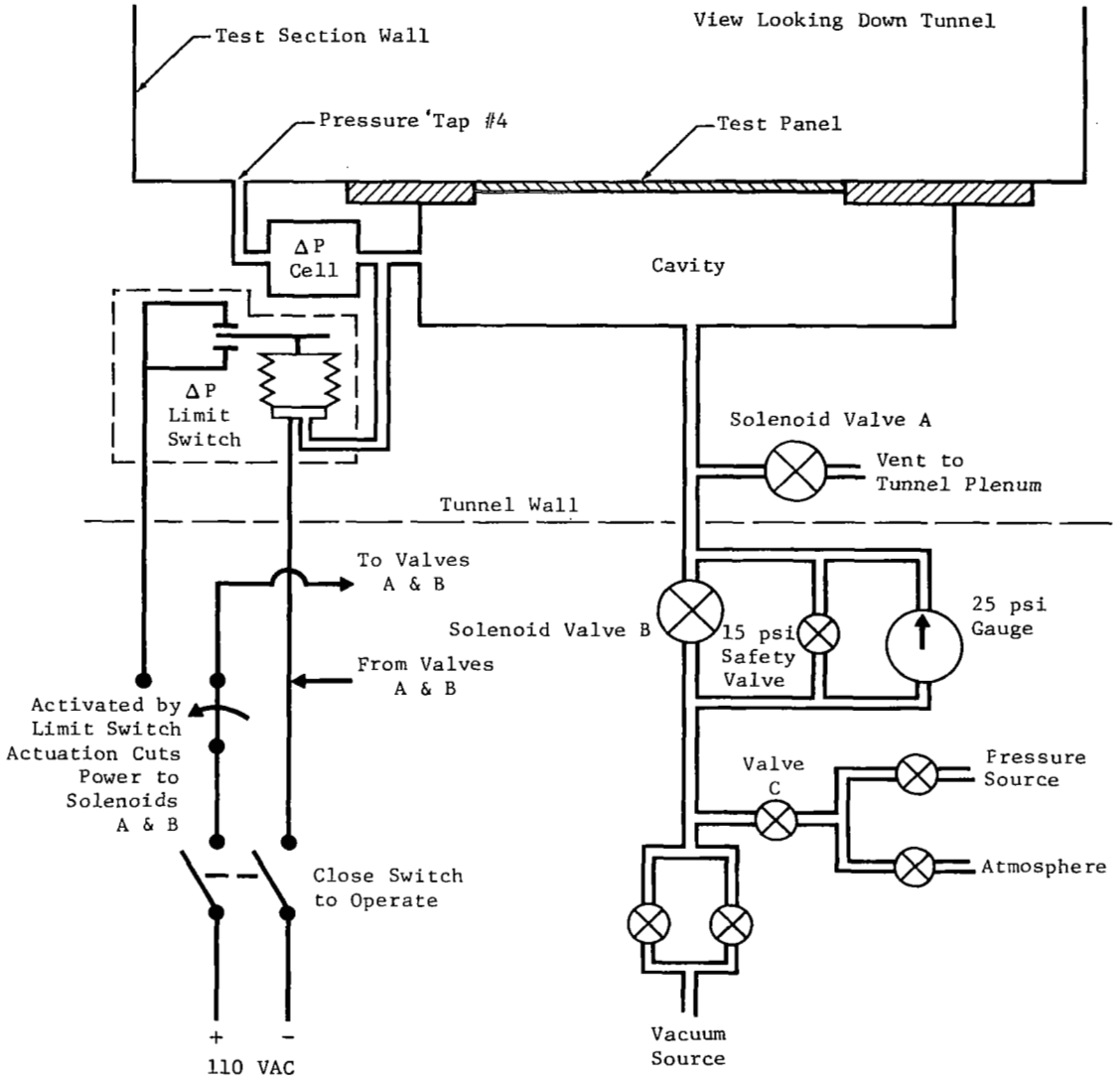

Figure 6 Schematic of Cavity Pressurization System

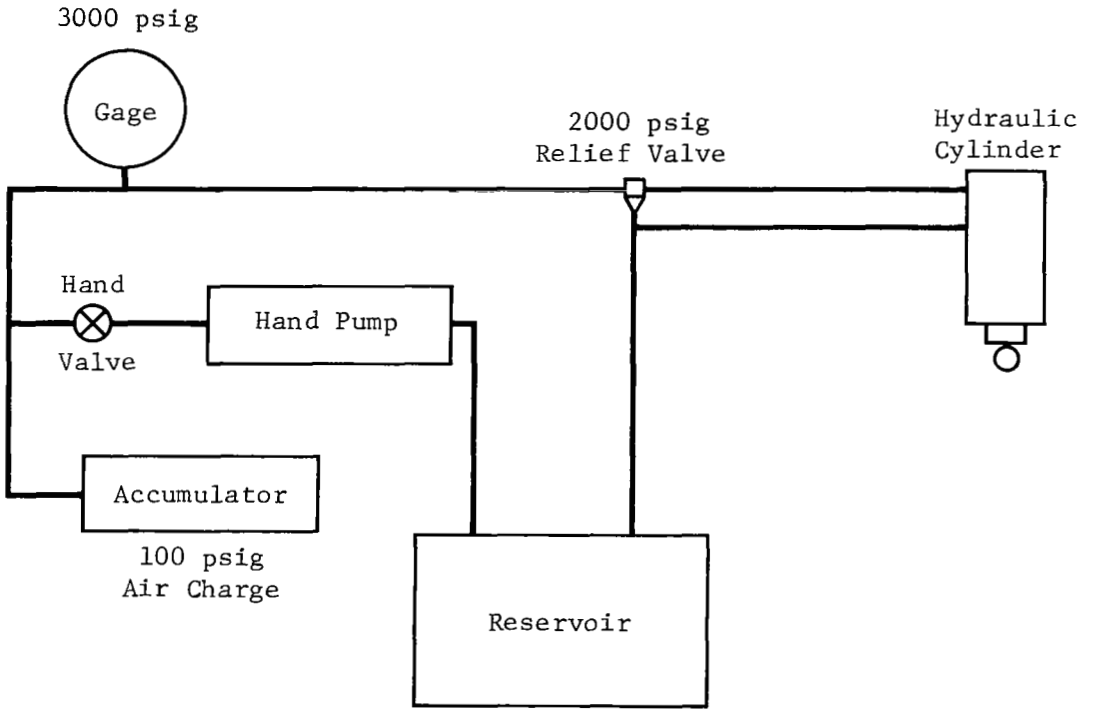

Figure 7 Schematic of Compressive Load System

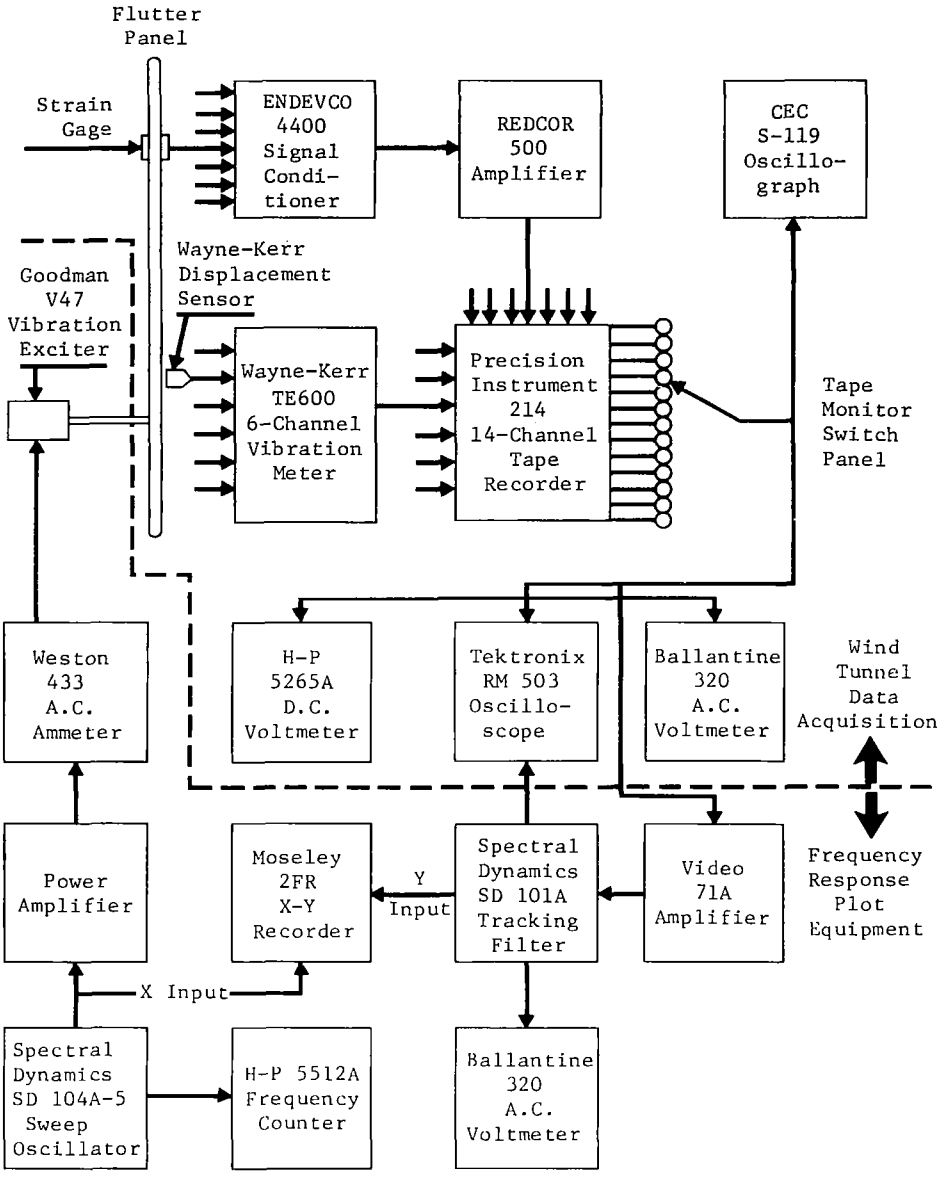

Instrumentation Specifications

Strain Gauges: Micro-Measurements 1/4" Foil Gauges
Type EA-06-250BF-350
Gauge Factor 2.105 $\pm$ 0.5%

Wayne-Kerr Vibration Meter: Main Unit - TE600, 6 Channel, Vibration Meter
Displacement Pickup - PCIB Holder with ME1 Head
Displacement Range 0.002 + 0.100 Inches
Frequency Accuracy $\pm$ 2%

Tape Recorder: Precision Instruments Corporation PS214
Flat Frequency Response to 1000 Hz
14 Channel Data Recorded at 3-3/4 ips

Figure 8 Data Acquisition Network and Instrumentation Specifications

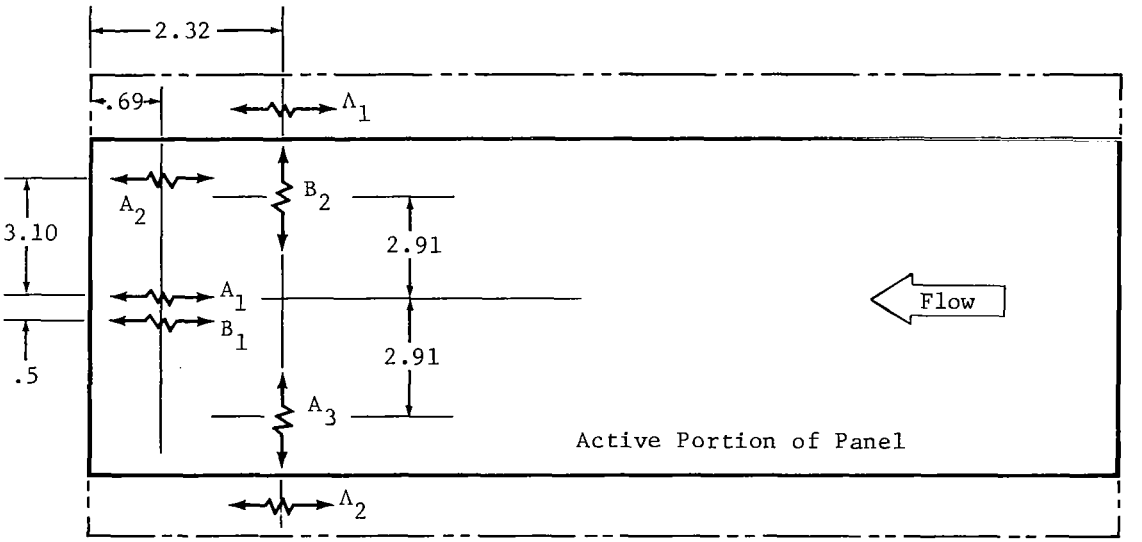

A - Panel Gauges Measuring Axial Strain
B - Panel Gauges Measuring Bending Strain
Λ - Longeron Gauges Measuring Axial Strain

Strain is Measured in the Directions Indicated

Figure 9 Location of Panel Strain Gauges

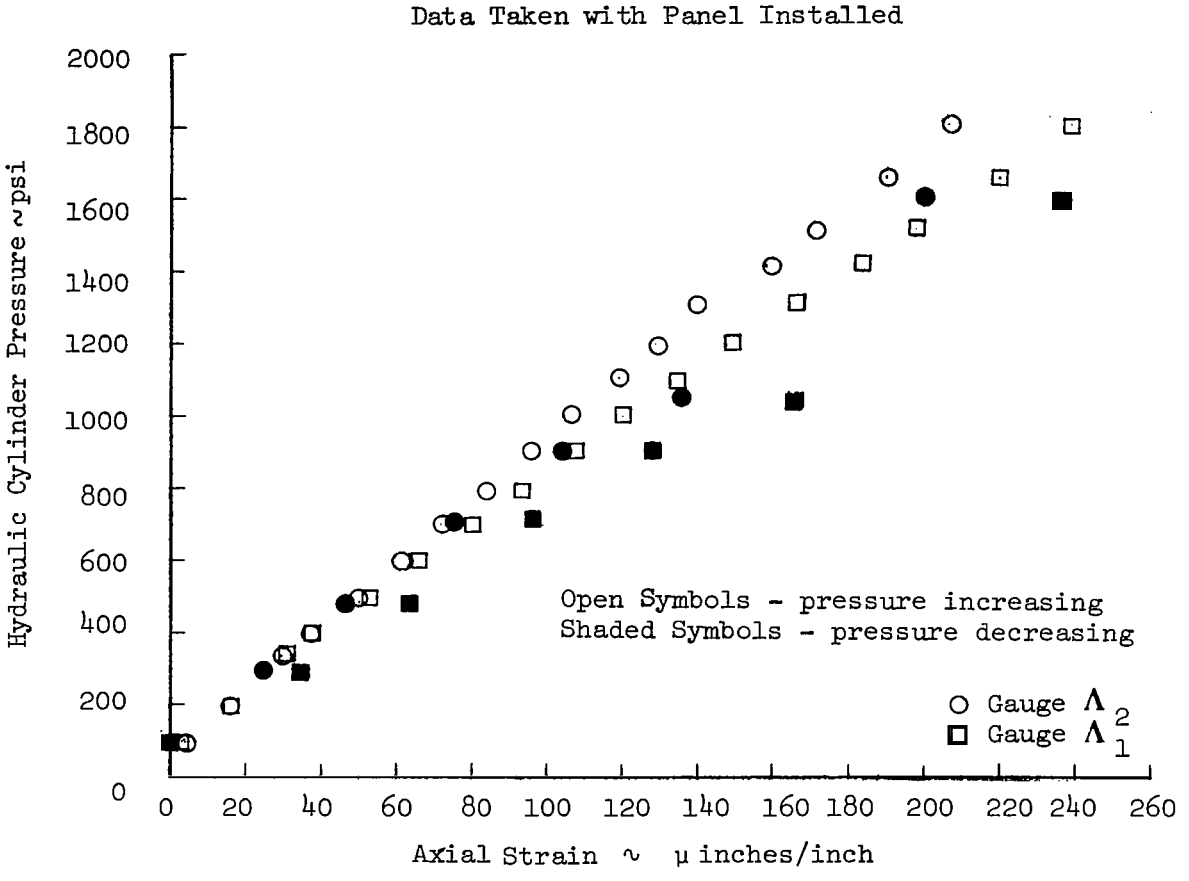

Figure 10 Longeron Strain Versus Hydraulic Cylinder Pressure Before Rail Screw Adjustment

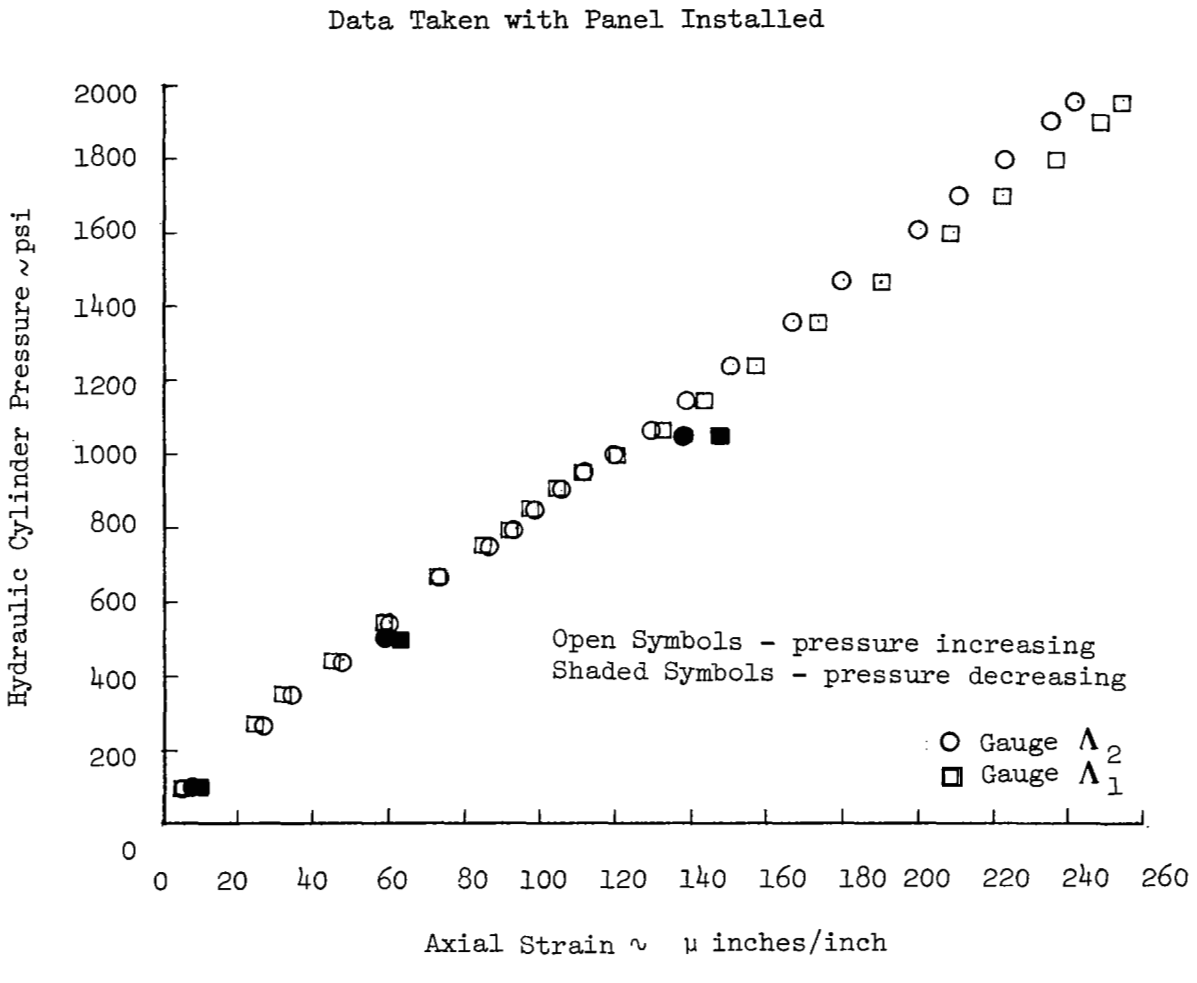

Figure 11 Longeron Strain Versus Hydraulic Cylinder Pressure After Rail Screw Adjustment

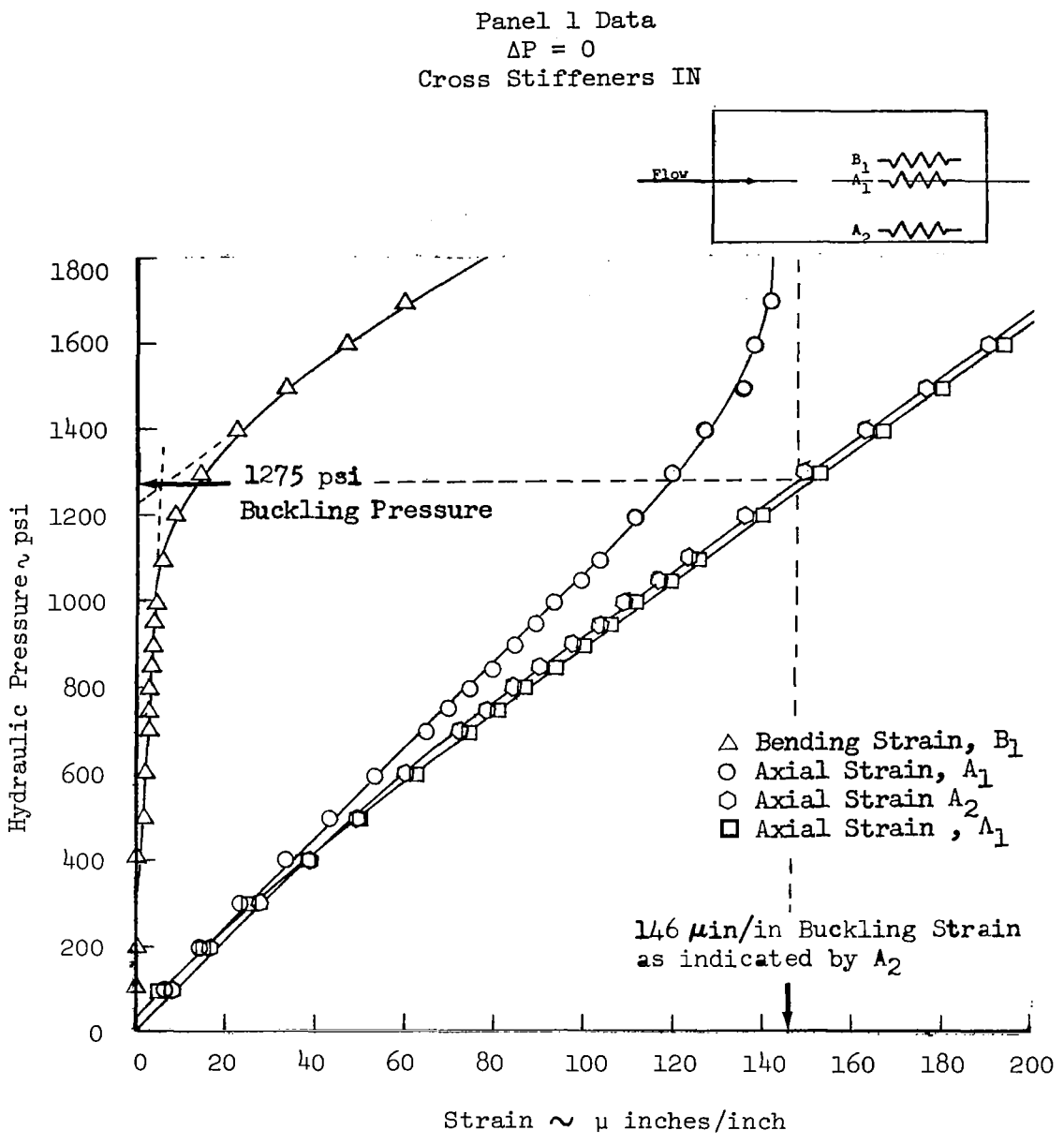

Figure 12 Determination of Panel Buckling Load

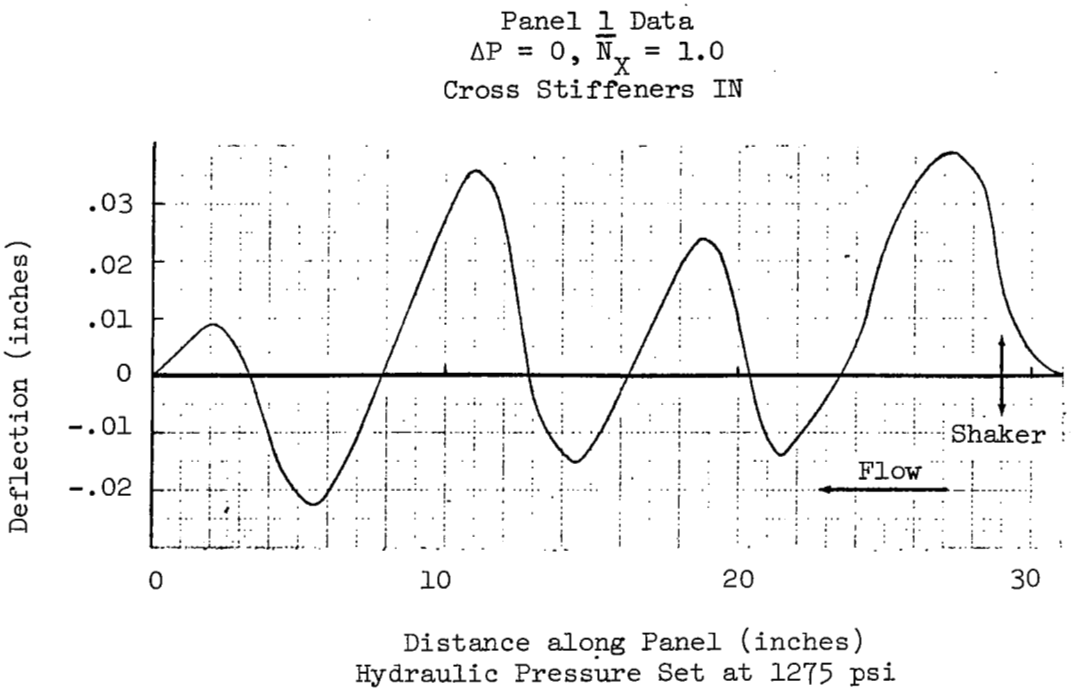

Figure 13 Test Panel Buckling Mode

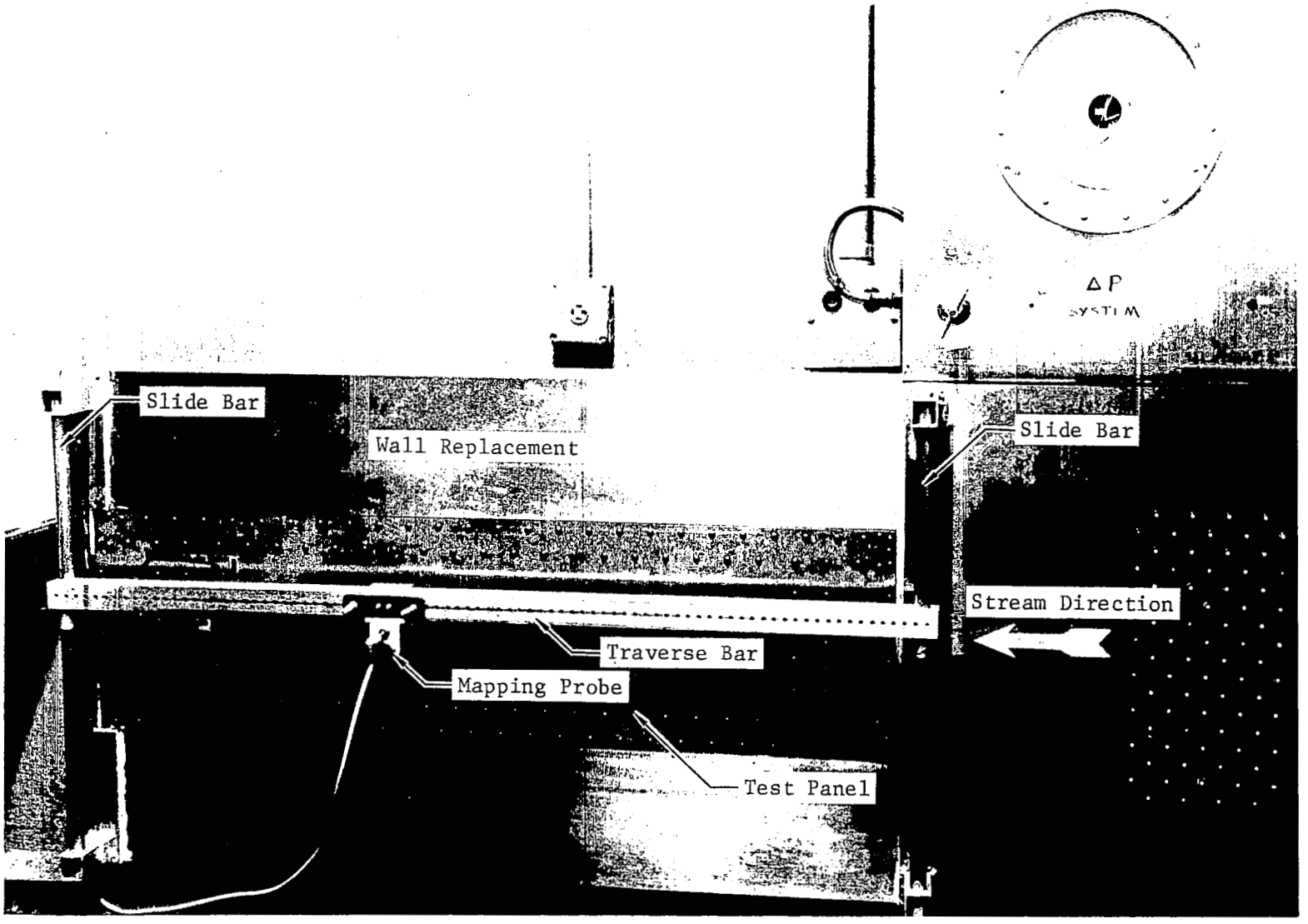

Figure 14 Modeshape Mapping Assembly

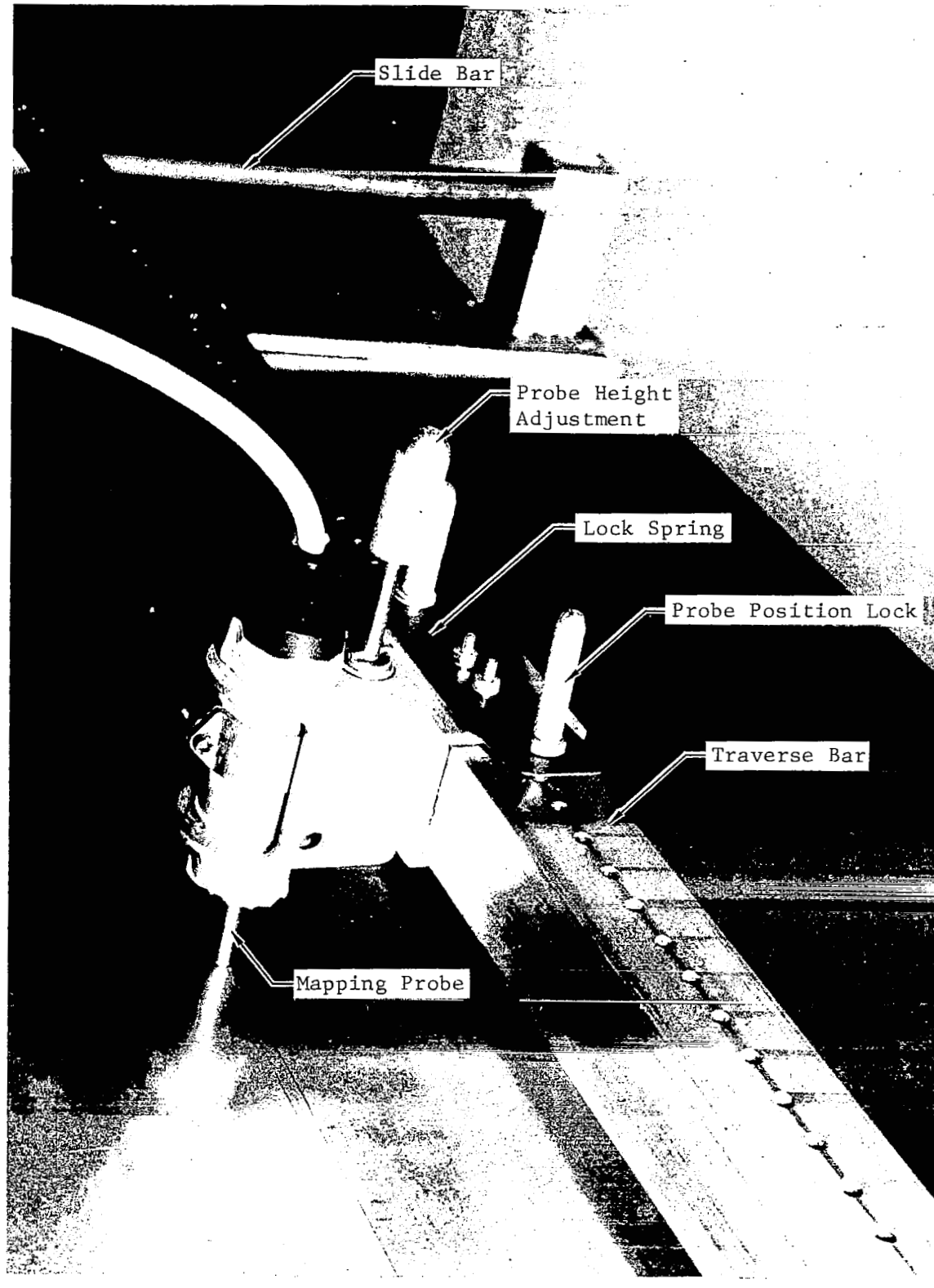

Figure 15 Mapping Probe and Traverse Assembly

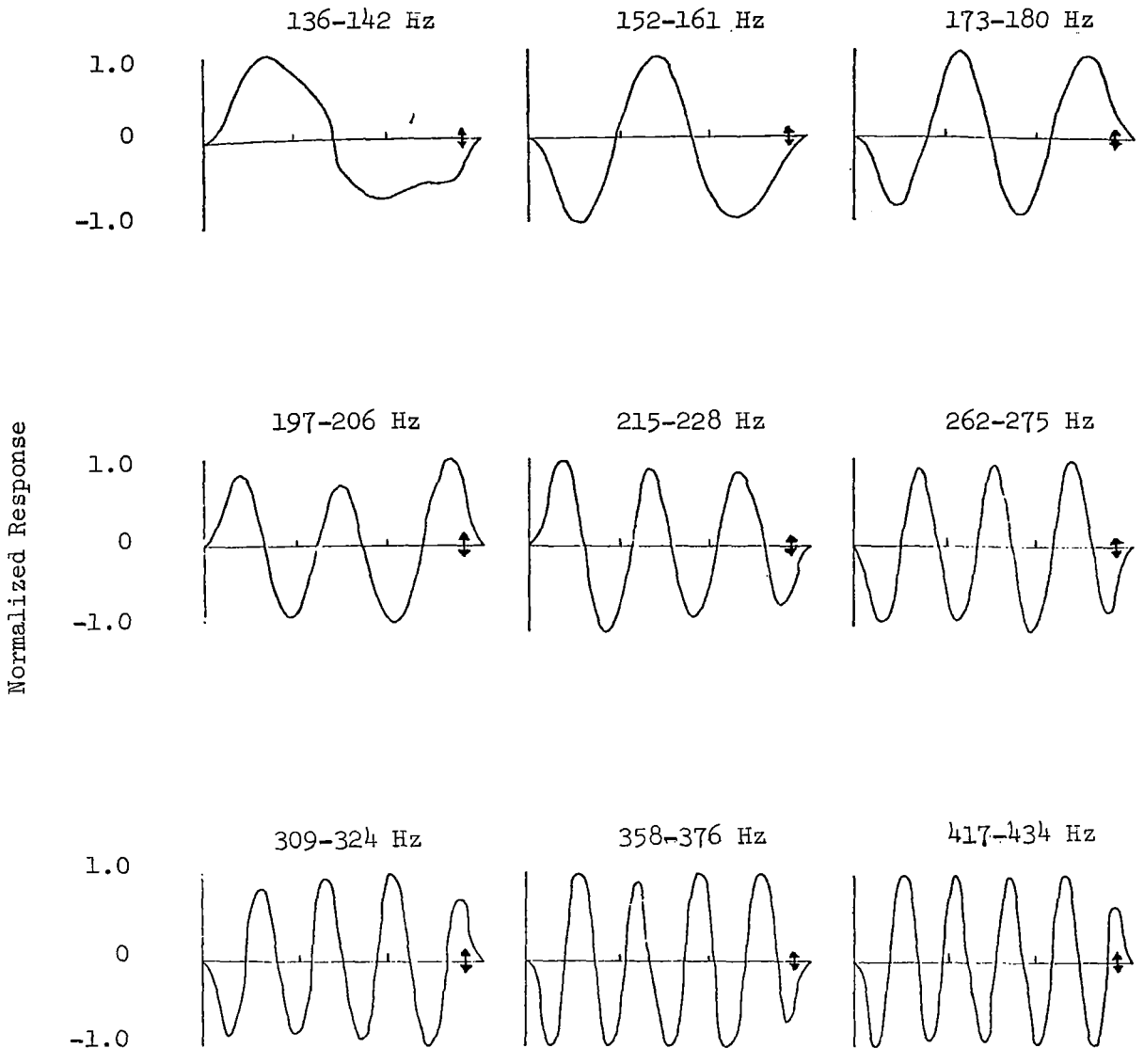

↕Shaker Position
Panel 1 Data
$\Delta P = 0$, $\bar{N}_x = 0$
Cross Stiffeners IN

Figure 16 Panel Vibration Mode Shapes

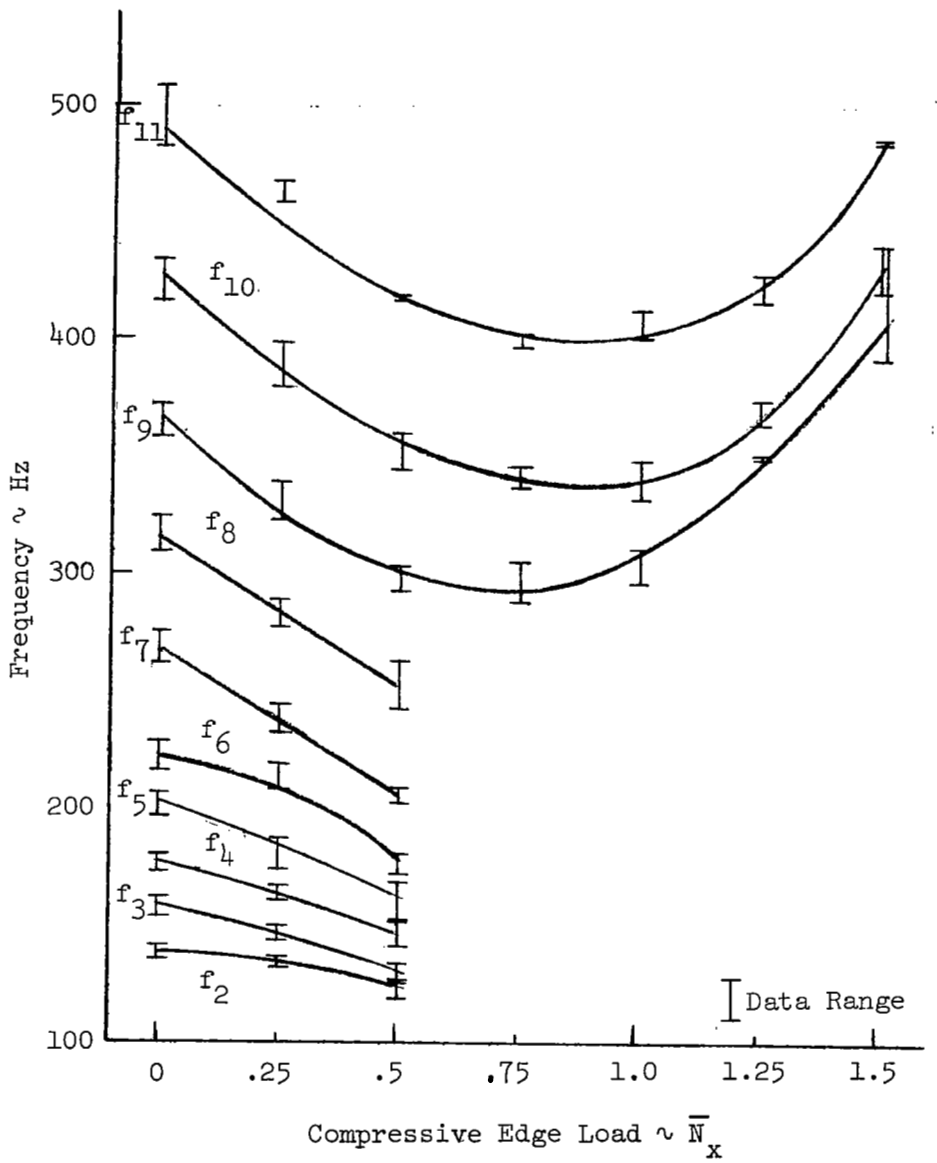

Figure 17 Effect of Compressive Edge Load on Panel Modal Frequencies

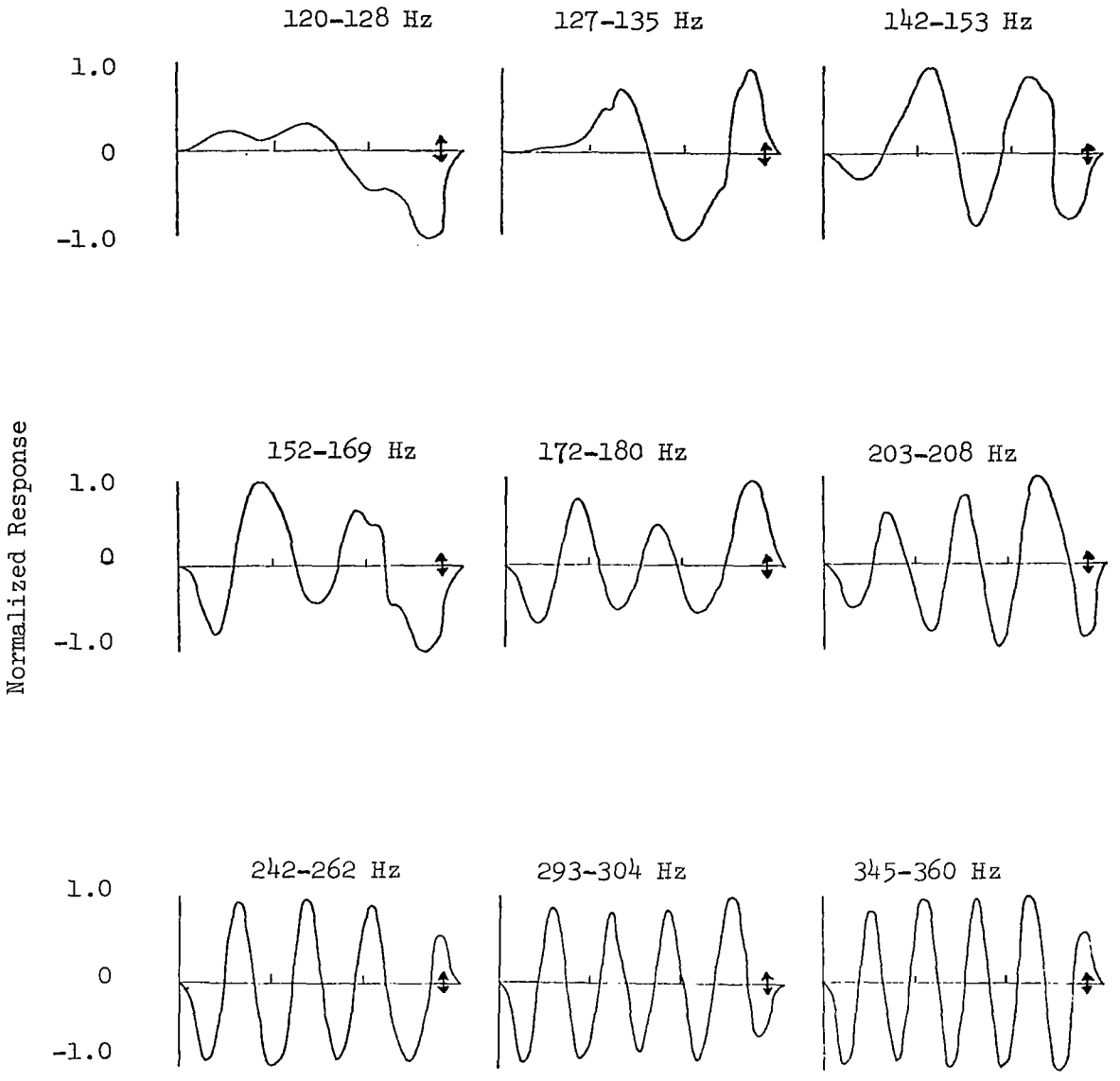

↕Shaker Position
Panel 1 Data
$\Delta P = 0$
Cross Stiffeners IN

Figure 18 Panel Vibration Mode Shapes, $\overline{N}_x = .5$

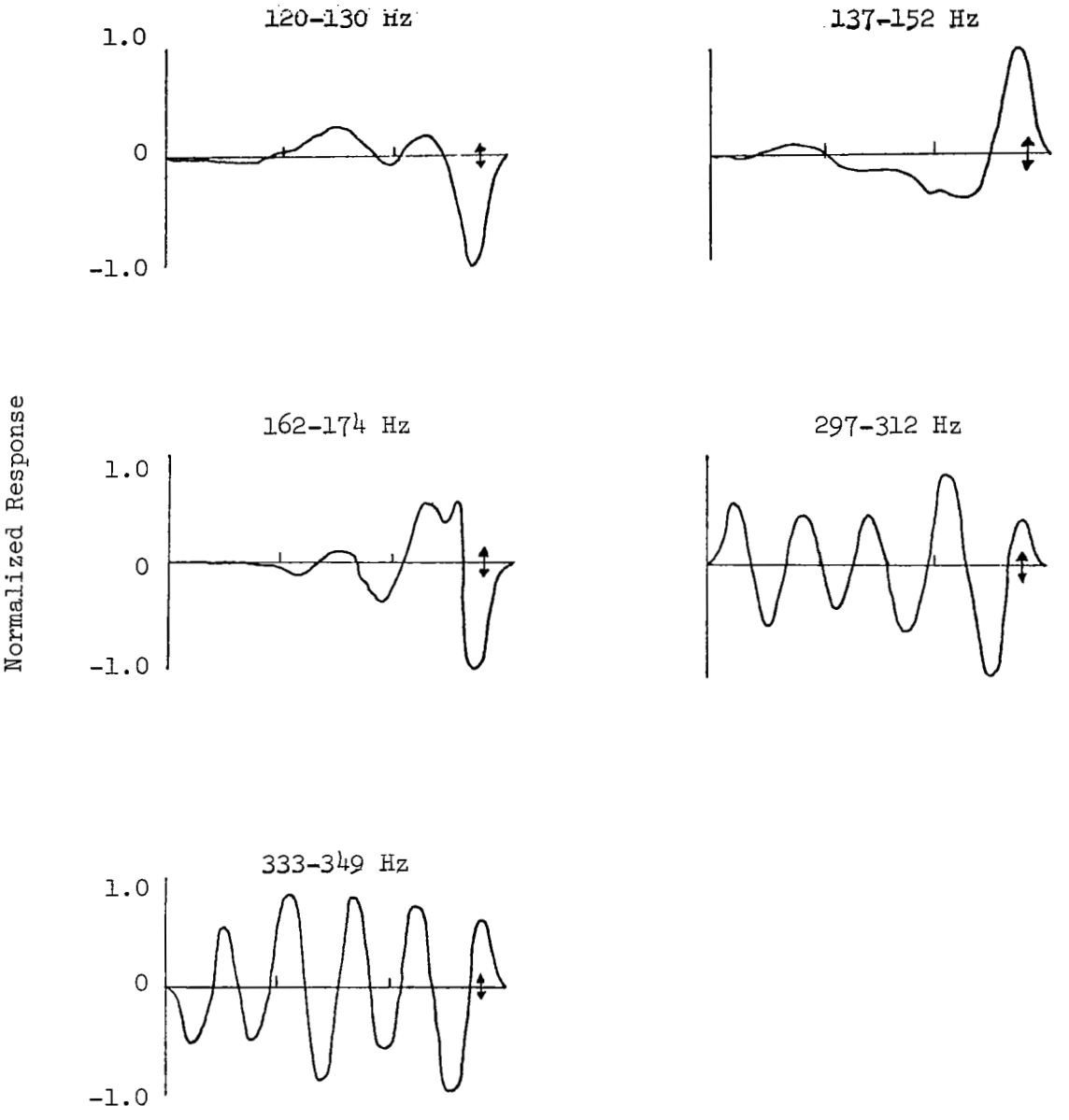

Figure 19 Panel Vibration Mode Shapes, $\overline{N}_X = 1.0$

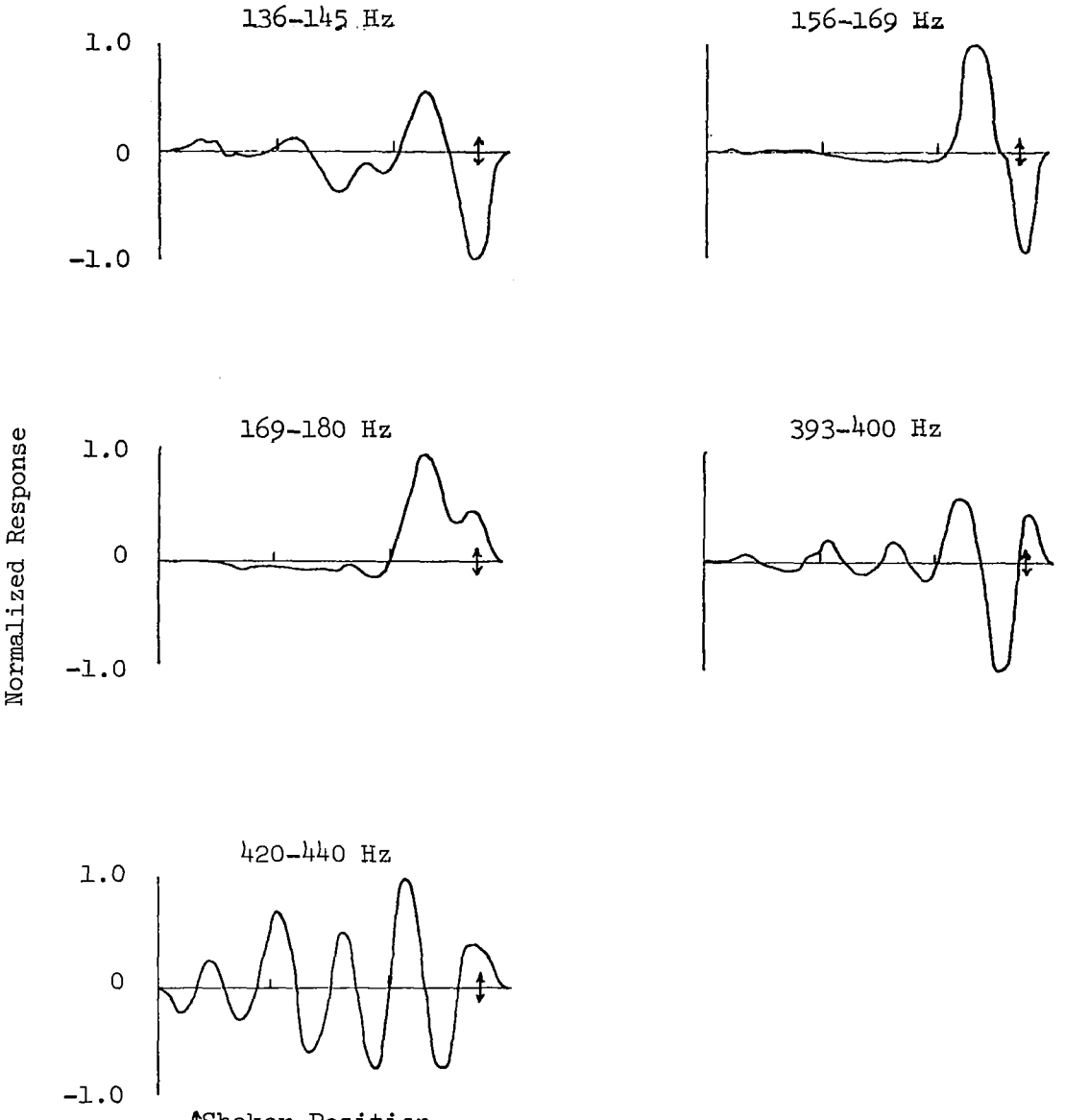

Panel 1 Data
$\Delta P = 0$
Cross Stiffeners IN

Figure 20 Panel Vibration Mode Shapes, $\overline{N}_x = 1.5$

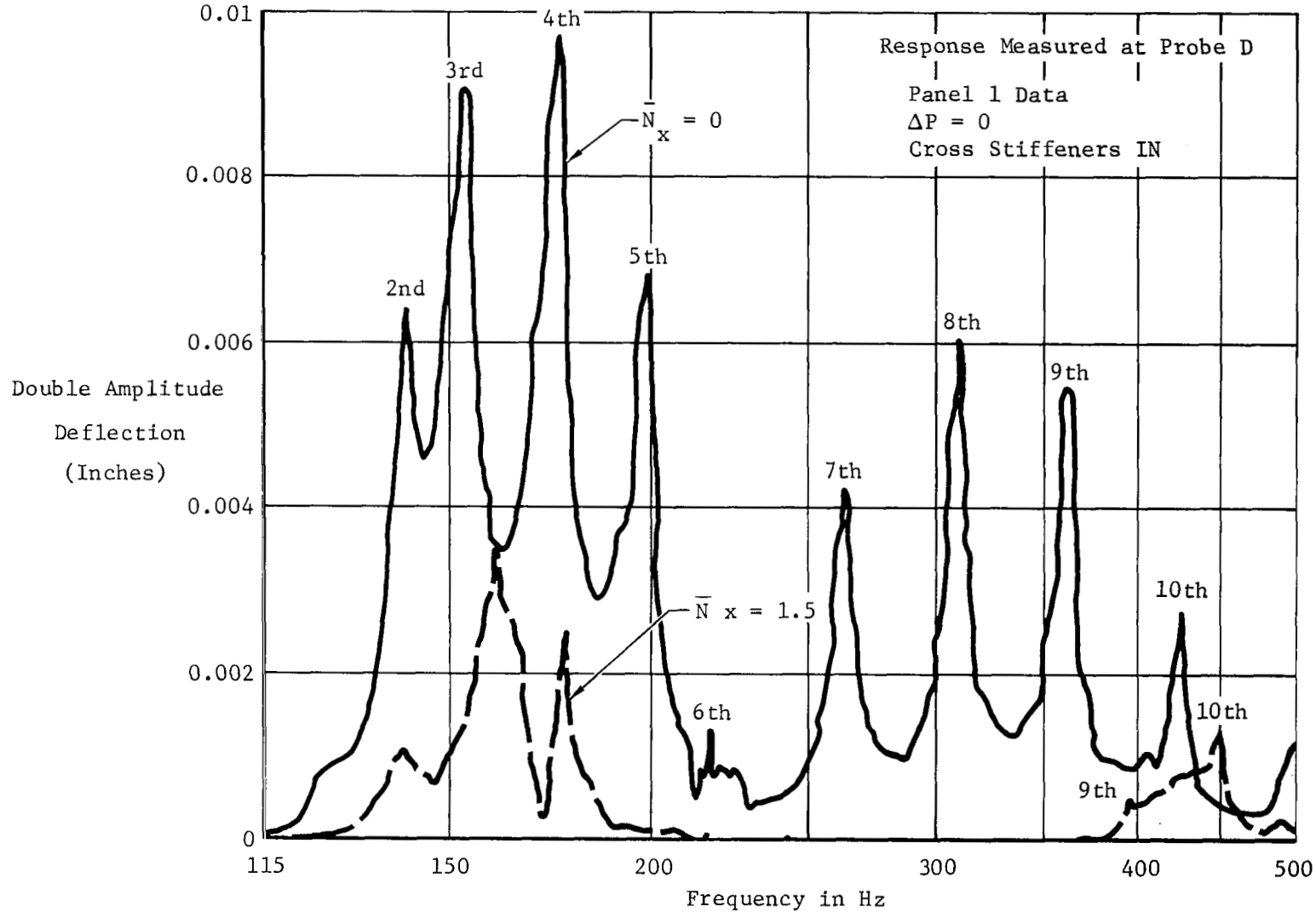

Figure 21 Panel Frequency Response Plots for $\bar{N}_x = 0$ and $\bar{N}_x = 1.5$

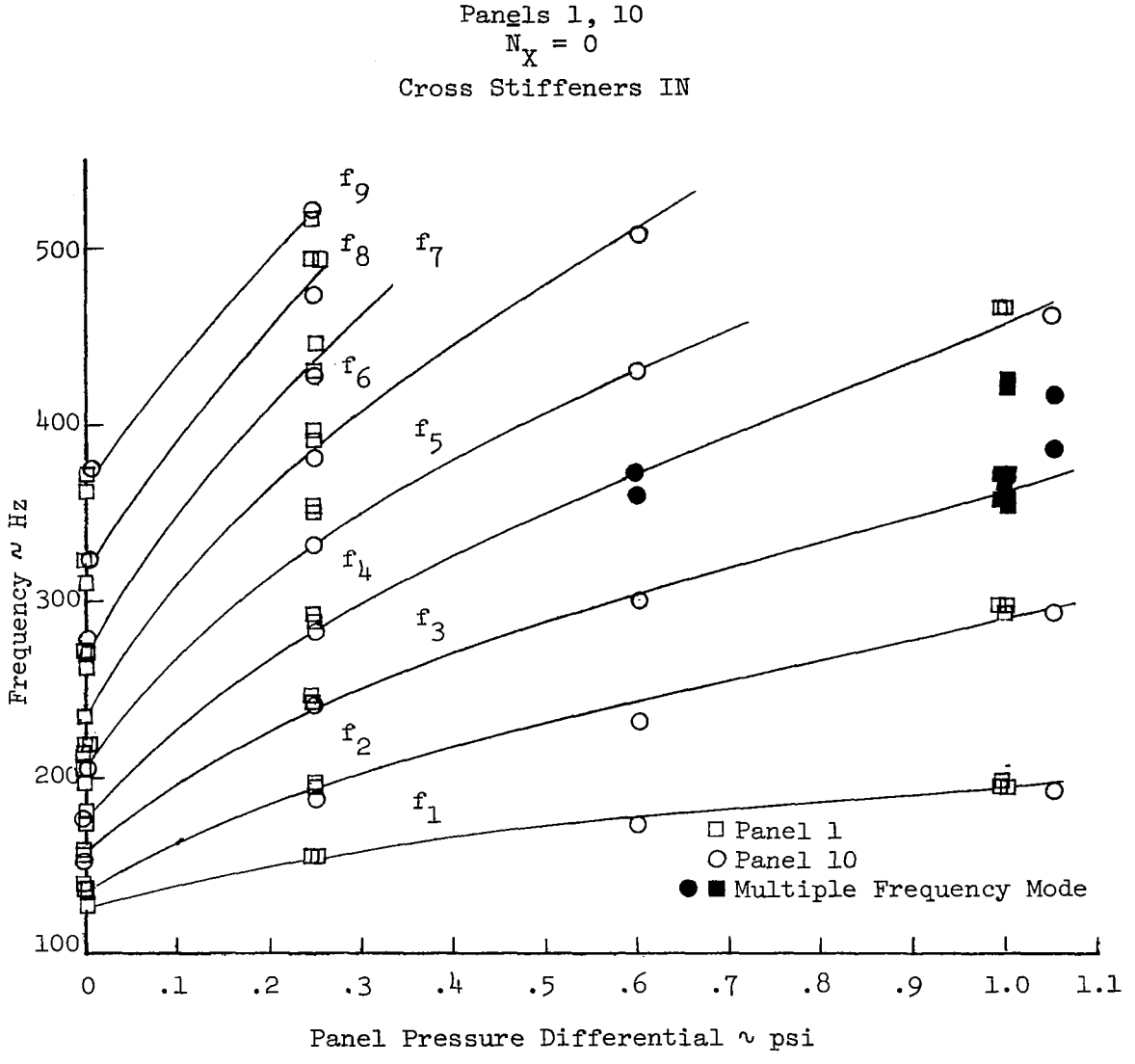

Figure 22 Effect of Static Pressure Differential on Panel Modal Frequencies

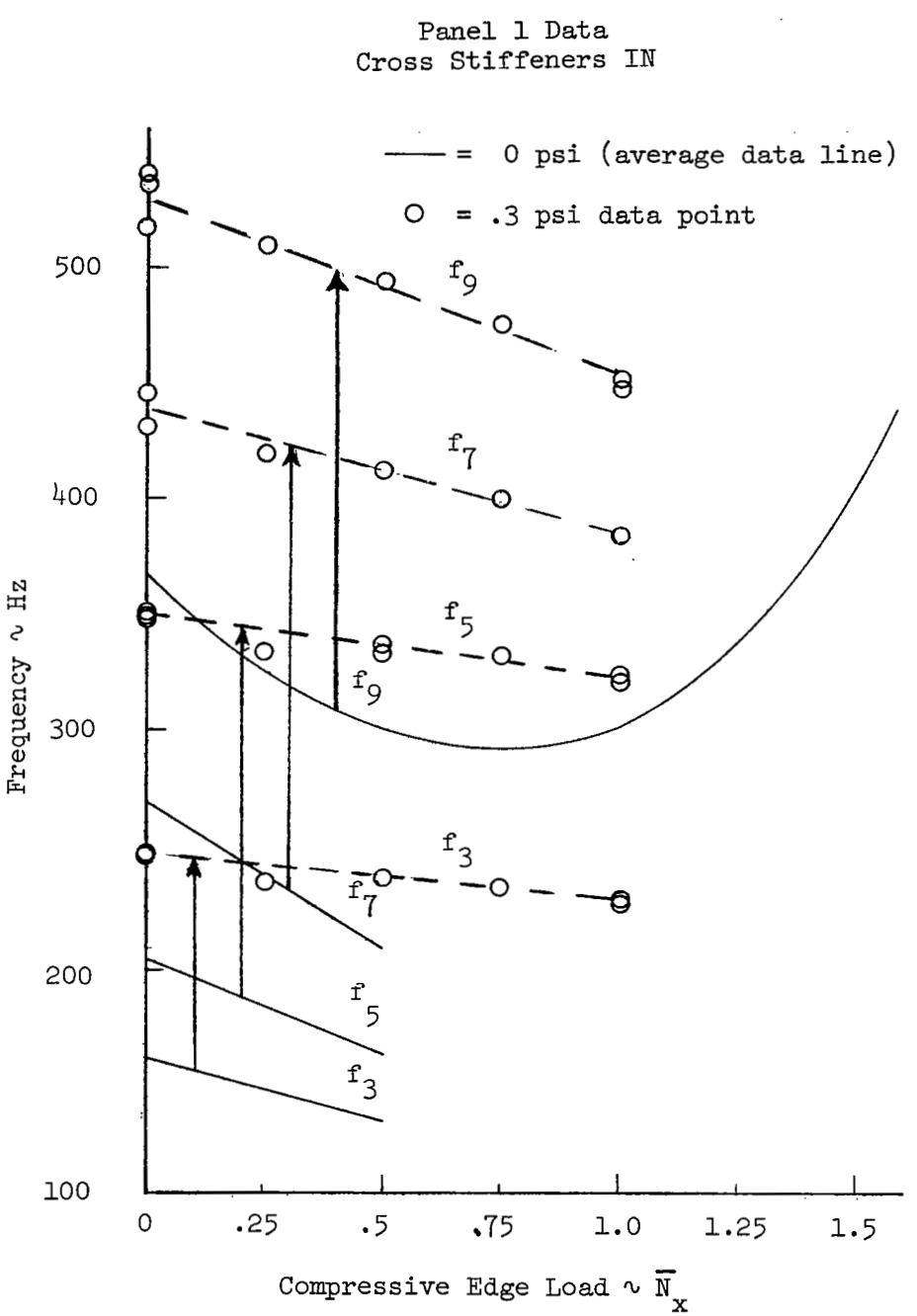

Figure 23 Effect of a Static Pressure-Compressive Edge Load Combination on Panel Frequencies

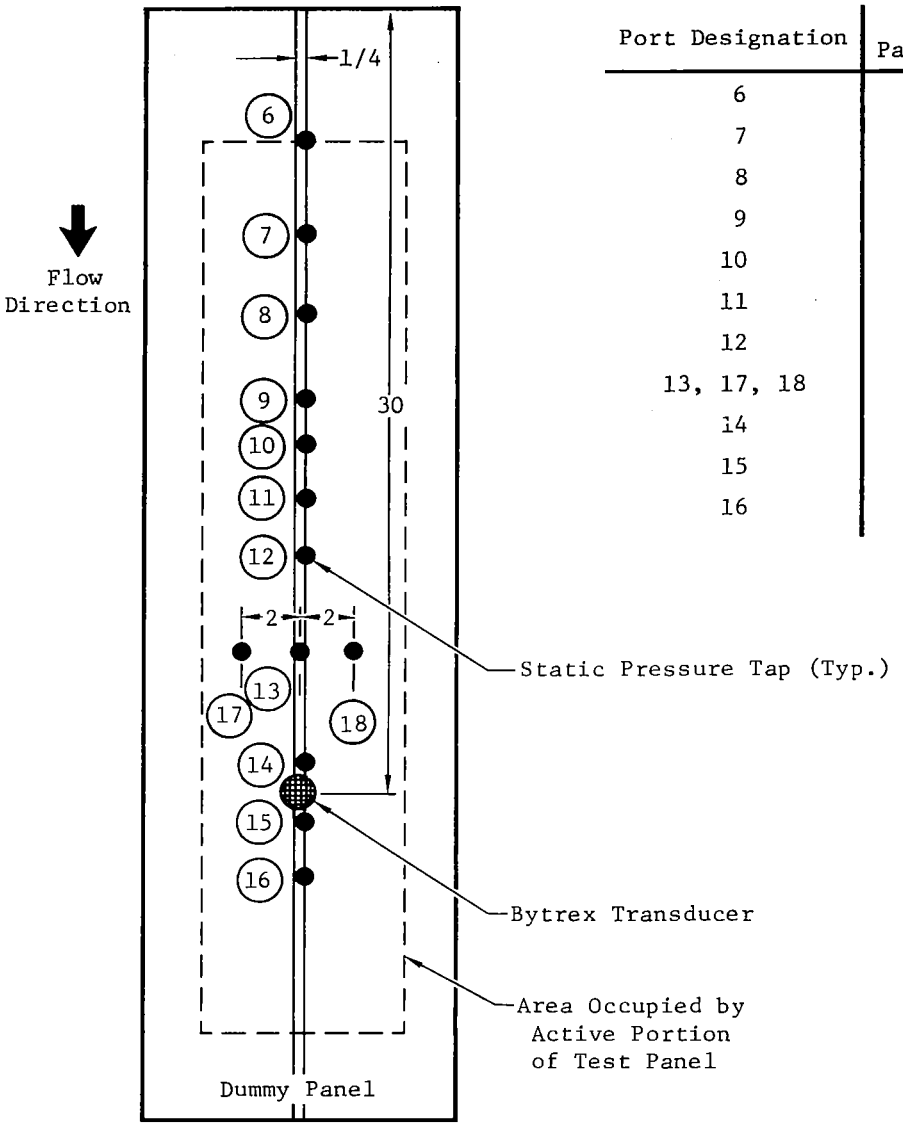

Port Designation	Distance from Panel L.E. (in.)
6	4.50
7	7.86
8	10.75
9	13.75
10	15.50
11	17.50
12	19.50
13, 17, 18	23.00
14	27.00
15	29.10
16	31.10

Figure 24 Locations of Static Pressure Ports on Rigid Panel

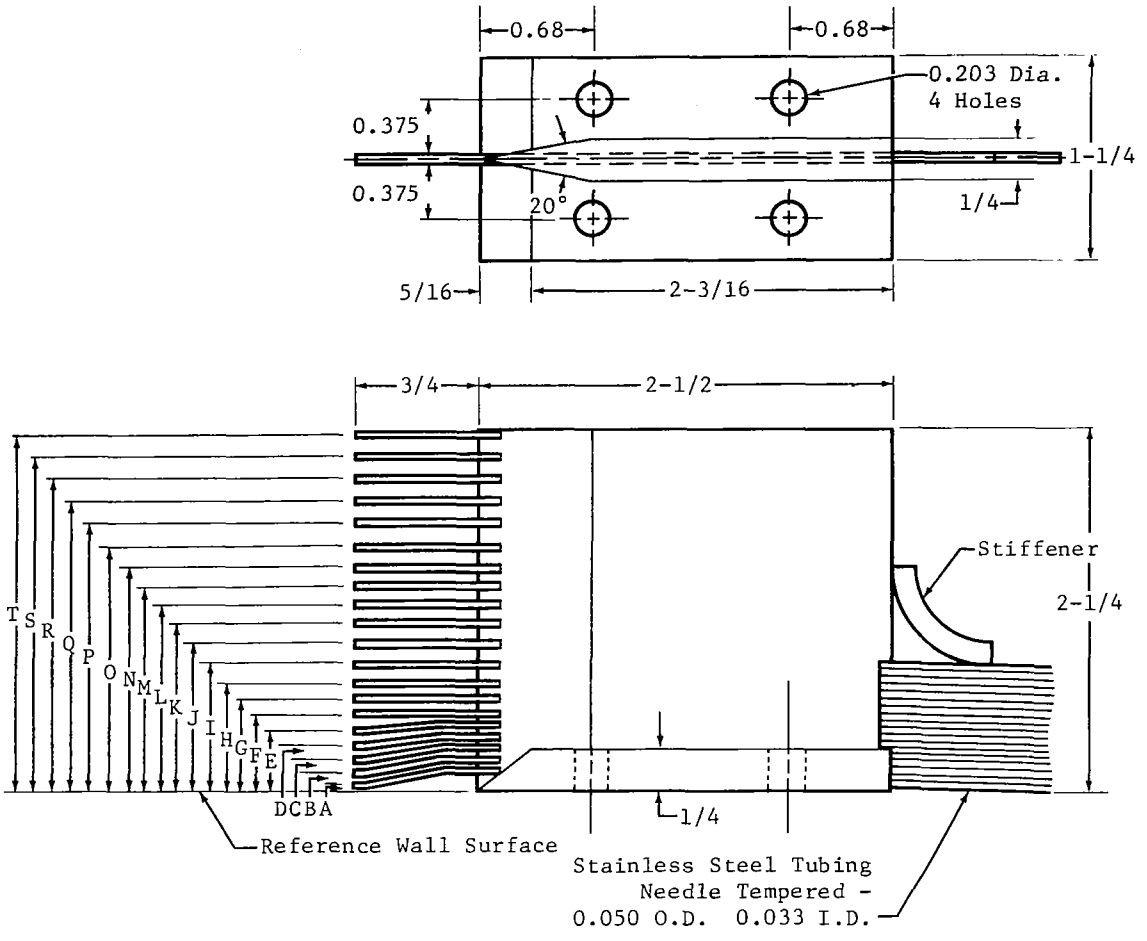

Note: All Dimensions in Inches

Probe Position	Dimensions to ℄ of Probe	Probe Position	Dimensions to ℄ of Probe
A	0.025	K	0.800
B	0.080	L	0.940
C	0.140	M	1.100
D	0.200	N	1.260
E	0.265	O	1.420
F	0.335	P	1.580
G	0.410	Q	1.740
H	0.490	R	1.900
I	0.580	S	2.060
J	0.680	T	2.220

Figure 25 Boundary Layer Rake

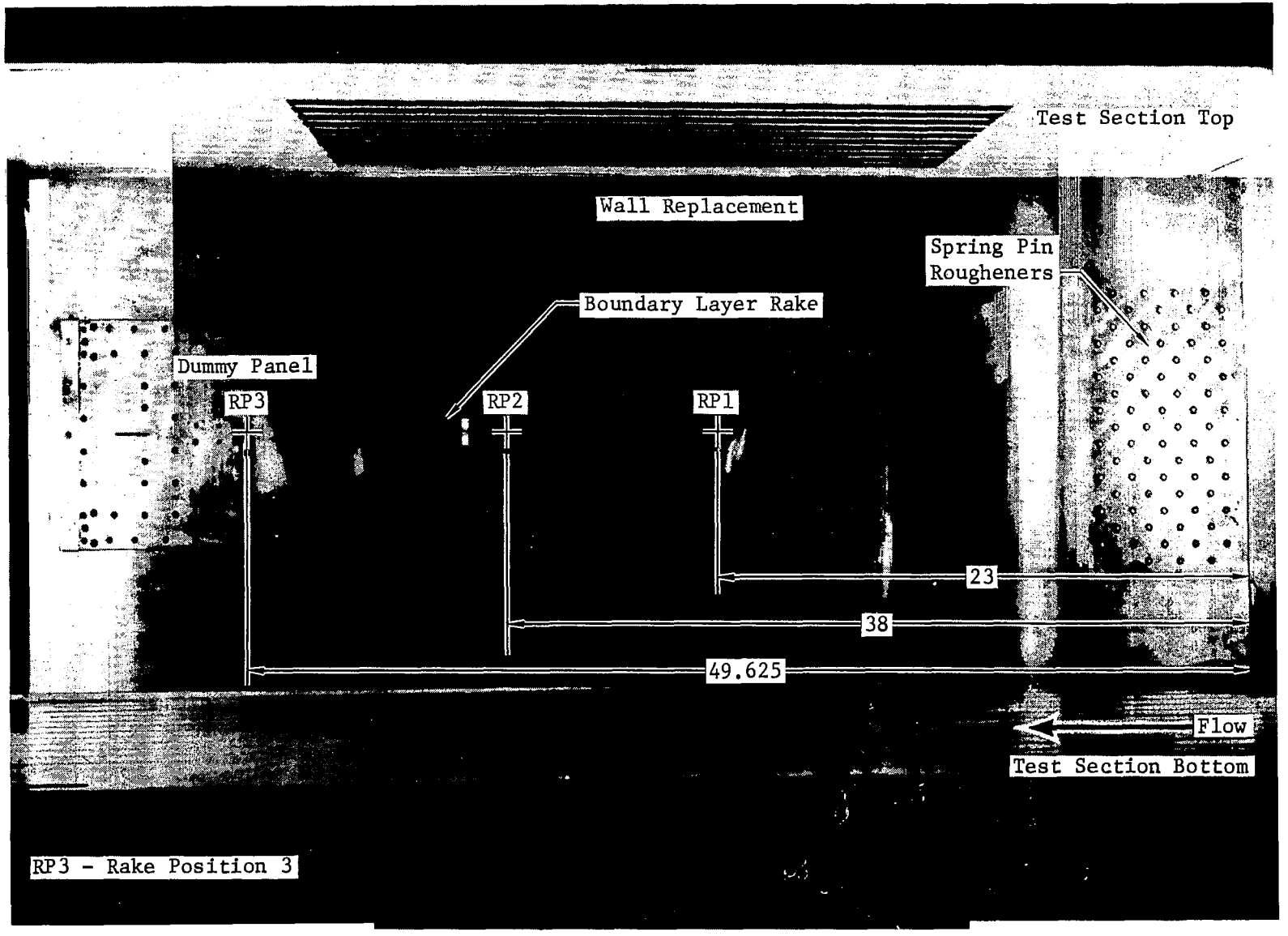

Figure 26 Boundary Layer Rake Positions

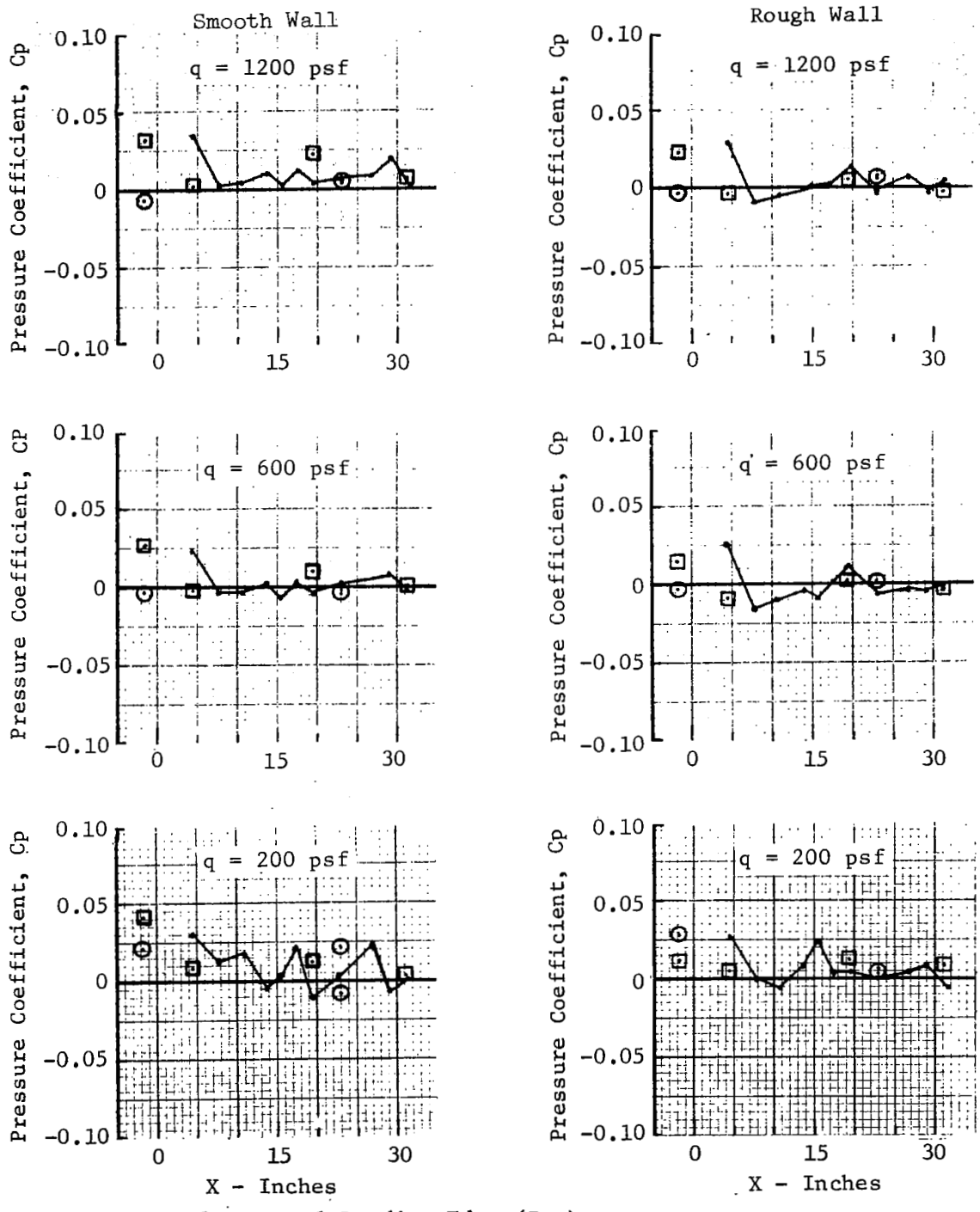

X = Distance from Panel Leading Edge (In.)

$$C_P = \frac{P_{Static} - P_{Static\ (Plenum)}}{q_{Freestream}}$$

——— 1/4" Off Centerline

⊙ 2" Off Centerline

⊡ 10" Off Centerline

Figure 27 Static Pressure Distribution over Test Panel at Mach 1.3

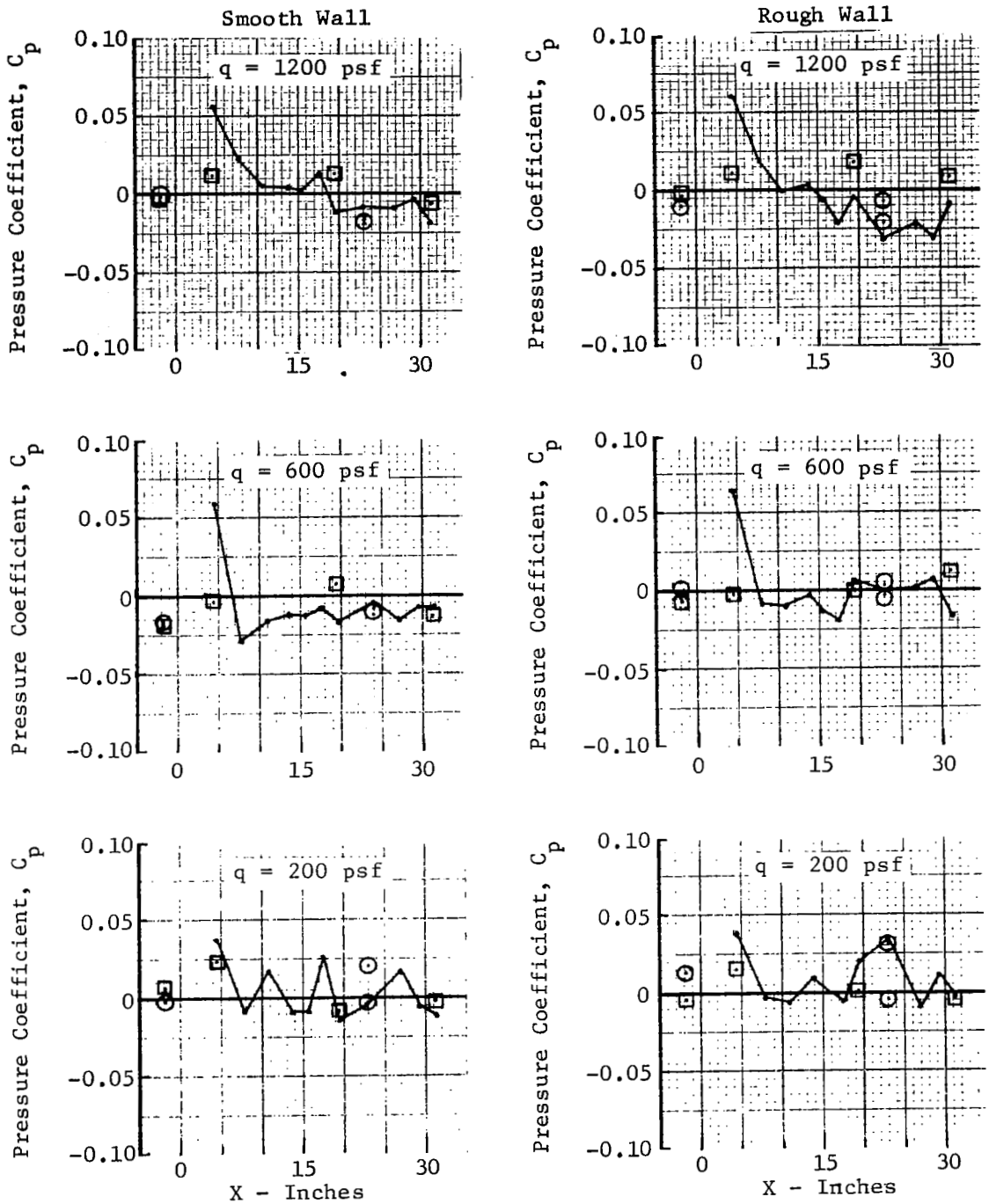

X = Distance from Panel Leading Edge (In.)

$$C_p = \frac{P_{Static} - P_{Static\ (Plenum)}}{q_{Freestream}}$$

— 1/4" Off Centerline

⊙ 2" Off Centerline

⊡ 10" Off Centerline

Figure 28 Static Pressure Distribution over Test Panel at Mach 1.4

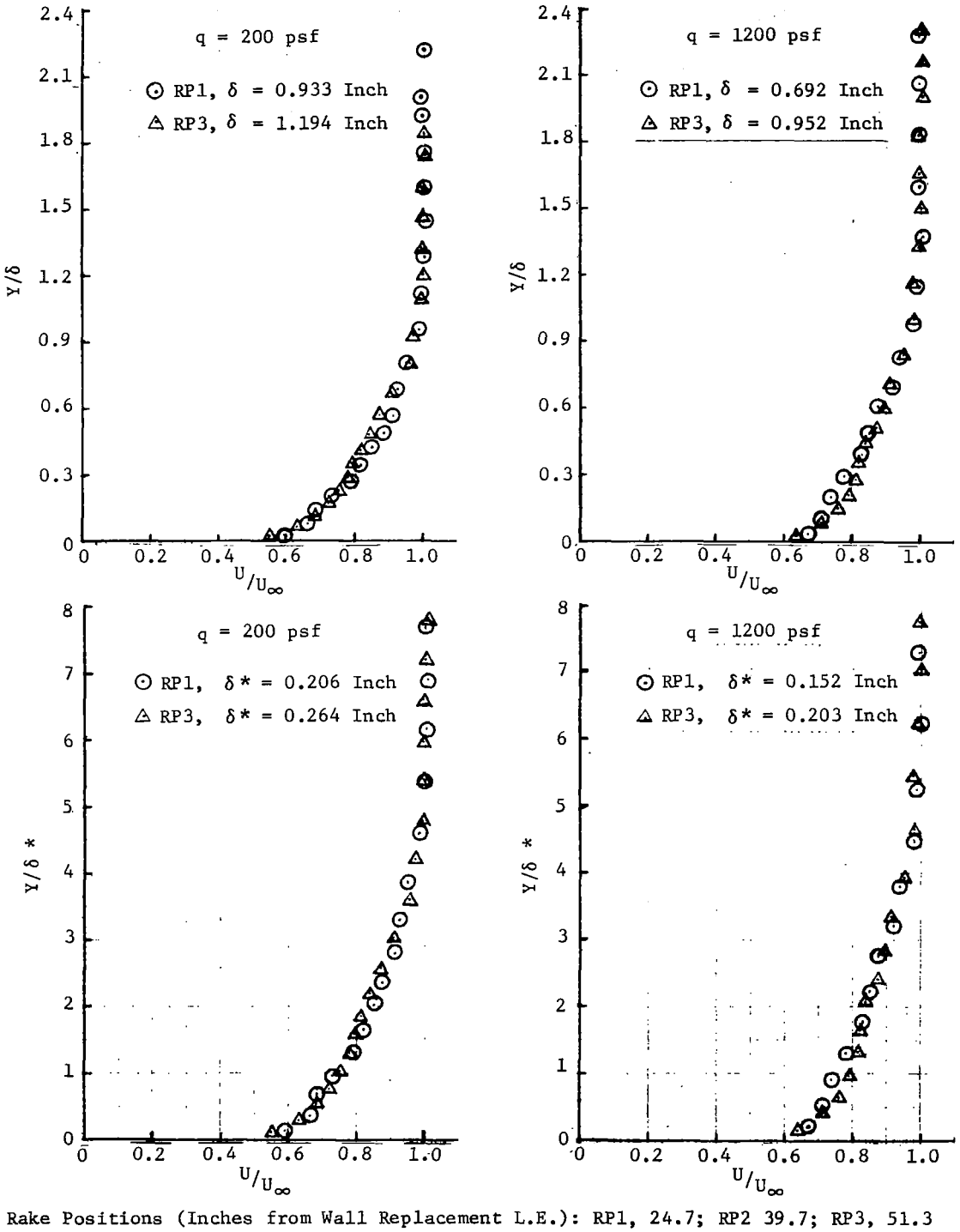

Rake Positions (Inches from Wall Replacement L.E.): RP1, 24.7; RP2 39.7; RP3, 51.3

δ^* = Boundary Layer Displacement Thickness $\quad$ δ = Boundary Layer Thickness

Y = Height Above Wall $\quad$ U_∞ = Free Stream Velocity

Figure 29 Experimental Smooth Wall Boundary Layer Profiles at Mach 1.4

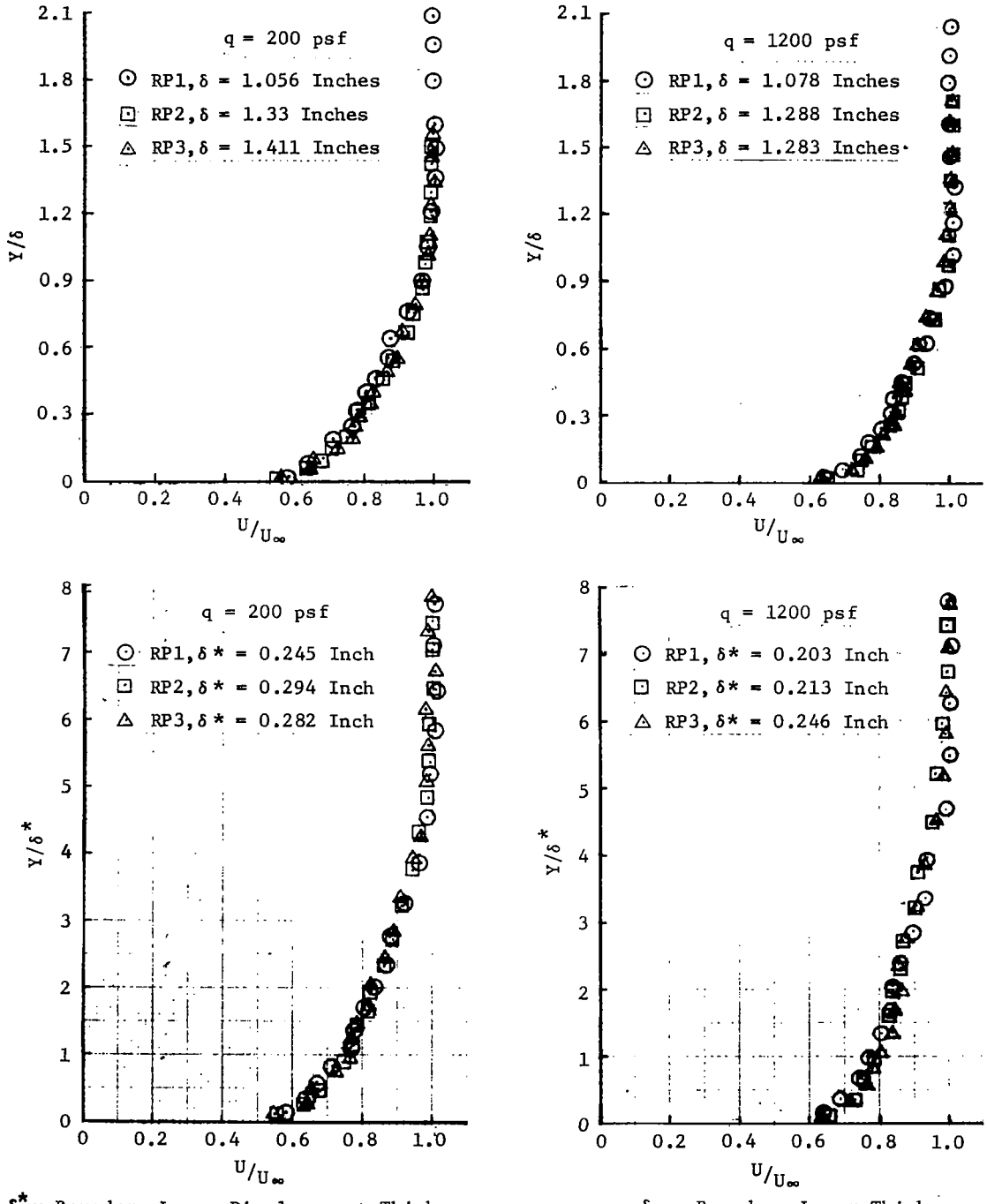

δ^* = Boundary Layer Displacement Thickness

Y = Height Above Wall

δ = Boundary Layer Thickness

U_∞ = Freestream Velocity

Figure 30 Experimental Rough Wall Boundary Layer Profiles at Mach 1.4

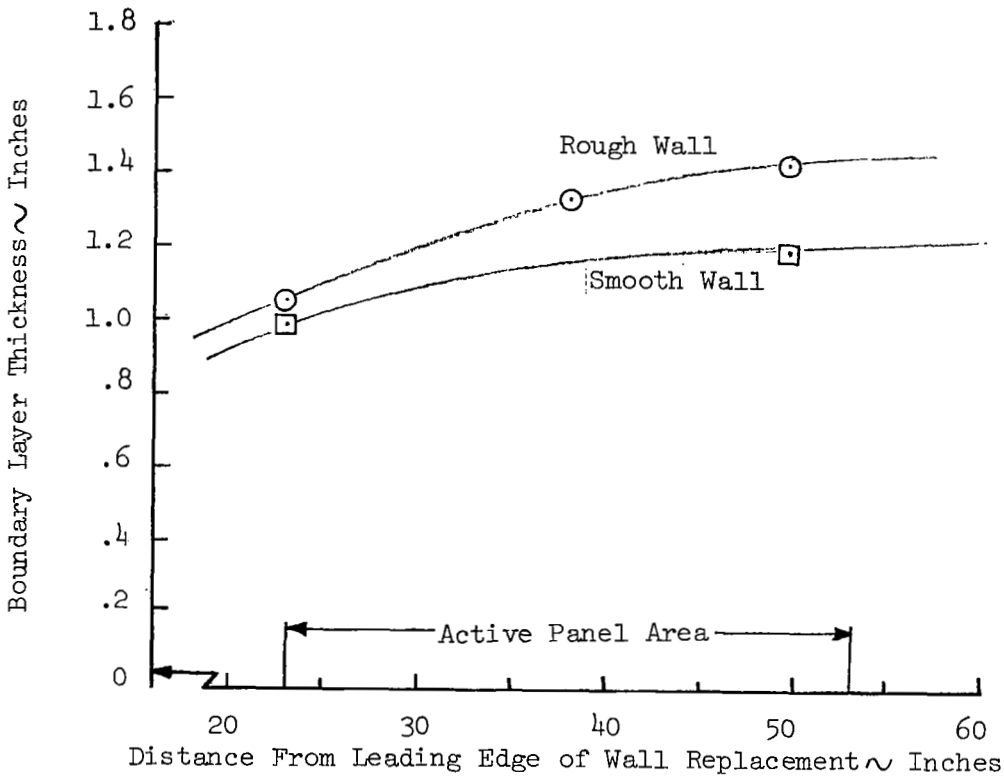

Note: Boundary layer thickness is measured at $U/U_\infty = .98$

Figure 31 Boundary Layer Thickness over the Test Panel at Mach 1.4 and q = 200 psf

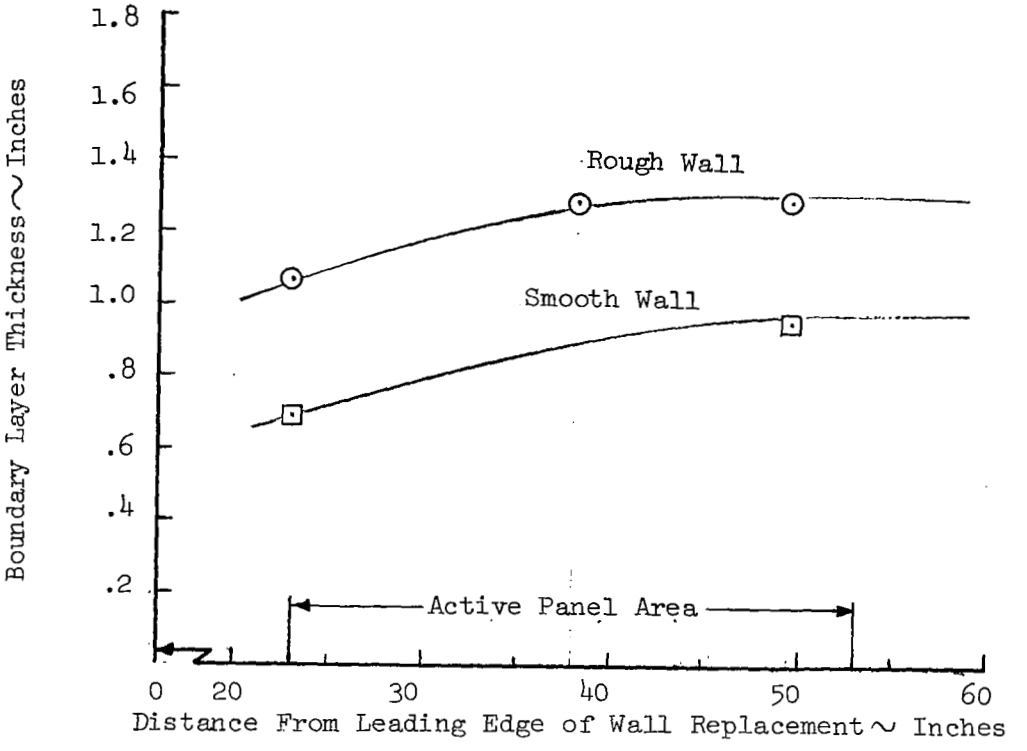

Note: Boundary layer thickness is measured at U/U_{∞} = .98

Figure 32 Boundary Layer Thickness Over the Test Panel at Mach 1.4 and q = 1200 psf

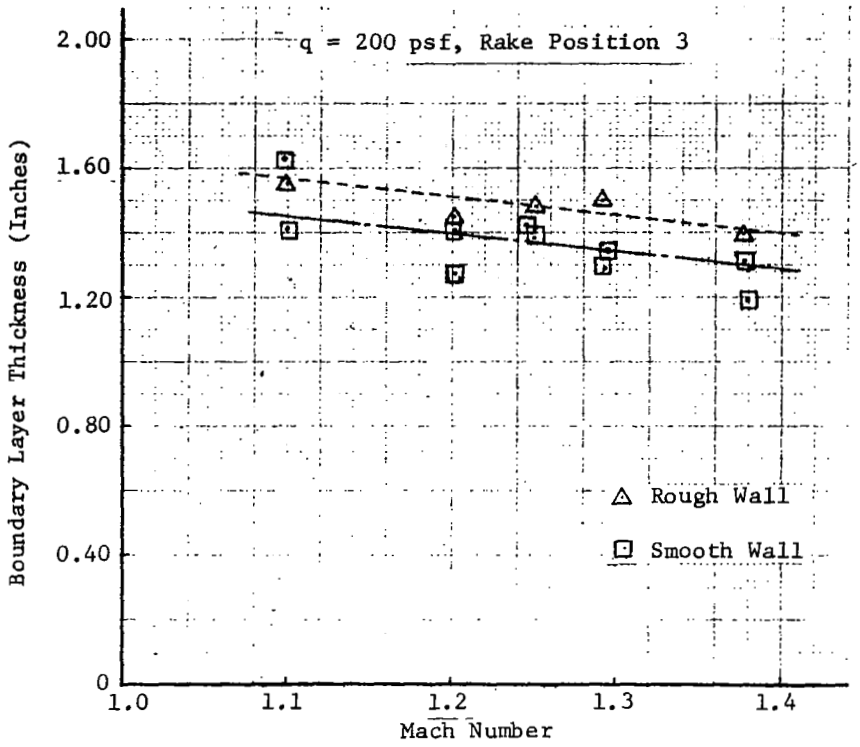

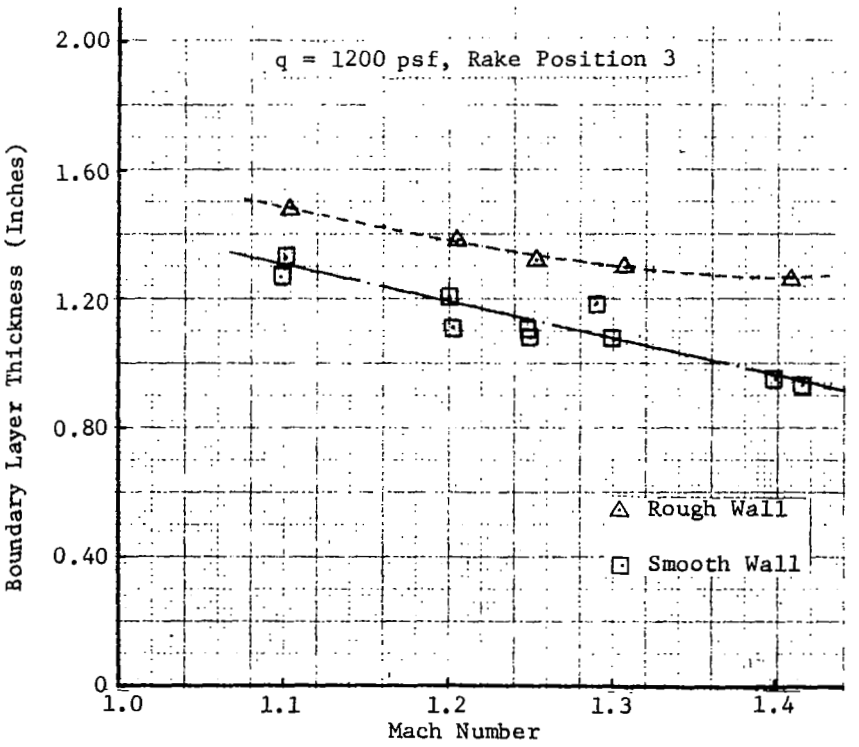

Note: Boundary Layer Thickness is Measured at $U/U_\infty = 0.98$

Figure 33 Variation of Boundary Layer Thickness with Mach Number

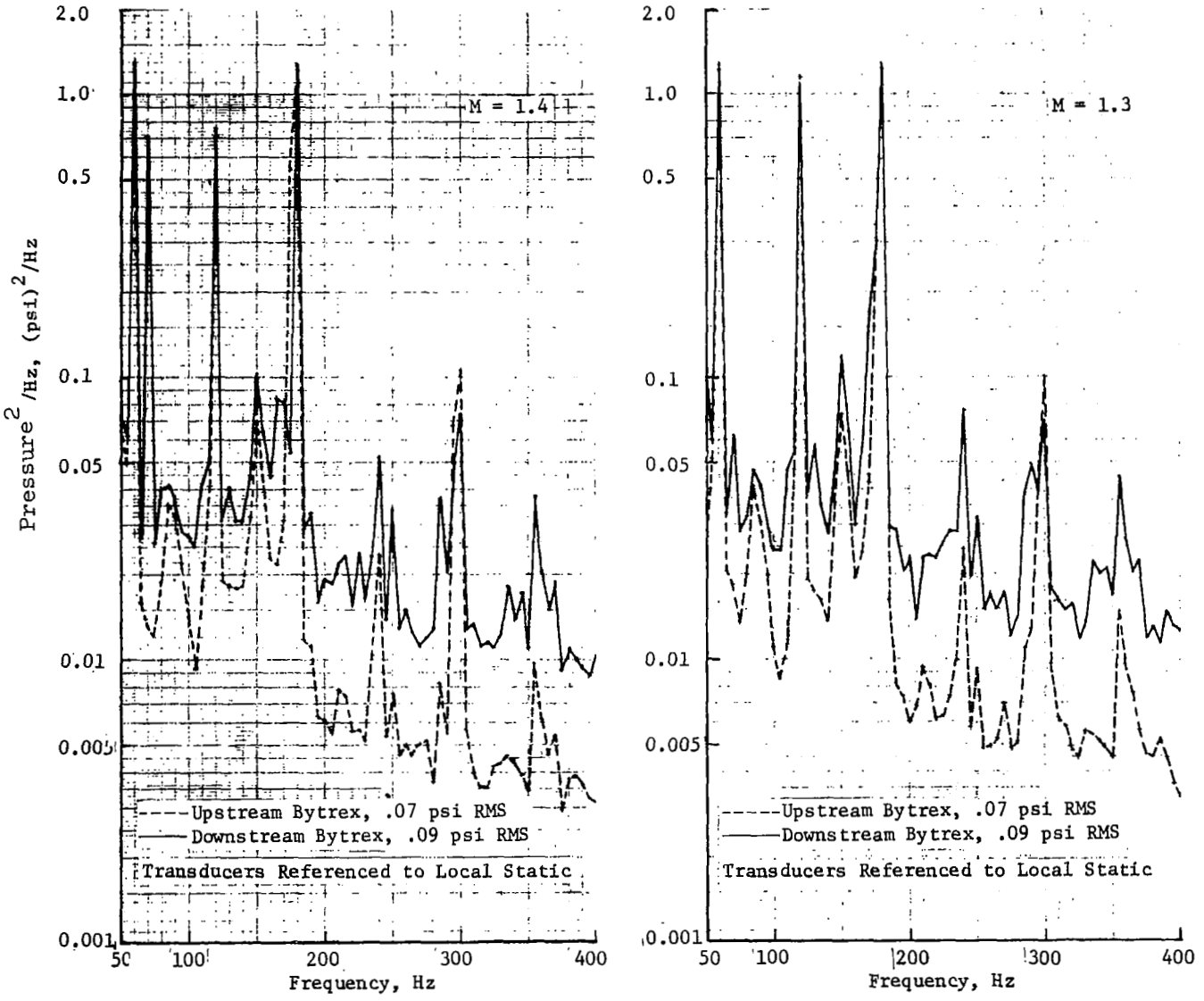

Figure 34 PSD Plots of Tunnel Wall Fluctuating Pressure (q = 200 psf, Smooth)

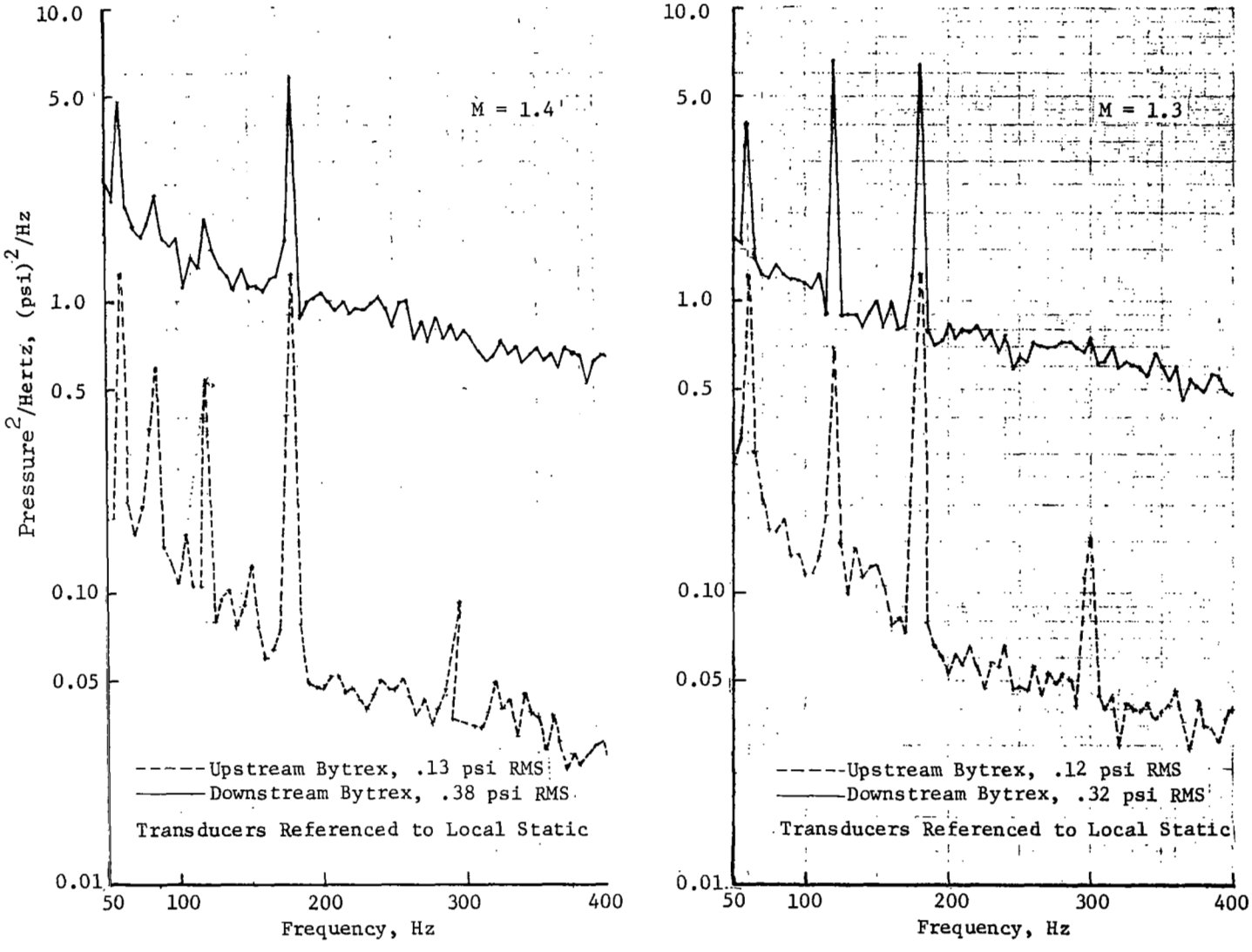

Figure 35 PSD Plots of Tunnel Wall Fluctuating Pressure (q = 1200 psf, Smooth)

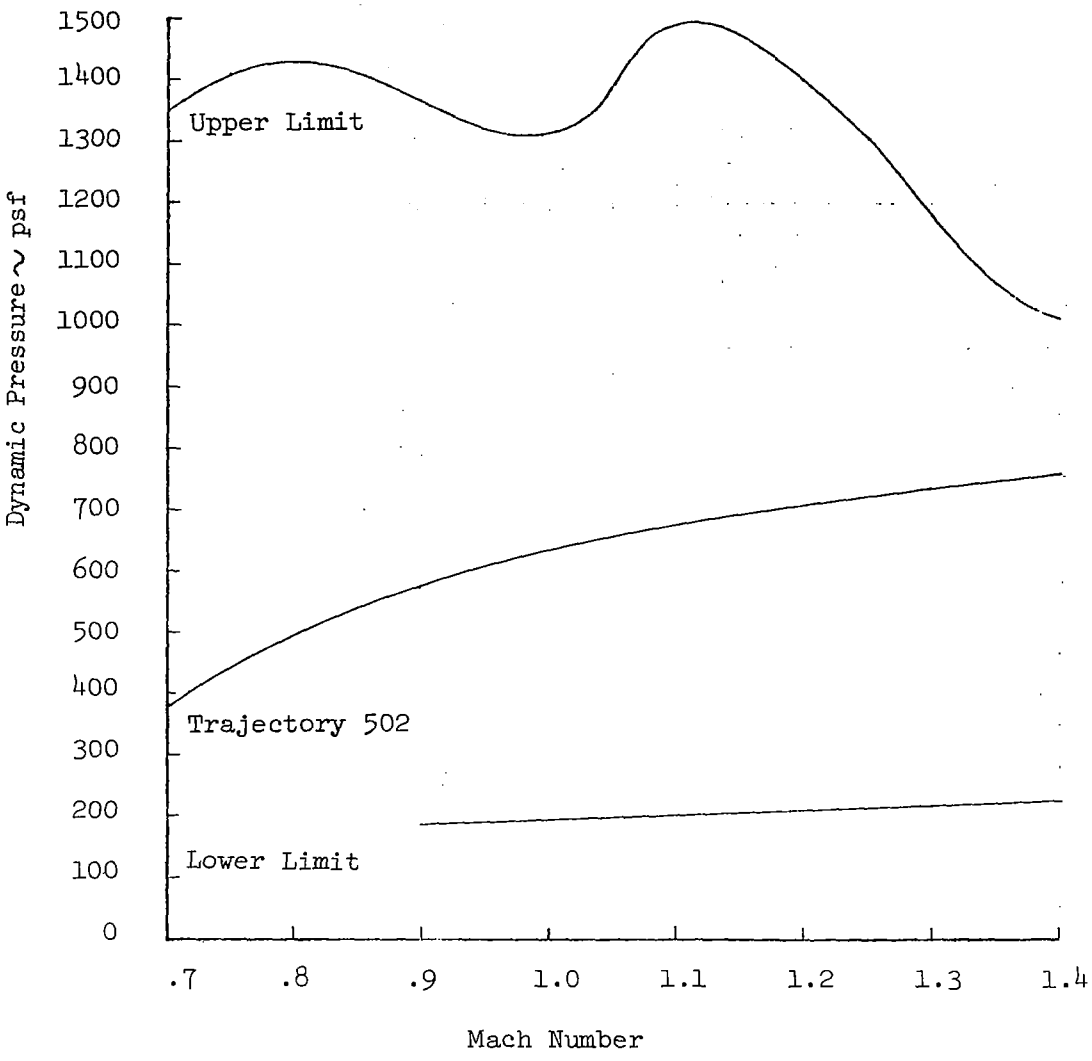

Figure 36 Operating Envelope for the Ames 2' x 2' Transonic Tunnel

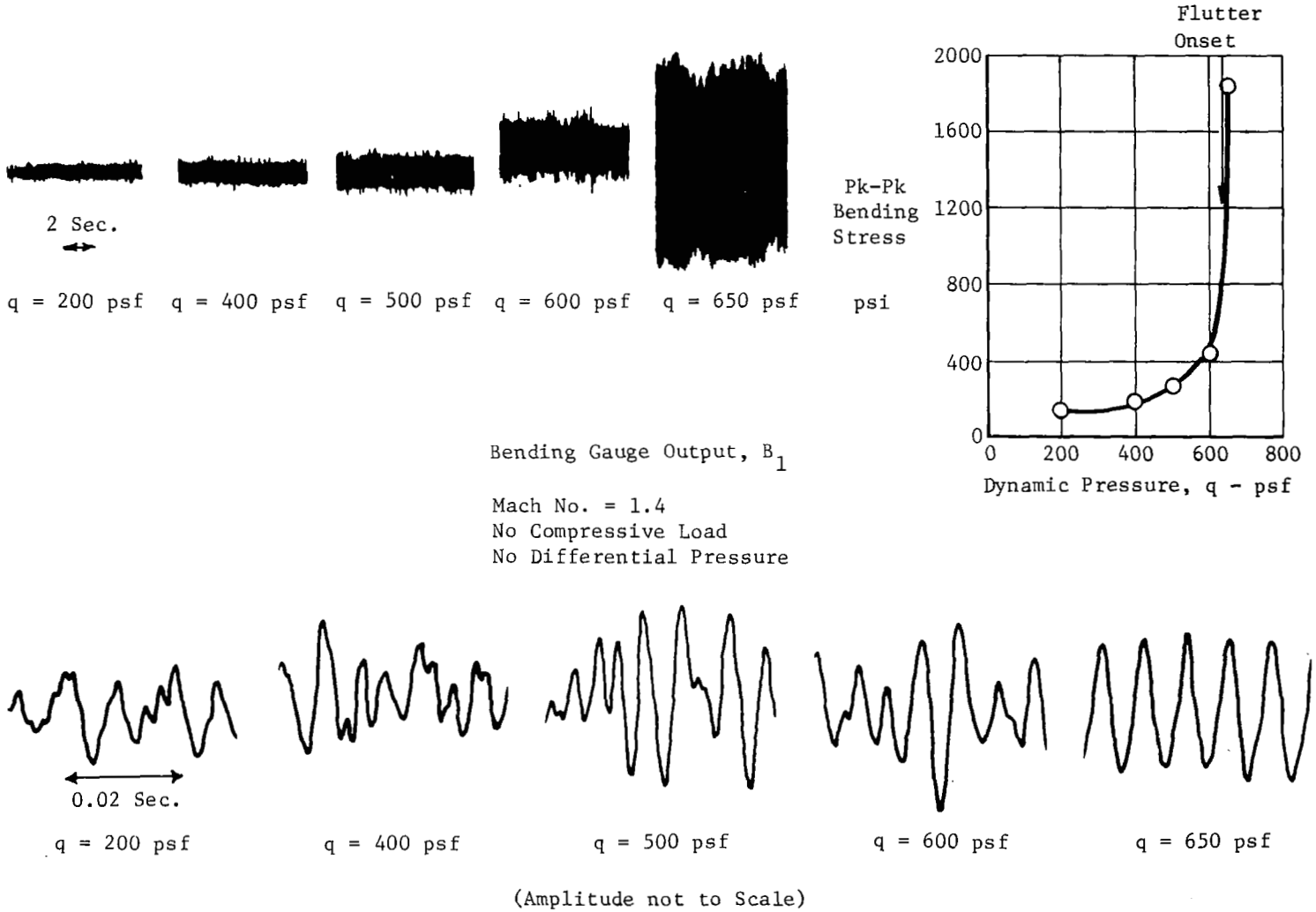

Figure 37 Determination of the Flutter Onset Dynamic Pressure

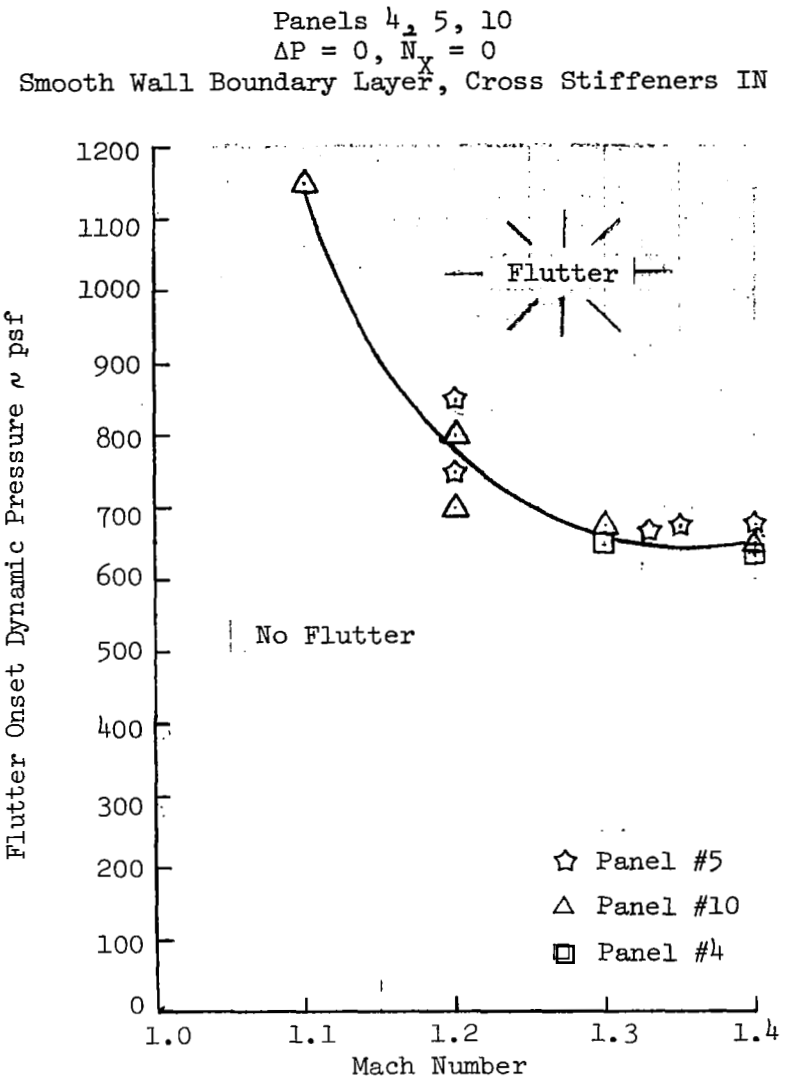

Figure 38 Variation of Onset Dynamic Pressure with Mach Number (Panels 4, 5, 10)

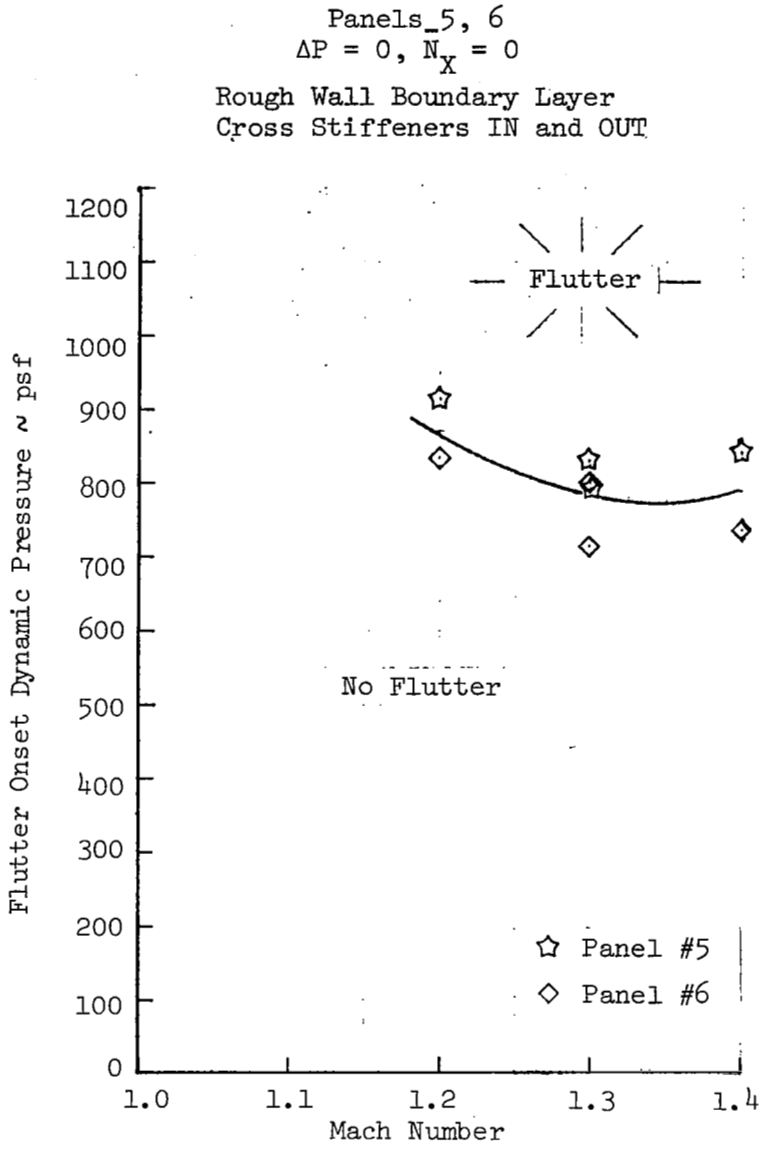

Figure 39 Variation of Onset Dynamic Pressure with Mach Number (Panels 5, 6)

Panel 6 Data
M = 1.3, $\Delta P = 0$
Rough Wall Boundary Layer, Cross Stiffeners OUT

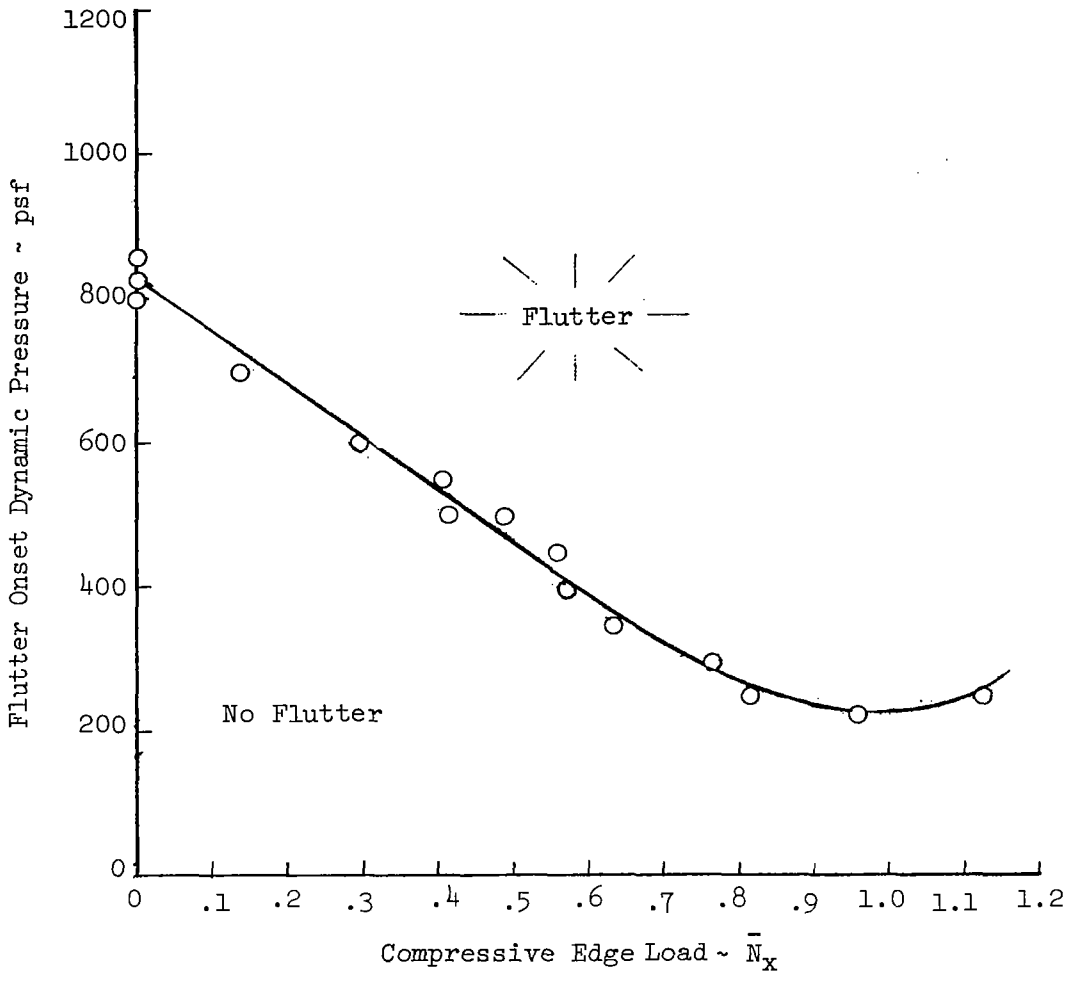

Figure 40 Variation of Flutter Onset Dynamic Pressure with Compressive Edge Load (Panel 6)

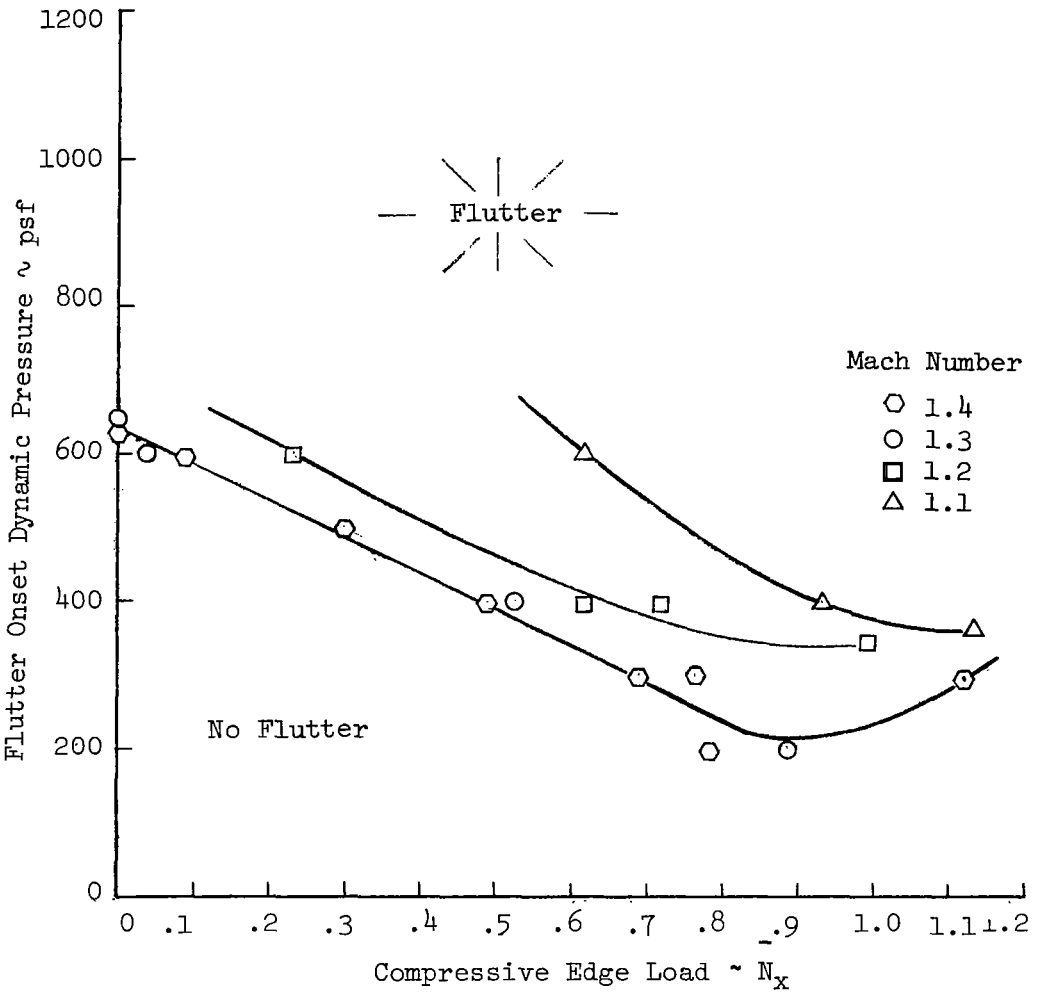

Figure 41 Variation of Flutter Onset Dynamic Pressure with Compressive Edge Load (Panel 4)

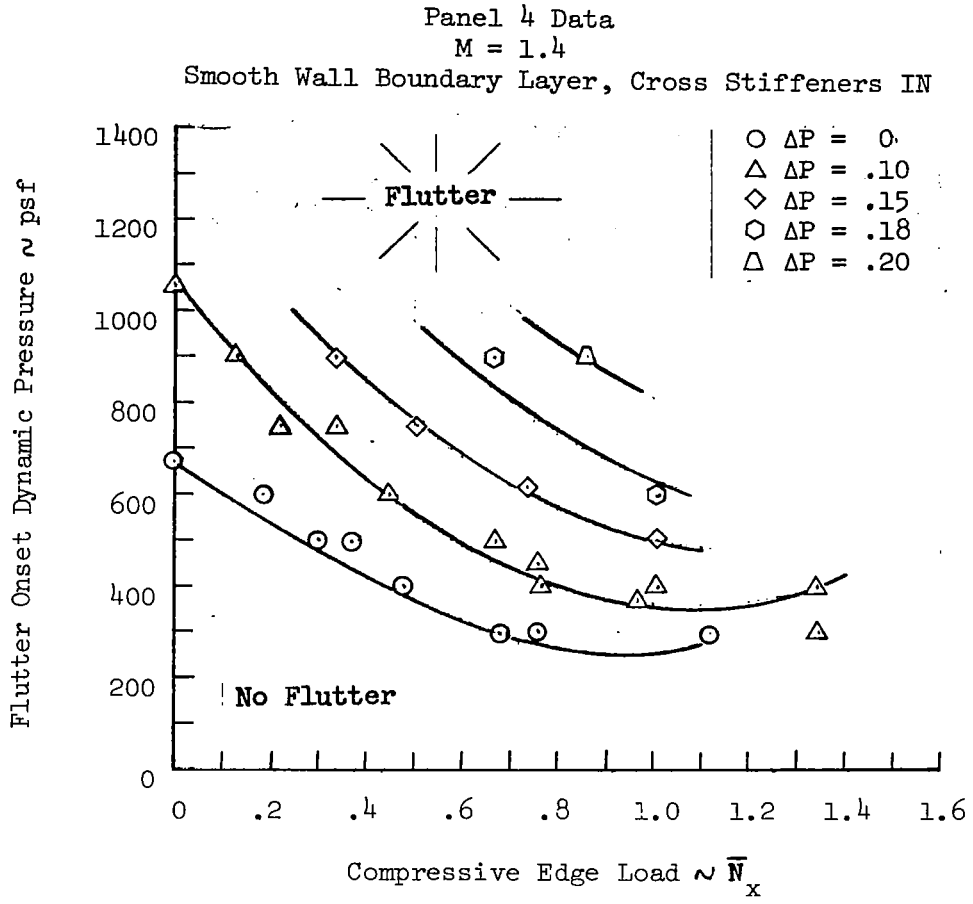

Figure 42 Effect of $\bar{N}_x$ on Flutter Onset Dynamic Pressure (with Variation in ΔP)

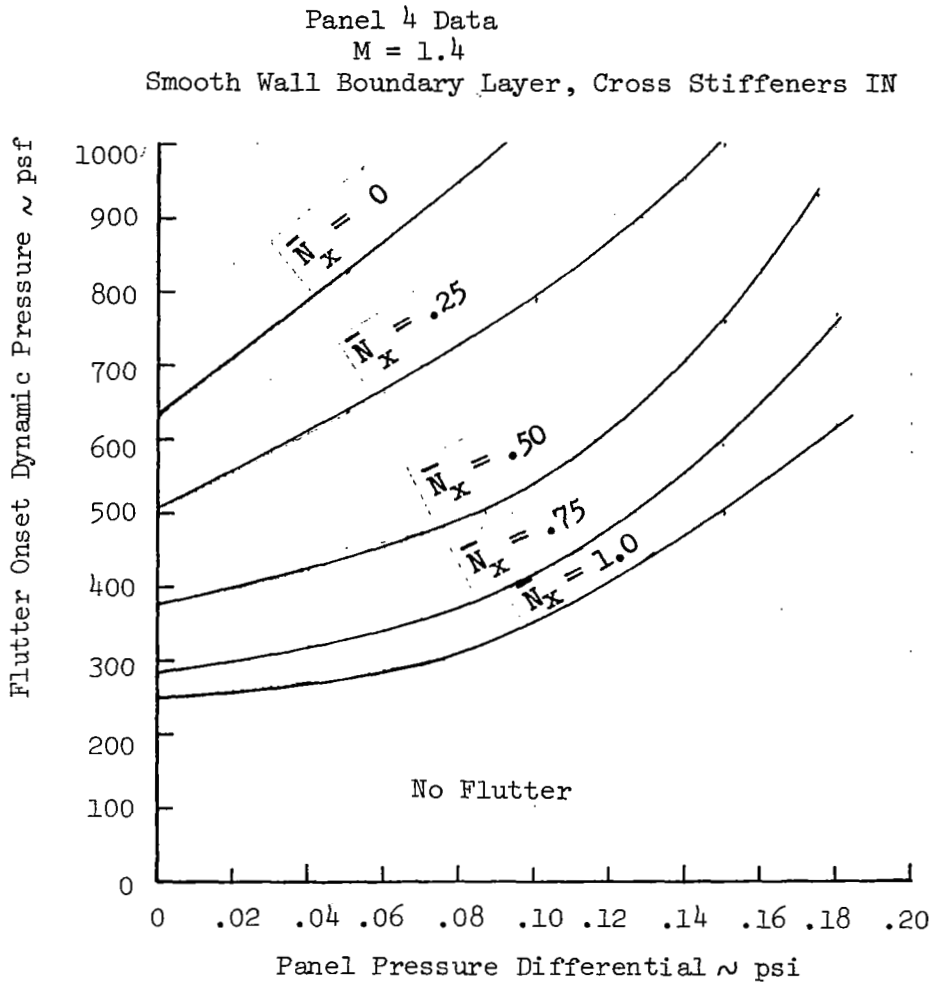

Figure 43 Effect of ΔP on Flutter Onset Dynamic Pressure (with Variation in $\bar{N}_x$)

Panel 5 Data
M = 1.3
Rough Wall Boundary Layer, Cross Stiffeners OUT

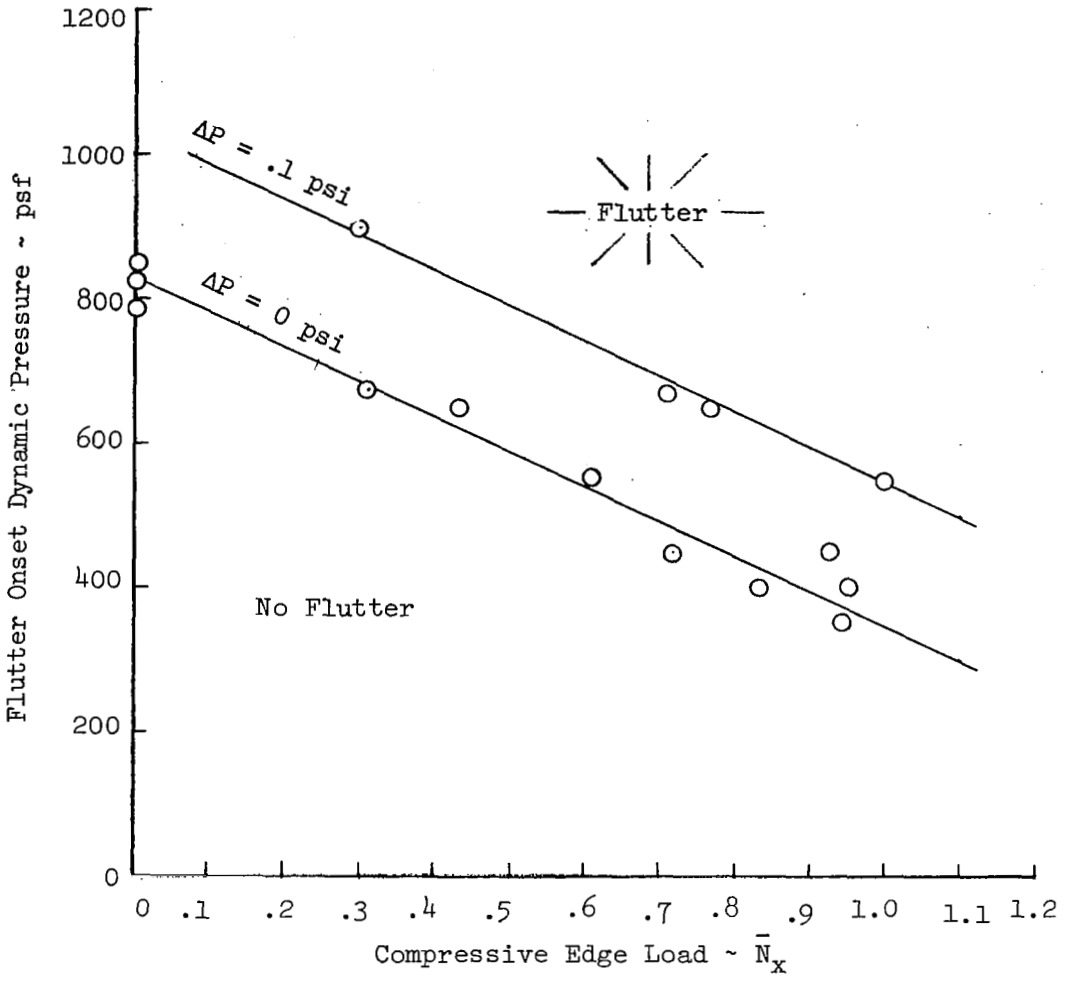

Figure 44 Effect of a 0.1 psi Differential Pressure on Flutter Onset

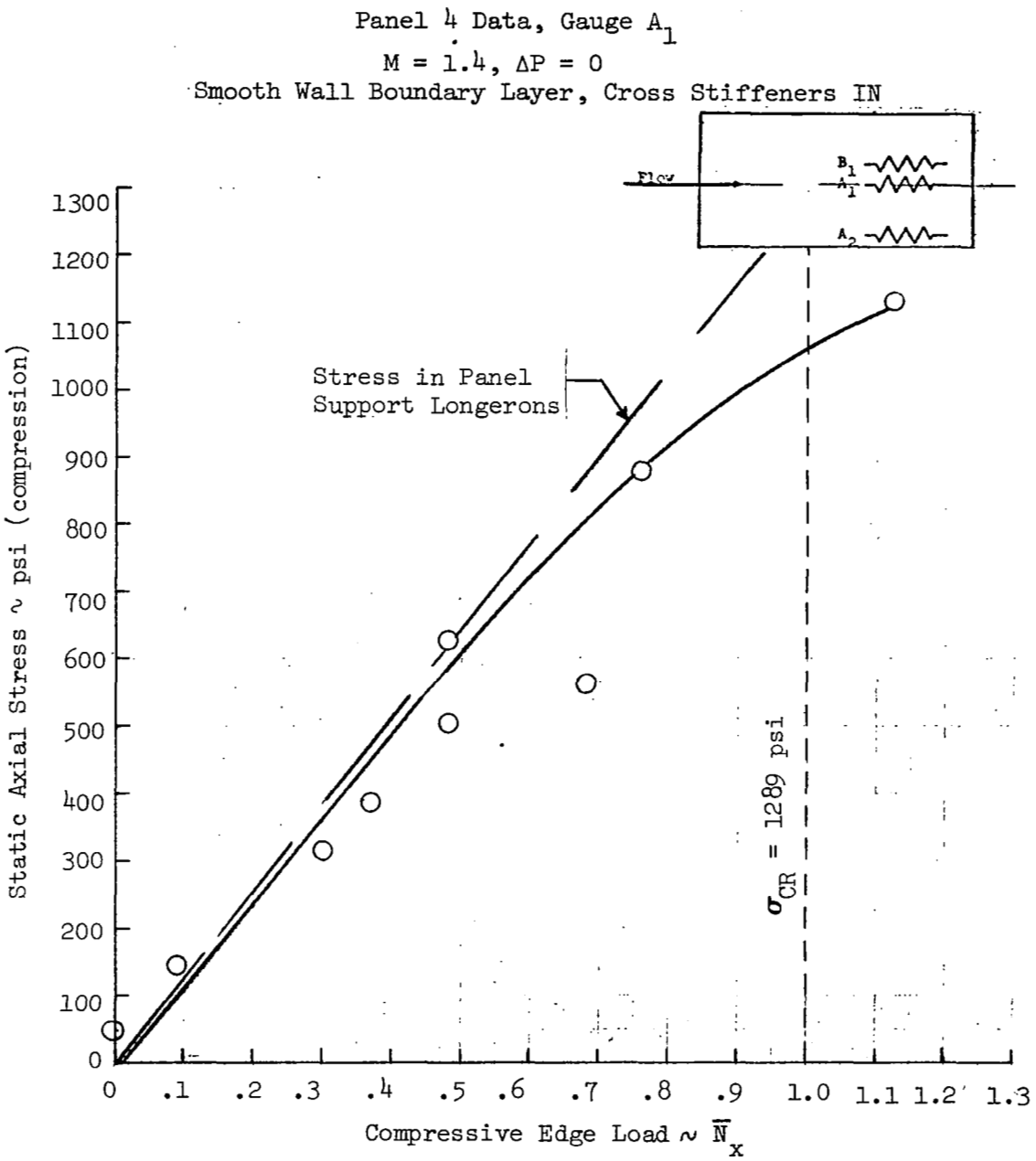

Figure 45 Variation of Static Axial Stress with $\bar{N}_x$ at Flutter Onset

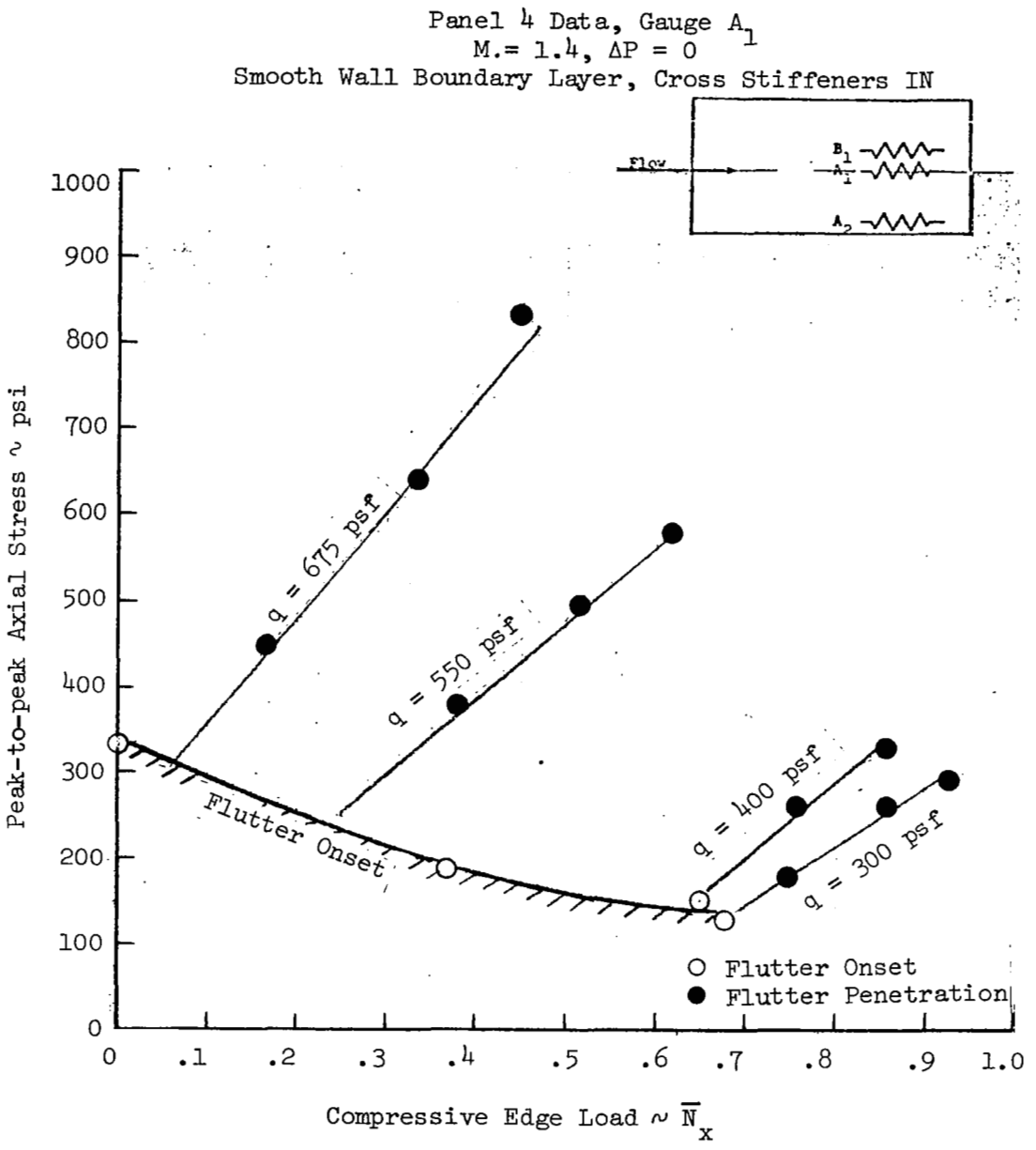

Figure 46 Oscillatory Axial Stress During Flutter Penetration (Panel 4)

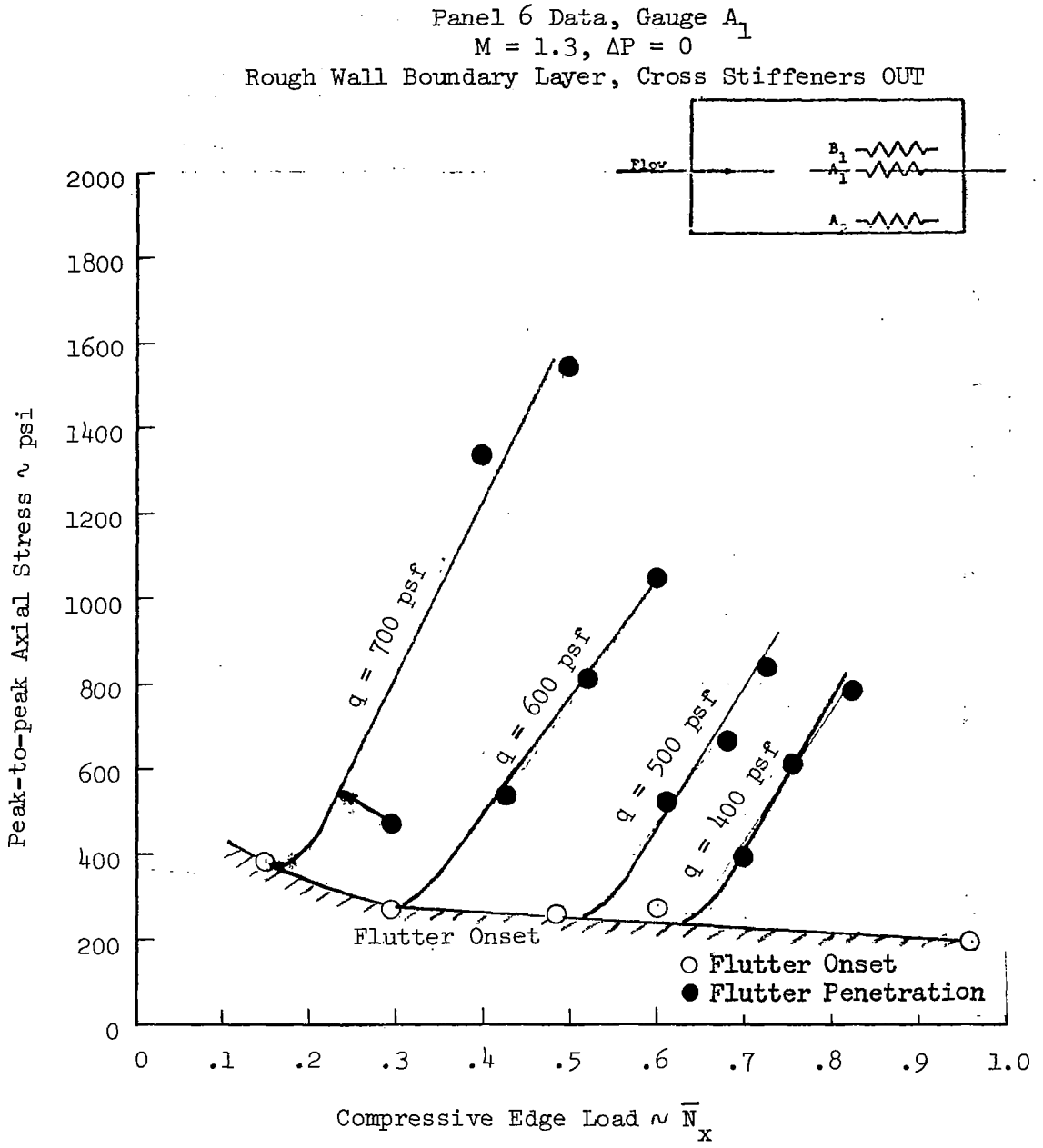

Figure 47 Oscillatory Axial Stress During Flutter Penetration (Panel 6)

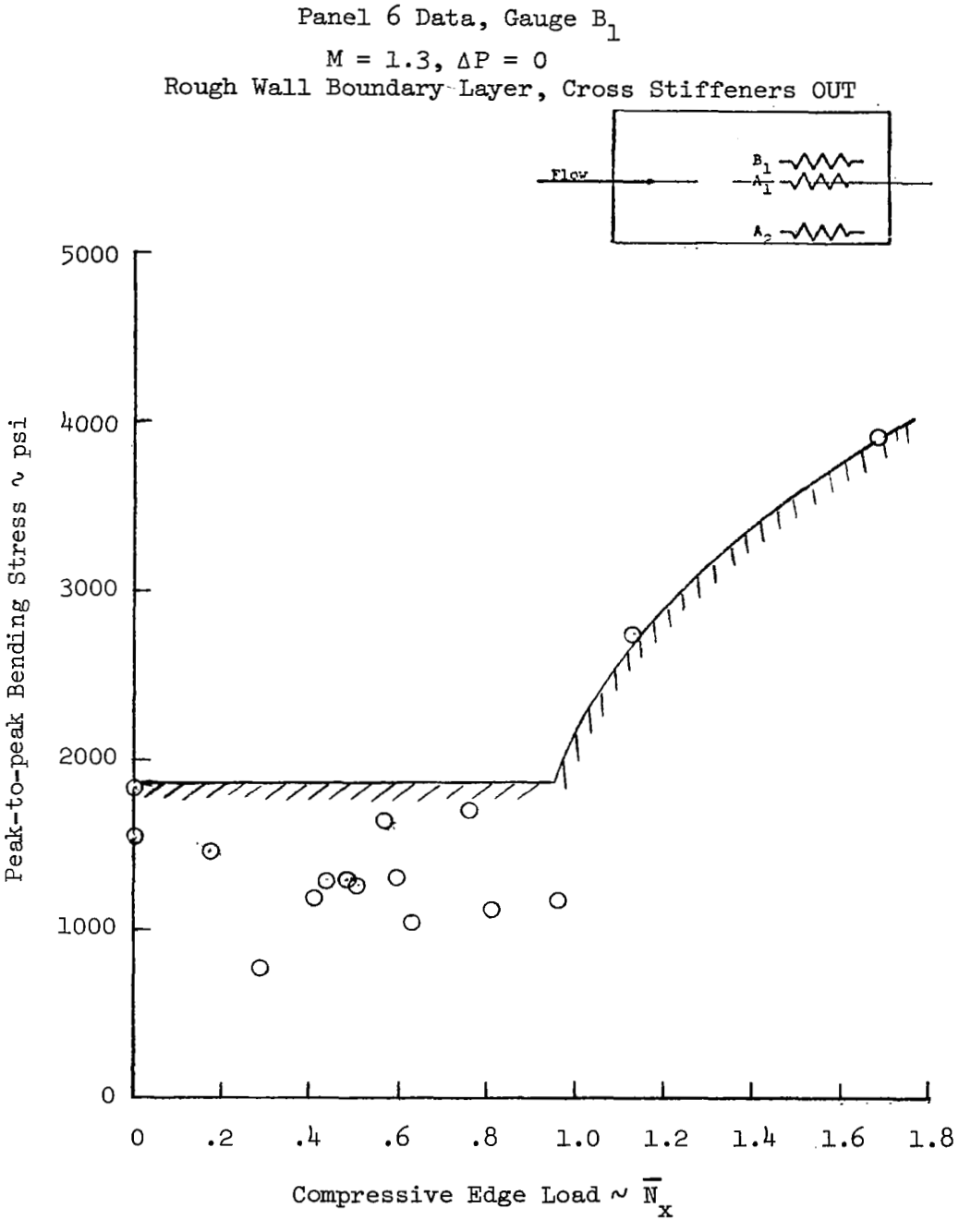

Figure 48 Variation of Oscillatory Bending Stress at Flutter Onset, ΔP = 0

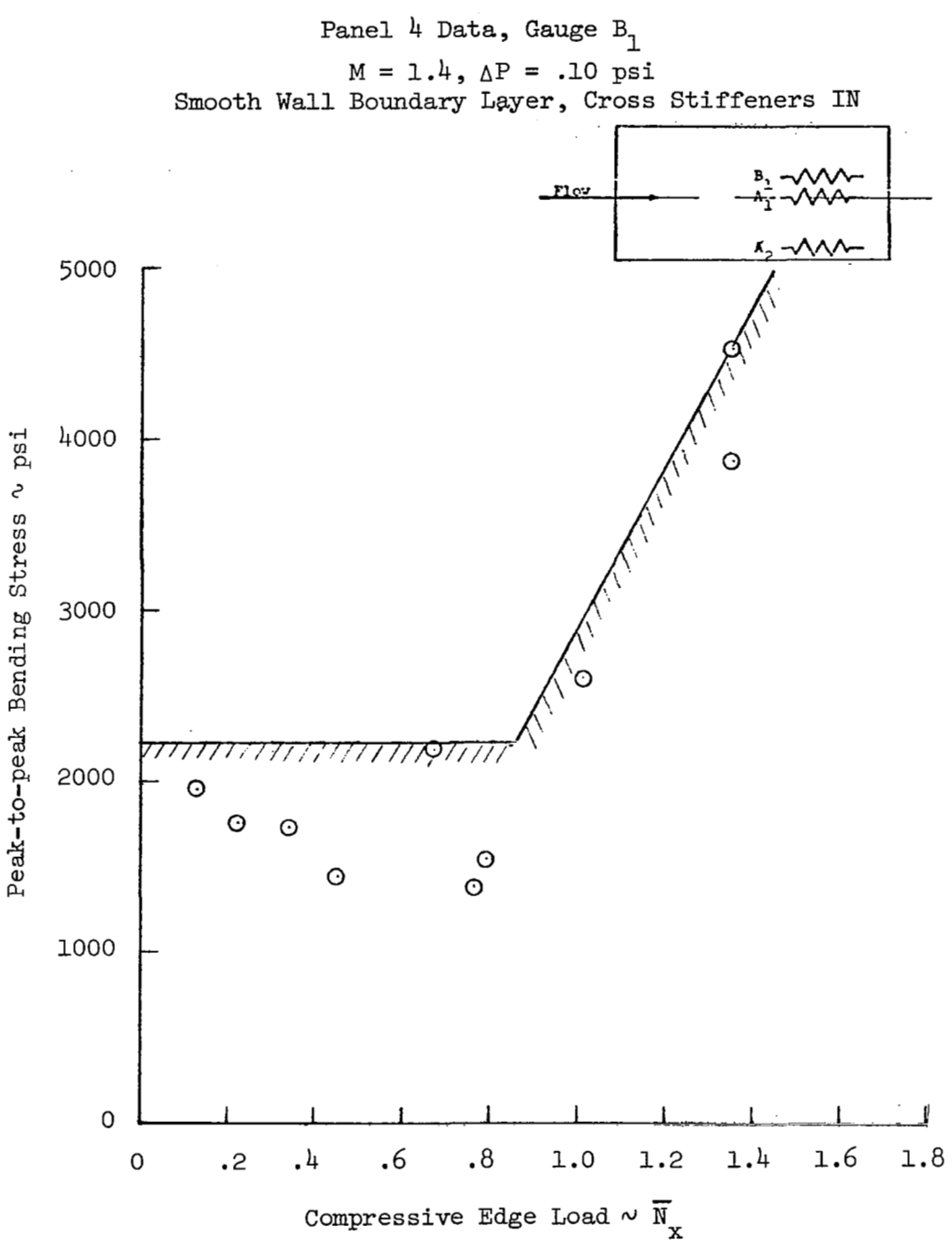

Figure 49 Variation of Oscillatory Bending Stress at Flutter Onset, ΔP = .10 psi

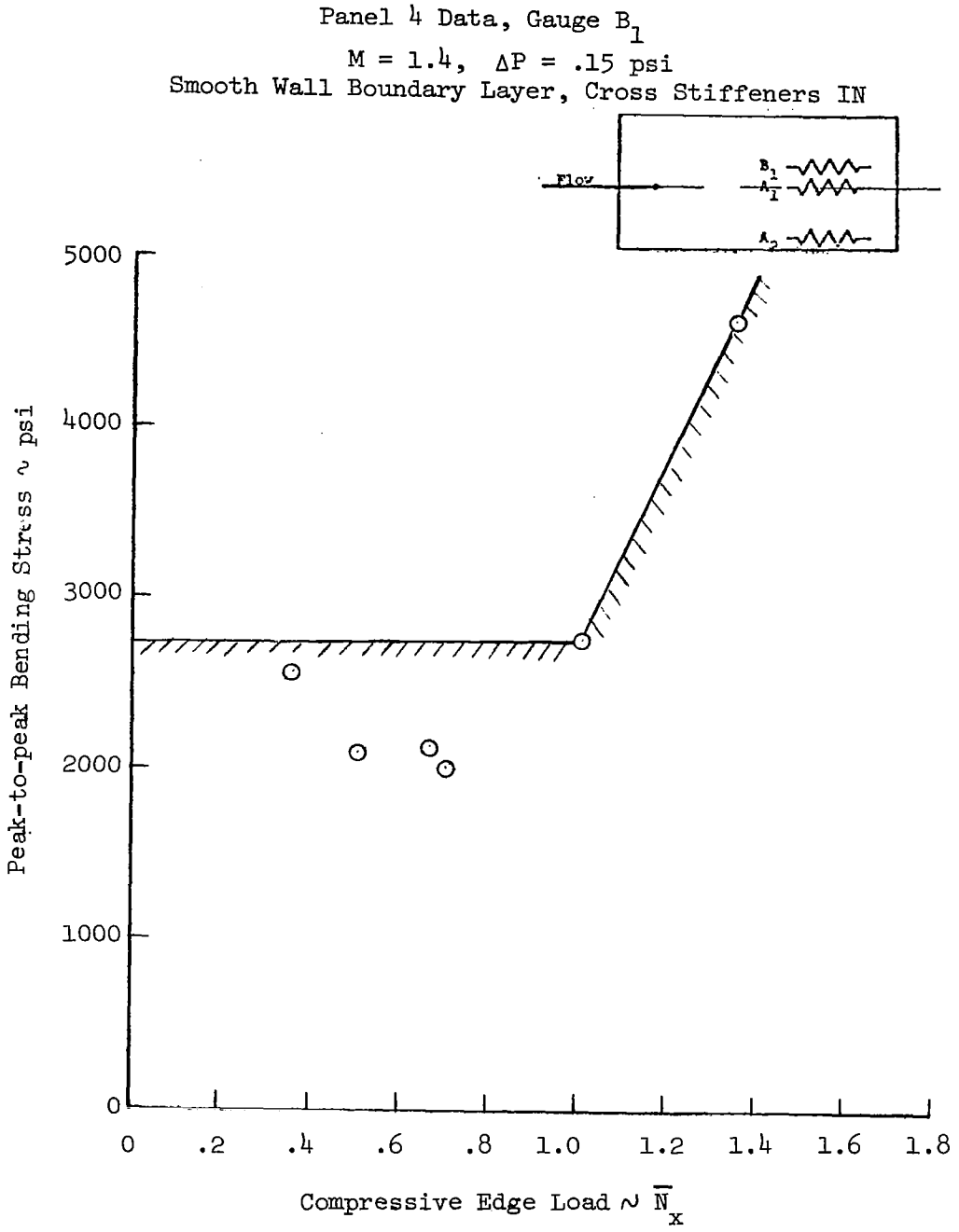

Figure 50 Variation of Oscillatory Bending Stress at Flutter Onset, ΔP = .15 psi

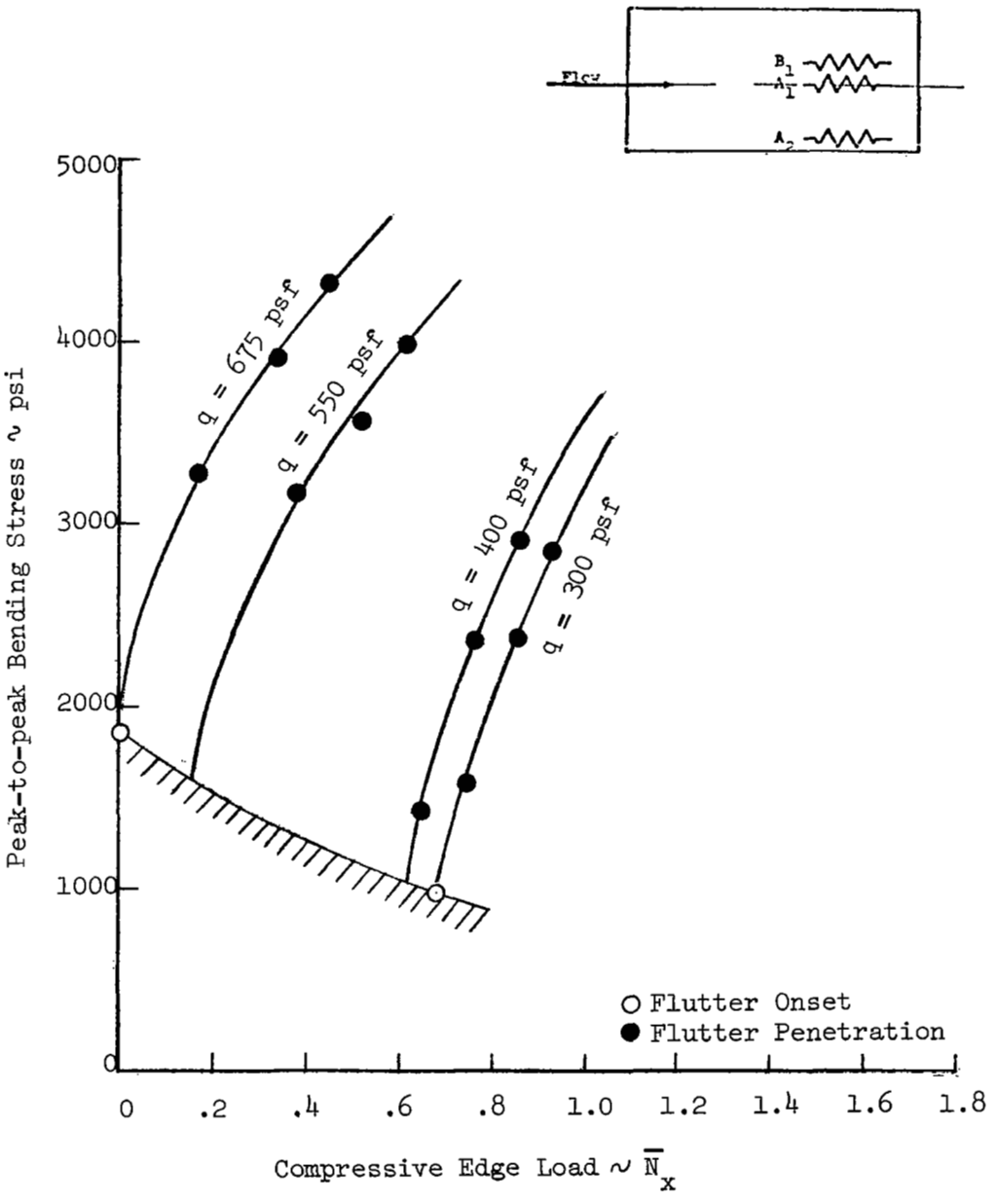

Figure 51 Oscillatory Bending Stress During Flutter Penetration (Panel 4)

Panel 6 Data, Gauge B_1

M = 1.3, ΔP = 0

Rough Wall Boundary Layer, Cross Stiffeners OUT

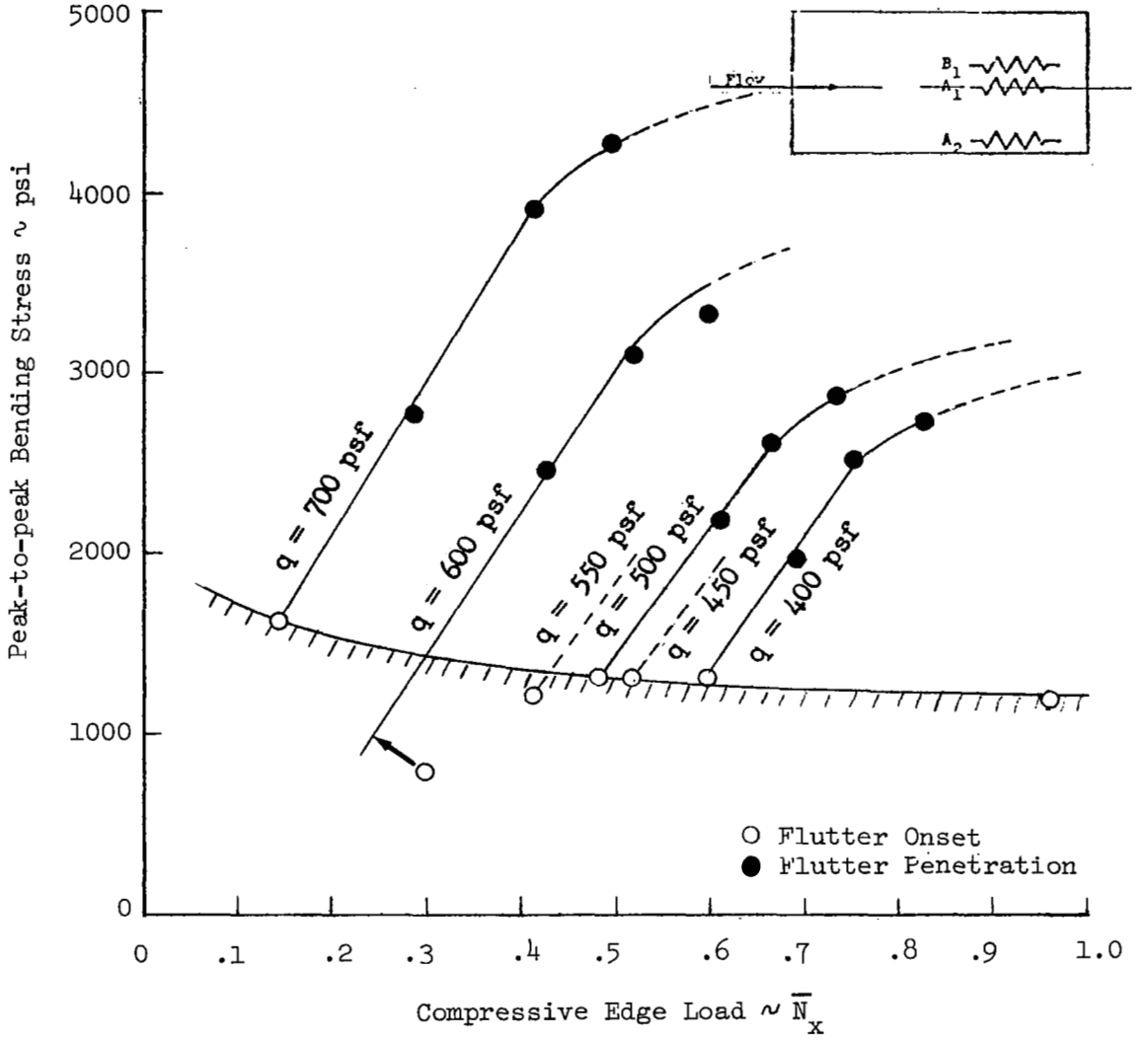

Figure 52 Oscillatory Bending Stress During Flutter Penetration (Panel 6)

Panel 6 Data
M = 1.3, ΔP = 0
Rough Wall Boundary Layer, Cross Stiffeners OUT

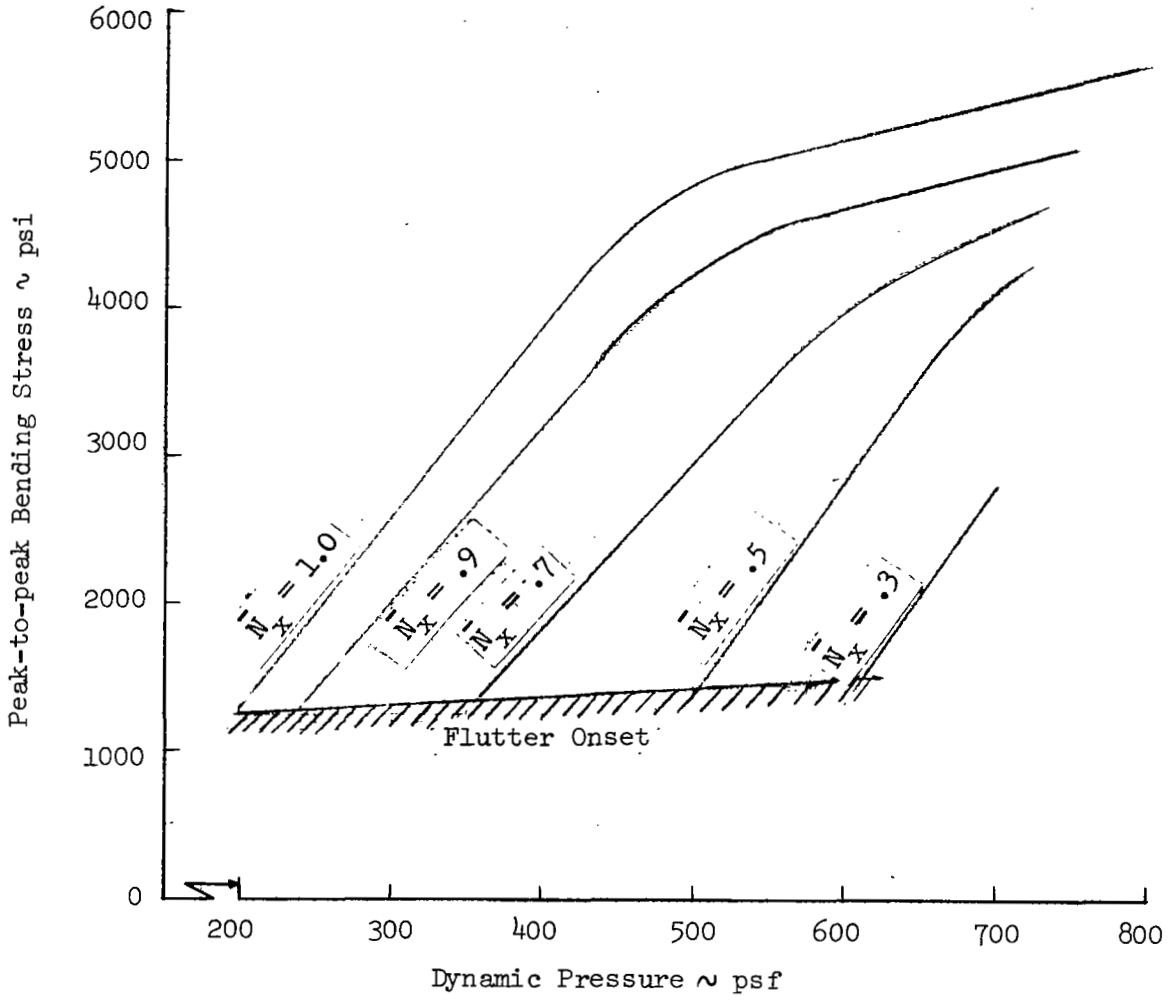

Figure 53 Variation of Oscillatory Bending Stress with q for Several Values of $\bar{N}_x$

Panel 6 Data, Gauge B_1
M = 1.3, $\Delta P = 0$
Rough Wall Boundary Layer, Cross Stiffeners OUT

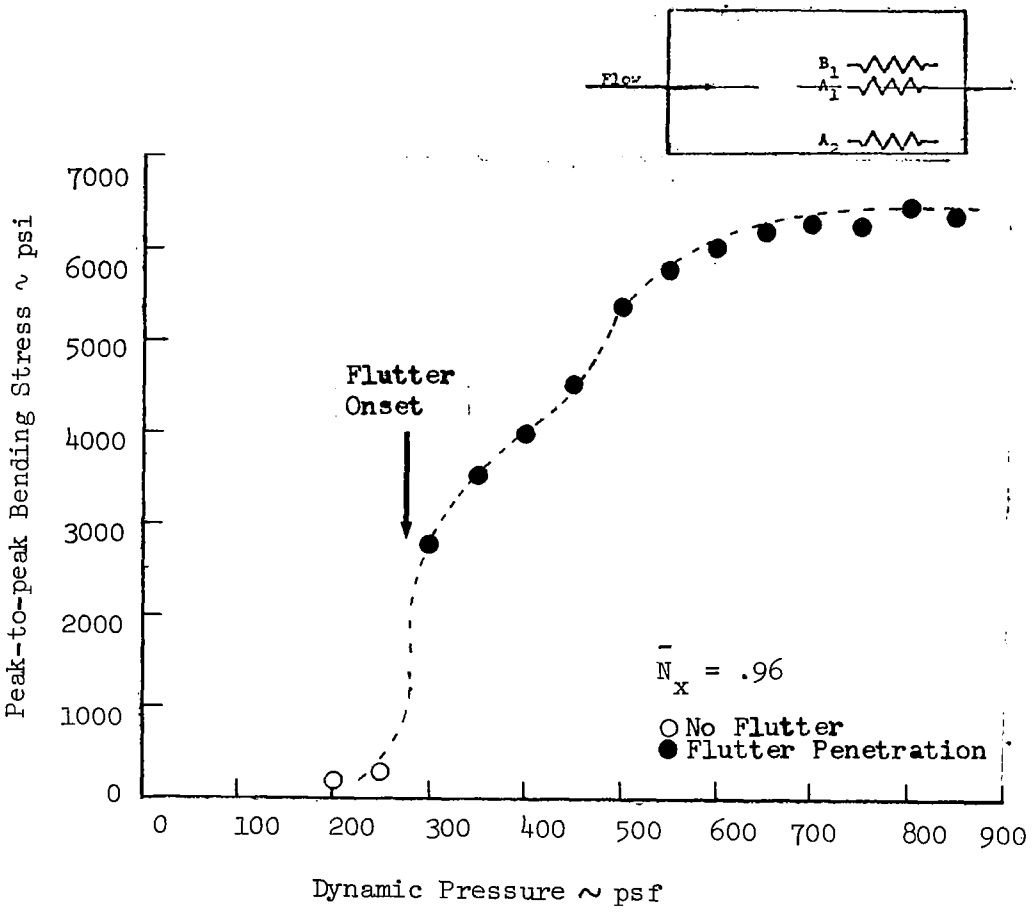

Figure 54 Oscillatory Bending Stress of a Buckled Panel During Flutter Penetration

Panel 4 Data
ΔP = 0
Smooth Wall Boundary Layer, Cross Stiffeners IN

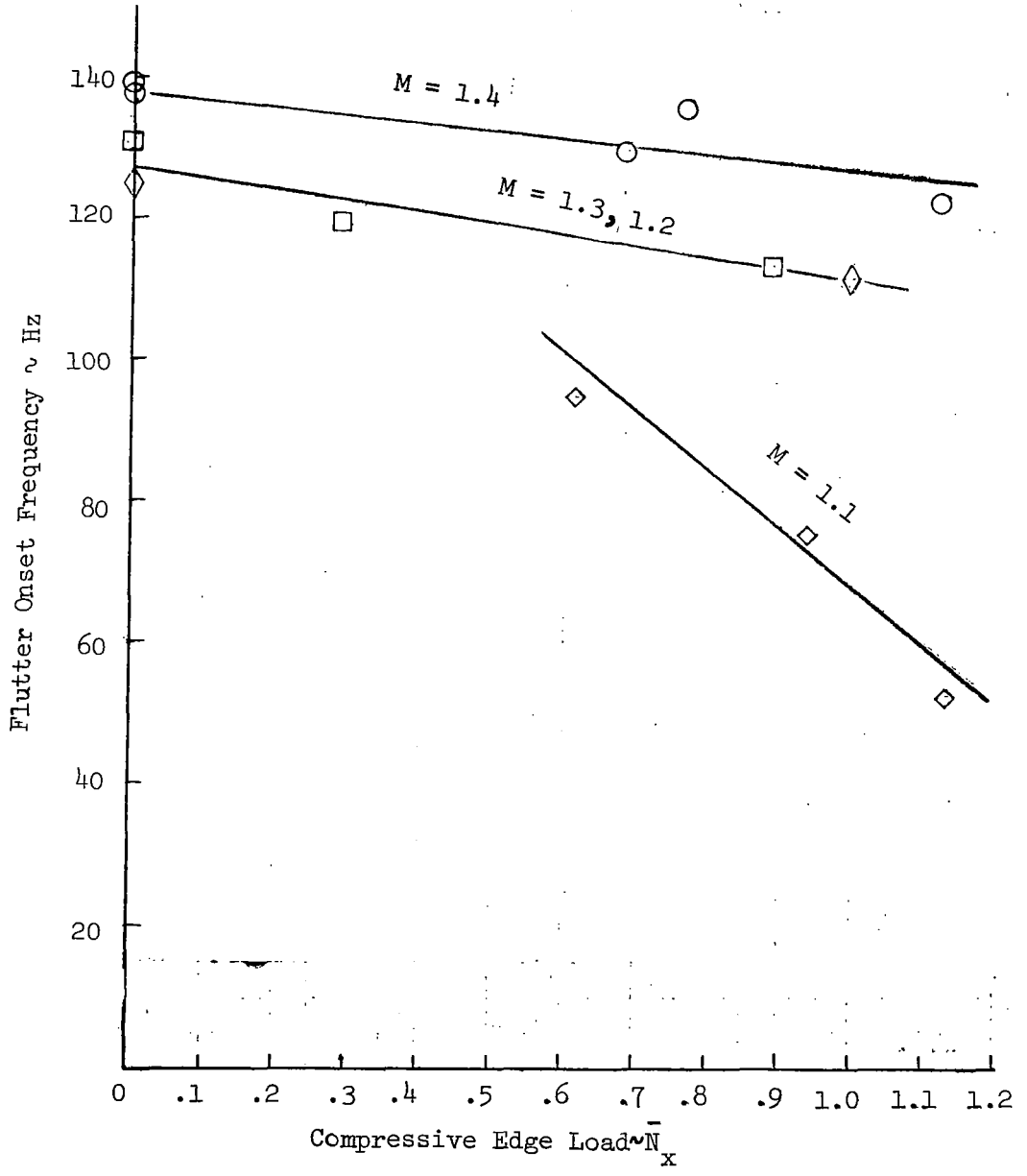

Figure 55 Effect of Compressive Edge Load and Mach Number on Flutter Onset Frequency

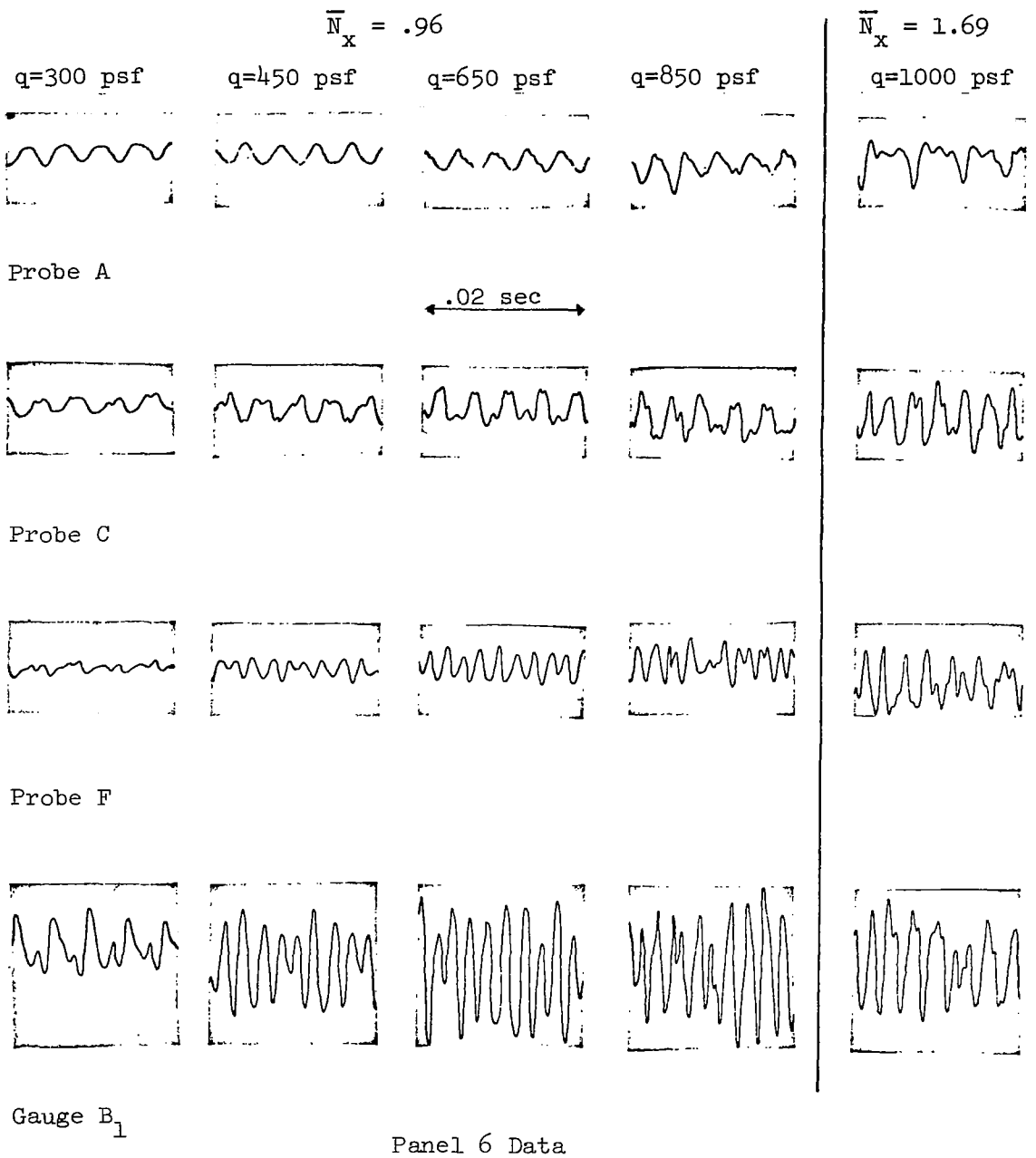

Panel 6 Data
M = 1.3, ΔP = 0
Rough Wall Boundary Layer, Cross Stiffeners OUT
(Amplitudes Not to Scale)

Figure 56 Time Histories of Panel Displacement and Strain During Flutter Penetration

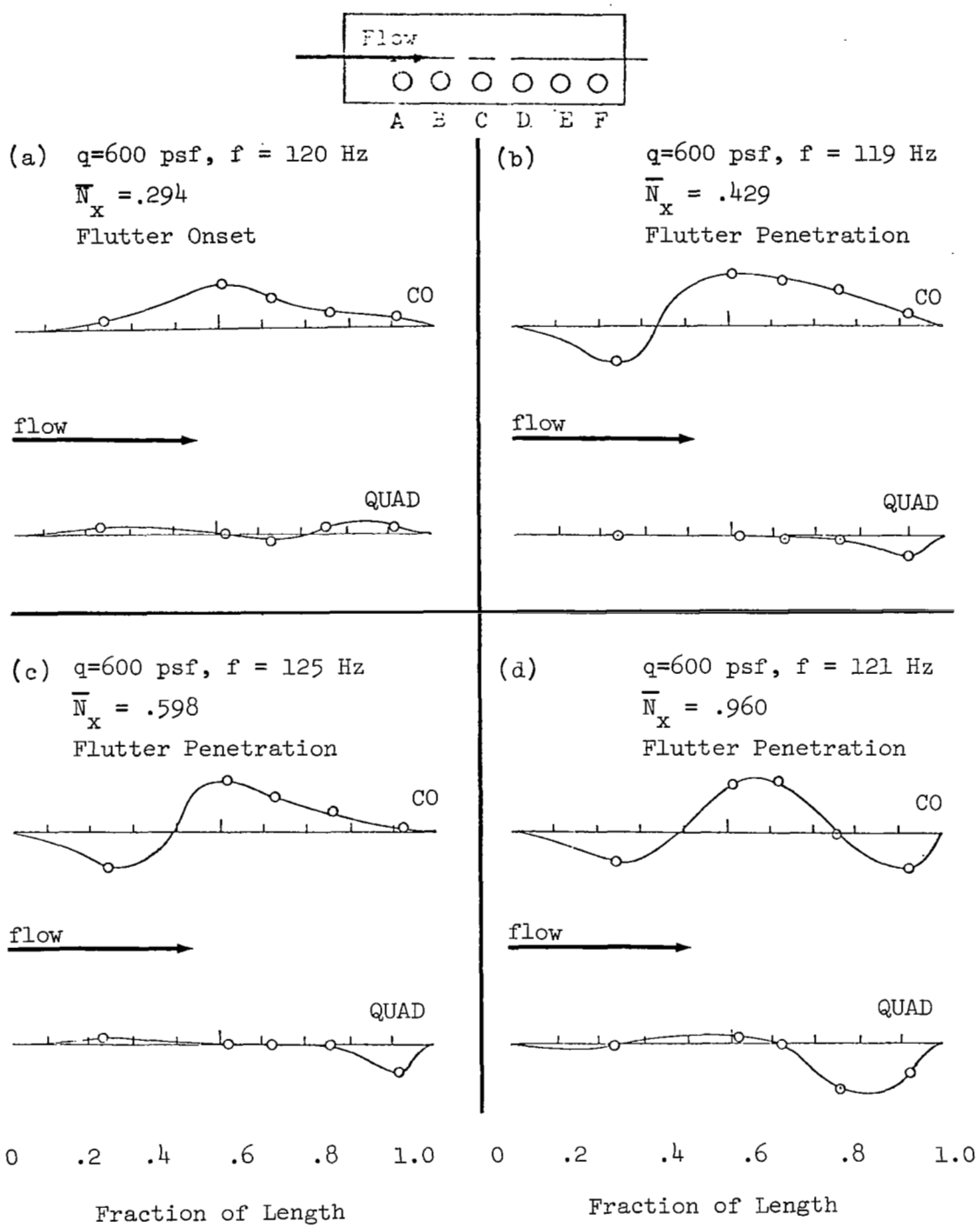

Panel 6 Data
M = 1.3, ΔP = 0
Rough Wall Boundary Layer, Cross Stiffeners OUT

Figure 57 Panel Flutter Mode Shapes

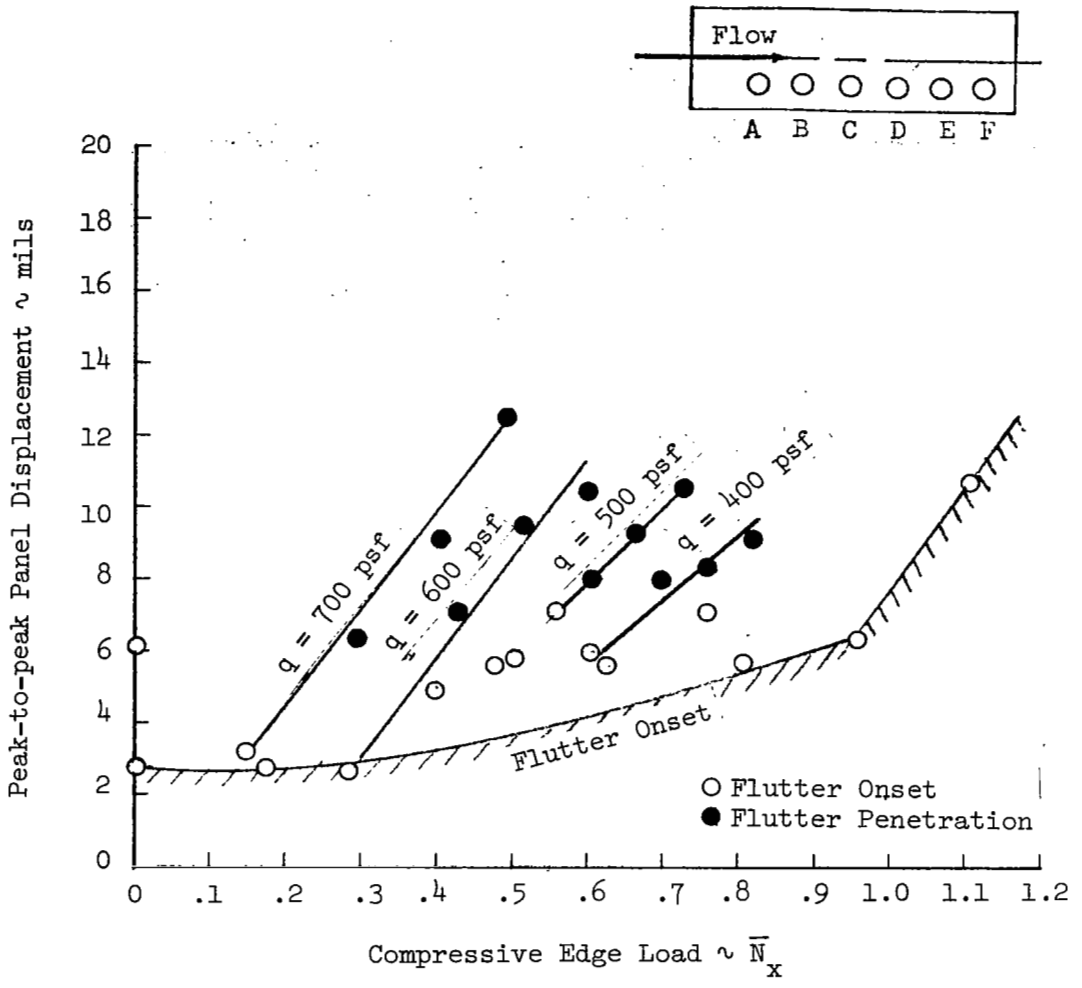

Figure 58 Panel Oscillatory Displacement During Flutter (Probe A)

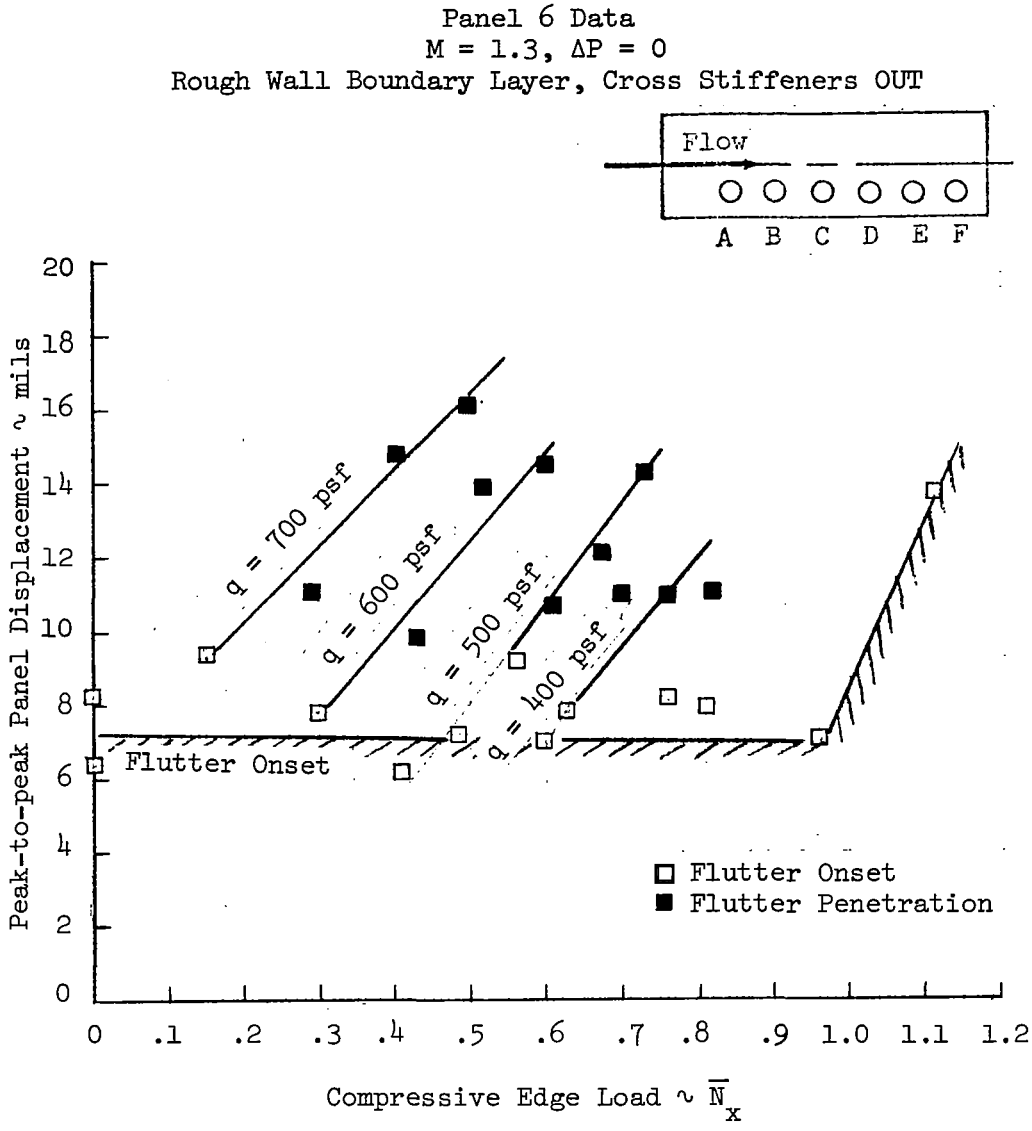

Figure 59 Panel Oscillatory Displacement During Flutter (Probe D)

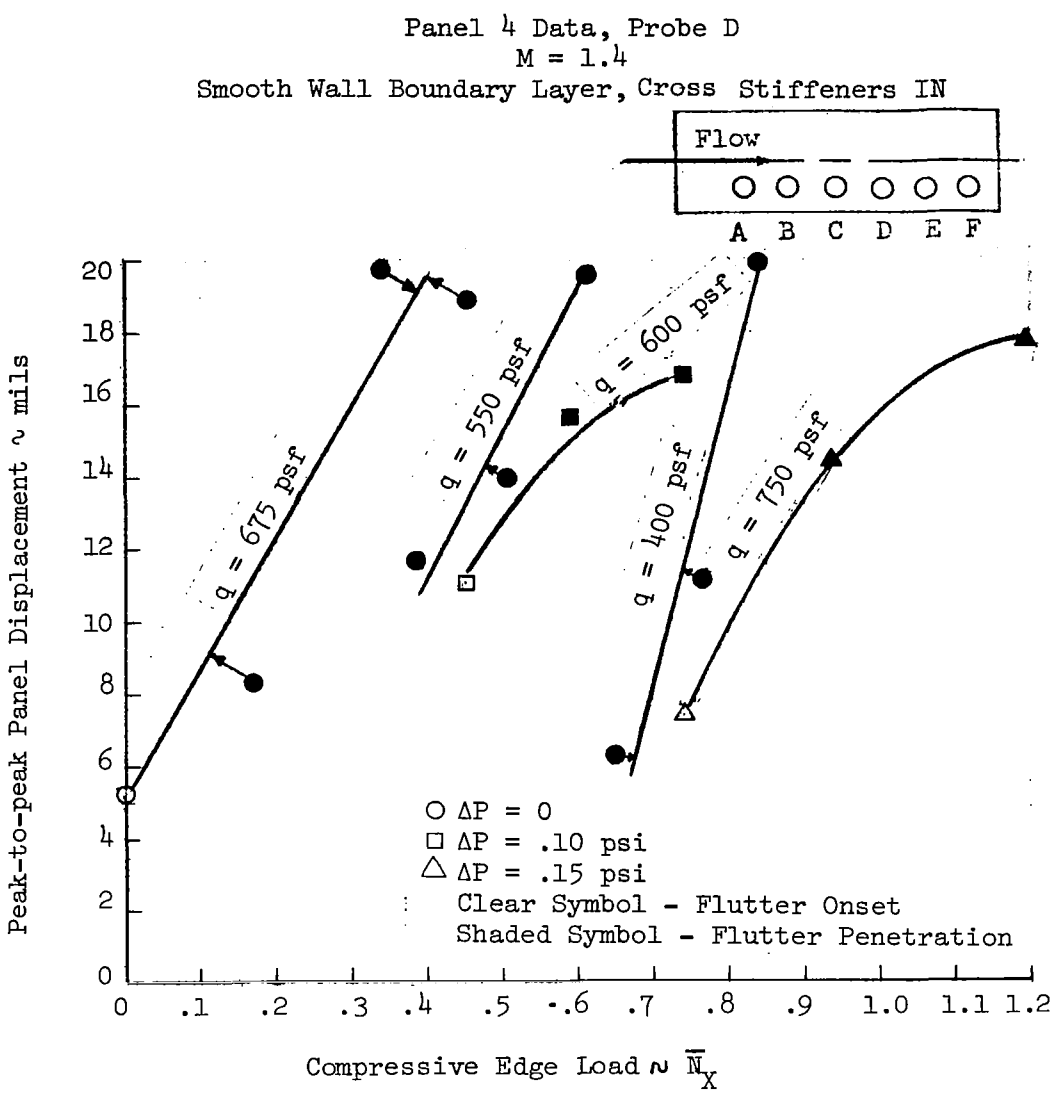

Figure 60 Panel Oscillatory Displacement During Flutter Showing the Effects of ΔP

Panel 6 Data

$M = 1.3$, $\bar{N}_x = .96$, $\Delta P = 0$

Rough Wall Boundary Layer, Cross Stiffeners OUT

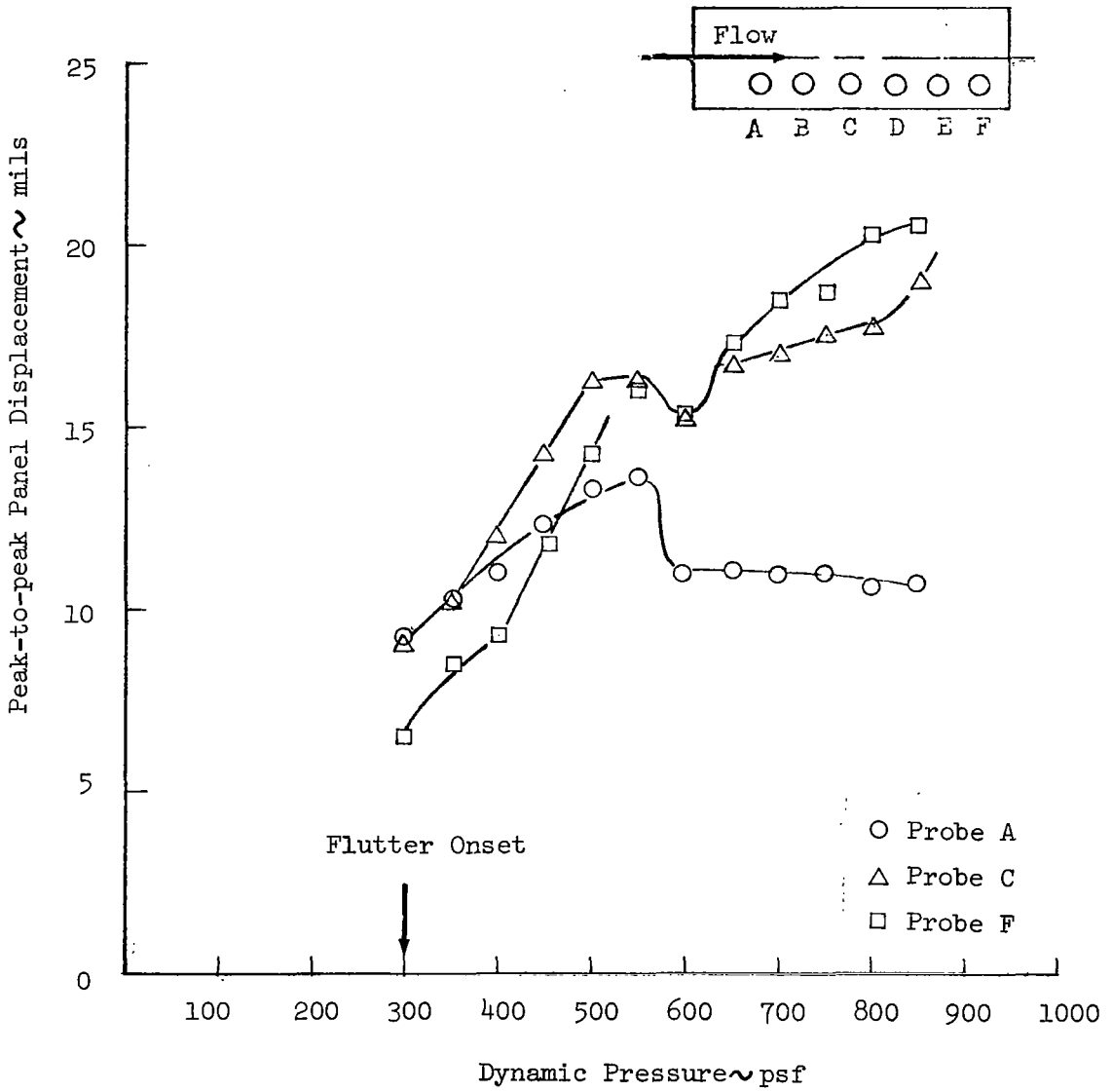

Figure 61 Panel Oscillatory Displacement During Flutter Penetration at $\bar{N}_x = .96$

REFERENCES

1. Perkins, T.M., "Flutter Test of an Array of Full-Scale Panels from the Saturn S-IVB Stage," AEDC-TR-68-30, February, 1968.

2. Nichols, J.J., "Final Report, Saturn V, S-IVB Panel Flutter Qualification Test," NASA TN-D 5439, October 1969.

3. Lemley, Clark E., "Design Criteria for the Prediction and Prevention of Panel Flutter," AFFDL-TR-67-140, Vol. II, August,1968.

4. Dugundji, John, "Theoretical Considerations of Panel Flutter at High Supersonic Mach Numbers," AFOSR 65-1907, August, 1965.

5. Hodson, C.H., and Stocker, J.E., "Commercial Supersonic Transport Panel Flutter Studies," RTD-TDR-63-4036, May, 1964.

6. Johns, David J., "A Survey on Panel Flutter," November 1965.

7. Swan, William, "Non-Linear Analysis of the Flutter of an Infinitely Long Plate," AMS Report No. 845," August, 1968.

8. Ventres, Charles, S., "Non-Linear Flutter of Clamped Plates," PhD Thesis, Princeton University, October, 1969.

9. Dowell, Earl H., "Non-Linear Oscillations of a Fluttering Plate," AIAA Journal, Vol. 4, No. 7, July 1966, pp. 1267-1275.

10. Grant NGR 05-020-102, Status Report 4, "Theoretical Studies of Some Nonlinear Aspects of Hypersonic Panel Flutter," Stanford University, August, 1967.

11. Dowell, Earl H. and Voss, H.M., "Experimental and Theoretical Panel Flutter Studies in the Mach Number Range of 1.0 to 5.0," Technical Documentary Report No. ASD-TDR-63-449, December, 1963.

12. "A Method for Predicting the Panel Flutter Fatigue Life of Saturn V Panels," McDonnell Aircraft Company Report, to be released February, 1970.

13. Schlichting, H., Boundary Layer Theory, Fourth Edition, McGraw-Hill Book Company.

14. Clever, II, William, W., "Results of an Experimental Turbulent Boundary Layer Control Investigation," NASA TM-53899, September 11, 1969.

15. Warburton, G.B., "The Vibration of Rectangular Plates," Proceedings of the Institute of Mechanical Engineering, Vol. 168, No. 12, 1953, pp. 371-384.

16. Weeks, George E. and Shideler, J.L., "Effect of Edge Loadings on the Vibration of Rectangular Plates with Various Boundary Conditions," NASA TN D-2815, May 1965.

17. Gaspers, P.A., and Muhlstein, L., "An Experimental Study of the Influence of the Turbulent Boundary Layer on Panel Flutter," NASA TN D-4486, March, 1968.

18. "High Amplitude Saturn S-IVB Panel Flutter Tests, Volume II - Technical Proposal," McDonnell Aircraft Company Report F687, September 25, 1967.

19. Timoshenko, S., and Woinowsky-Krieger, S., "Theory of Plates and Shells , 2nd Edition, McGraw-Hill Book Company, 1959.

20. Young, Dana, "Vibration of Rectangular Plates by the Ritz Method," Journal of Applied Mechanics, December, 1950, pp. 448-453.

21. Liepman, H.W., and Puckett, A.E., Introduction to Aerodynamics of a Compressible Fluid, John Wiley and Son, New York, 1947, p. 146.

APPENDIX A

EFFECT OF MASS LOADING ON PANEL FREE VIBRATIONS

A vibration analysis using Ritz's Method, as described in Reference 20 was performed on the test panel to examine the effect of the concentrated shaker mass. The theoretical mass was located on the panel centerline 2 inches behind the leading edge to simulate the mass load due to the shaker armature and stem. Clamped beam mode shapes presented in Reference 21 were used in the analysis (six stream direction modes and one cross-stream mode). Table A.1 summarizes the frequency results of the analysis and shows that increasing mass loading lowers panel frequencies. The first mode experienced the greatest modal distortion especially at the higher mass loadings as shown in Figure A.1. The actual mass loading due to the shaker (shaker mass/panel mass = .049) had a small effect on the panel vibration modes.

Table A.1 - Theoretical Frequencies for the Test Panel Using a Mass Load at the Shaker Position

Mass Ratio	Resonant Frequency - Hz					
	f_1	f_2	f_3	f_4	f_5	f_6
0	153	160	173	192	218	252
.049	152	159	170	187	212	243
.100	151	156	166	182.6	208	240

Panel Properties

Length: 30 inches Width: 6.7 inches Thickness: .032 inches

Young's Modulus: 10.5×10^6 psi
Panel Density: .101 lbs/in^3

$$\text{Mass Ratio} = \frac{\text{Concentrated Mass}}{\text{Panel Mass}}$$

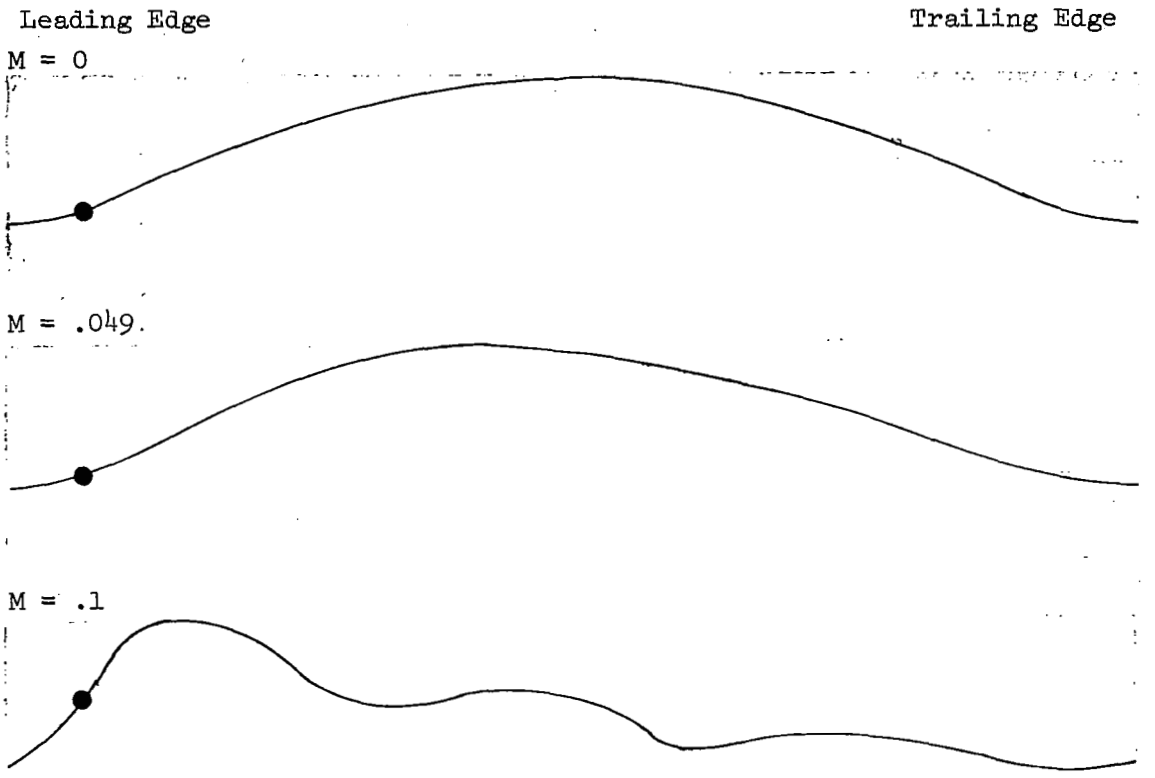

M = Concentrated Mass Divided by Total Panel Mass
Dot indicates position of concentrated mass

Figure A.1 Distortion of the 1st Mode Due to a Mass Loading at the Shaker Attachment Point (Theory)

APPENDIX B

EFFECT OF IMBALANCED COMPRESSION LOAD ON PANEL RESONANCES

The test fixture was designed so that the compressive load from the hydraulic cylinder was very nearly equally divided between the two side longerons. However, small load imbalances were measured (about 5% difference between longerons) during the GVT and it was decided to experimentally investigate the effect of load imbalances on panel modeshape and frequency.

The fixture used for the investigations is shown in Figure B.1. It consisted of a panel (similar to the test panel: thickness = .032", L/W = 4.2, L = 26.5", W = 6.3") riveted to a rectangular frame of diamond-shaped cross-section tubes with steel butt locks. A threaded rod was run through each of the tubular side pieces. The panel could be subjected to a compressive edge load of any desired imbalance by individually tightening the nuts which capped the exposed ends of the rod. Three panel mounted strain gauges were used to determine the compressive edge load.

Vibration measurements were made for edge loads ranging from zero load to slightly over buckling with load imbalances as high as 40%. It was found that the mode shapes (as indicated by sand patterns) were relatively undistorted by the unbalanced loading. In addition it was found that the resonant frequencies were equal to the corresponding frequencies observed when the panel was subjected to a uniformly distributed load equal to the average of the imbalanced edge loading. Figure B.2 shows how closely these average edge loading frequencies compare with the uniform edge loading frequencies.

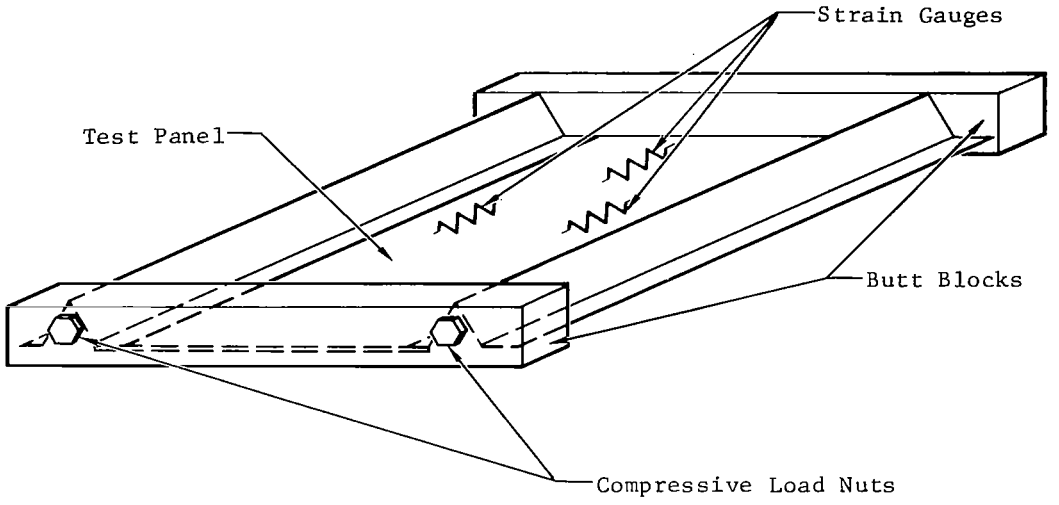

Figure B.1 Load Imbalance Test Fixture

Panel Properties: Length = 26.5 in. Thickness = .032 in.
Width = 6.7 in. Young's Modulus - 10.5×10^6 psi

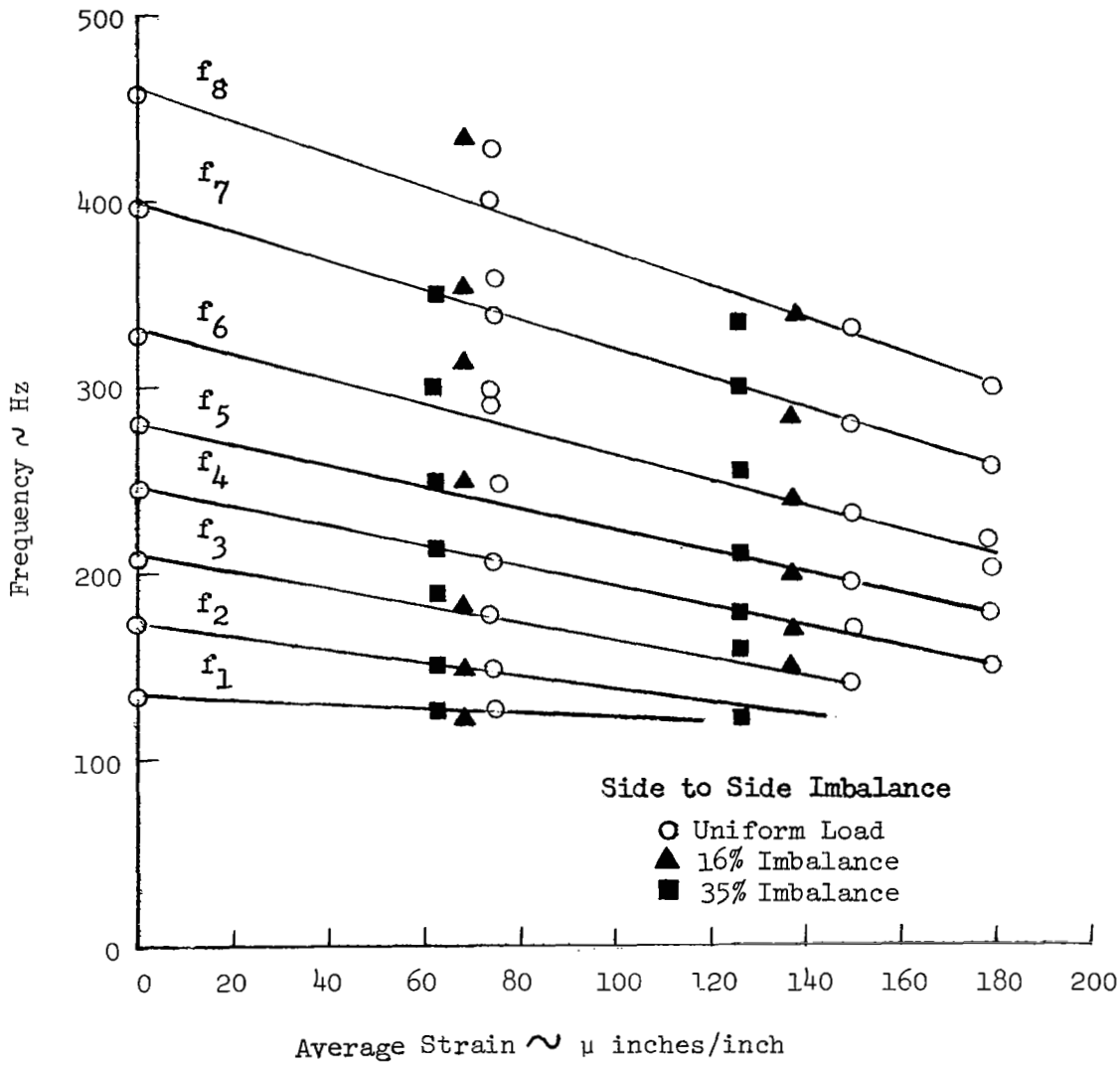

$$\varepsilon_{Buckling} = 155 \ \mu \text{ in/in}$$

$$\left\{\text{Percentage Imbalance} = \frac{\text{Strain Difference Between Sides}}{\text{Average Strain}}\right\}$$

Figure B.2 Panel Natural Frequencies Showing the Effects of an Imbalanced Compressive Load

APPENDIX C

LOG OF TEST DATA

This section presents a listing of all test points that were obtained during the tunnel portion of the test program. The information presented here includes the panel tested, the test fixture configuration (wall roughness, cavity, cross stream stiffening), the flow conditions (M and q), the flutter frequency, and comments concerning the nature of the flutter or panel response. Symbology and notation is explained below.

Notes:

Test fixture configuration code:

δ_1: smooth wall boundary layer

δ_2: rough wall boundary layer

CVO: cavity open

CVC: cavity closed

CS: cross stream stiffening

NCS: no cross stream stiffening

(Thus a configuration of δ_1 - CVO - CS means panel was tested with the smooth wall boundary layer, the cavity open, and the cross stream stiffeners installed.)

Explanation of terms in the comment column:

Onset - Point at flutter boundary, no subflutter data

Onset Survey - Point taken at flutter boundary preceded by subflutter data

Penet 1: 17% dynamic pressure penetration

Penet 2: 33% dynamic pressure penetration

Penet 3: 50% dynamic pressure penetration

Penetration sequence - refers to a complete set of penetrations: 1, 2, 3 accomplished by varying $\bar{N}_x$ and fixing all the other parameters.

Panel	Log	Configuration	M	q (psf)	$\bar{N}_x$	ΔP (psi)	f (Hz)	Comment
10	17	δ_1-CVC-CS	1.4	640	0	0	135	Onset
↓	19	↓	1.3	675	0	0	125	Onset
	20		1.2	700	0	0	125	Onset
	21		1.2	800	0	0	125	Onset
	22		1.2	775	.12	0	125	Onset
	23		1.2	800	0	0	125	Onset
	24		1.1	1150	0	0	125	Onset
4	7	δ_1-CVC-CS	1.3	200	.89	0	125	Onset
↓	8	↓	1.1	400	.93	0	70	Onset (Erratic panel response)
	9		1.2	400	.62	0	125	Onset (Erratic panel response)
	16		1.3	400	.53	0	130	Onset
	17		1.3	400	.46	0	130	Onset
	18		1.4	600	.09	0	135	Onset
	19		1.4	635	0	0	130	Onset
	20		1.3	600	.04	0	137.5	Onset
	21		1.3	650	0	0	135	Onset
	22		1.2	600	.24	0	130	Onset
	23		1.1	600	.62	0	100	Onset
	26		1.2	848	0	0	140	Onset
	27		1.2	400	.73	0	125	Onset
	28		1.2	350	1.00	0	120	Onset
	29		1.1	363	1.13	0	55	Onset (Erratic panel response)
	35		1.4	300	.76	0	120	Onset
	36		1.4	300	1.12	0	120	Onset
	37		1.4	400	.48	0	145	Onset
↓	38	↓	1.4	400	.79	.11	125	Onset
4	39	δ_1-CVC-CS	1.4	400	1.01	.125	115	Onset

Panel	Log	Configuration	M	q (psf)	$\bar{N}_x$	ΔP (psi)	f (Hz)	Comment
4	40	δ_1-CVC-CS	1.4	400	1.12	.13	110	Onset
	41		1.4	500	.30	0	130	Onset
	42		1.4	500	.67	.10	135	Onset
	43		1.4	500	1.01	.17	125	Onset
	44		1.4	500	1.23	.19	125	Onset
	45		1.4	600	.45	.13	130	Onset
	46		1.4	600	.79	.18	120	Onset
	47		1.4	600	1.01	.19	120	Onset
	48		1.4	400	1.35	.16	112.5	Onset
	54		1.4	1050	0	.11	130	Onset (Erratic panel response)
	55		1.4	1050	.34	.17	150	(Erratic panel response)
	56		1.4	1050	.67	.19	150	Onset
	57		1.4	750	0	0	125	Onset
	58		1.4	750	.34	.11	137.5	Onset
	59		1.4	750	.34	0	125	Penet 1
	60		1.4	750	1.01	.18	130	Onset
	61		1.4	750	.67	.16	125	Onset
	62		1.4	900	0	.18	145	Onset (Erratic panel response)
	63		1.4	900	.336	.125	135	Onset
	64		1.4	900	.67	.18	145	Onset
	68		1.4	500	.37	0	140	Onset
	69		1.4	400	.48	0	140	Onset
	70		1.4	675	00	0	140	Onset
	71		1.4	675	.17-.45	0	140	Penetration sequence
	74		1.4	550	.38-.62	0	135	Penetration sequence
	78		1.4	400	.65-.86	0	130	Penetration sequence
4	81	δ_1-CVC-CS	1.4	400	1.35	.12	100	Onset

Panel	Log	Configuration	M	q (psf)	$\bar{N}_x$	ΔP (psi)	f (Hz)	Comment
4	82	δ_1-CVC-CS	1.4	400	1.57	.14	107	Onset
	83		1.4	300	.68	0	130	Onset
	84		1.4	300	.75-.93	0	125	Penetration sequence
	87		1.4	300	1.35	.08	100	Onset
	88		1.4	300	1.57	.13	100	Onset
	94		1.4	900	0	.03	140	Onset (Erratic panel response)
	95		1.4	900	.13	.10	145	Onset
	98		1.4	900	.86	.20	140	Onset
	99		1.4	900	.26	.10	140	Penet 1
	100		1.4	900	.37	.10	145	Penet 2
	101		1.4	900	.50	.15	145	Onset (Erratic panel response)
	102		1.4	450	.76	.10	130	Onset
	103		1.4	450	1.0-1.5	.10	130	Penetration sequence
	105		1.4	450	1.41	.15	122	Onset
	107		1.4	600	.45	.10	130	Onset
	108		1.4	600	.59-.92	.10	130-140	Penetration sequence
	112		1.4	600	.94	.15	125	Penet 1
	113		1.4	600	1.22	.15	130	Penet 2
	114		1.4	750	.22	.10	135	Onset
	115		1.4	750	.29-.61	.10	135-140	Penetration sequence
	117		1.4	750	.50	.15	135	Onset
	119		1.4	375	.96	.10	120	Onset (Erratic panel response)
	120		1.4	375	1.35	.10	110	Penet 1
	121		1.4	375	1.6	.10	115	Penet 2
4	128	δ_1-CVC-CS	1.4	900	.15	.15	140	Onset (Erratic panel response)

Panel	Log	Configuration	M	q (psf)	$\bar{N}_x$	ΔP (psi)	f (Hz)	Comment
4	129	δ_1-CVC-CS	1.4	900	.68-.94	.15	130-150	Penetration sequence
	132		1.4	750	.71	.15	135	Onset
	133		1.4	750	.84-1.17	.15	130-140	Penetration sequence
	136		1.4	600	.90	.15	140	Onset
5	6	δ_1-CVO-CS	1.4	690	0	0	145	Onset
	7		1.33	668	0	0	125-130	Onset
	8		1.2	850		0	130	Onset
	9		1.35	675	0	0	125	Onset
	16		1.3	645	0	0	125	Onset
	18	δ_1-CVC-CS	1.4	675	0	0	130	Onset
	19		1.3	625	0	0	125	Onset (Erratic panel response)
	20		1.3	720	0	0	125	Onset
	21		1.2	750	0	0	125	Onset
	22		1.3	600	.14	0	135	Onset
	23		1.3	500	.29	0	125	Onset
	24		1.3	325	.99	0	130	Onset
	25		1.3	625	0	0	130	Onset
	26		1.3	675	0	0	125	Onset
	27		1.4	650	0	0	130	Onset
	28		1.4	720	0	0	130	Onset
	34	δ_2-CVC-CS	1.4	755	0	0	140	Penetration (Erratic panel response)
	36		1.3	670	0	0	135	Onset (Erratic panel response)
	37		1.2	795	0	0	130	Onset
	38		1.3	675	0	0	130	Onset
5	39	δ_2-CVC-CS	1.3	675	.31	.10	125	Onset (Erratic panel response)

Panel	Log	Configuration	M	q (psf)	$\bar{N}_x$	ΔP (psi)	f (Hz)	Comment
5	40	δ_2-CVC-CS	1.3	675	.71	.15	110	Onset (Erratic panel response)
	41		1.3	450	1.06	.09	125	Onset (Erratic panel response)
	42		1.3	450	.72	0	1.20	Onset
	43		1.3	450	1.01	.10	100	Penet 1
	44		1.3	350	.94	.07	110	Onset
	50		1.3	900	0	.09	125	Onset (Erratic panel response)
	51		1.3	550	.36	0	125	Onset
	52		1.3	550	.734	.10	105	Onset
	53		1.3	550	1.09	.15	90	Onset
	54		1.3	740	0	0	135	Onset (Erratic panel response)
	55		1.3	740	.29-.67	0	122-138	Penetration sequence (Erratic panel response)
	58		1.3	400	.831	.05	145	Onset
	59		1.3	400	1.09	.08	150	Penet 1
	60		1.3	400	1.02	.10	110	Onset
	61		1.3	825	0	0	135	Penetration (Erratic panel response)
	62		1.3	825	.09	.08	120	Penetration
	63		1.3	825	.40	.13	102	Penetration
	64		1.3	500	.39	0	130	Onset (Erratic panel response)
	66		1.3	500	.72-1.18		105-120	Penetration sequence (Erratic panel response)
	68		1.3	300	.93	.05	115	Onset
5	69	δ_2-CVC-CS	1.3	600	.25	0	125	Onset

Panel	Log	Configuration	M	q (psf)	$\bar{N}_x$	ΔP (psi)	f (Hz)	Comment
5	70	δ_2-CVC-CS	1.3	600	.48-.87	.01-.10	115-135	Penetration sequence
	73		1.3	300	.93	0	120	Onset
	74		1.3	350	.62	0	120	Stable
	75		1.3	350	.93	0	120	Penet 1
	81	δ_2-CVC-NCS	1.4	840-865	0	.05	135	Onset
	82		1.3	790	0	0	130	Onset
	83		1.2	915	0	0	130	Onset
	84		1.3	830	0	0	130	Onset (Erratic panel response)
	85		1.3	915	0	.08	125	Onset
	86		1.3	650	.41	0	135	Penetration
	87		1.3	650	.73	.10	110	Penetration
	88		1.3	650	1.04	.15	78	Penetration
	89		1.3	550	.58	0	125	Onset
	90		1.3	550	.97	.10	110	Onset
	91		1.3	550	1.31	.05	50	Onset
	92		1.3	450	.88	0	120	Onset
	93		1.3	450	1.4	.10	70	Onset
	94		1.3	850	0	0	140	Penetration
	95		1.3	850	.24	0	135	Penet 1
	96		1.3	850	.44	0	135	Penet 2
	102		1.3	900	0	0	135	Penetration
	103		1.3	900	.29	.10	115	Onset
	104		1.3	900	.68	.15	75	Onset
6	6	δ_2-CVC-NCS	1.4	735	0	0	125	Onset
	7		1.3	715	0	0	125	Onset (Erratic panel response)
	8		1.2	835	0	0	115	Onset
	10		1.3	550	.41	0	105	Onset
6	11	δ_2-CVC-NCS	1.3	450	.57	0	112.5	Onset (Erratic panel response)

Panel	Log	Configuration	M	q (psf)	$\bar{N}_x$	ΔP (psi)	f (Hz)	Comment
6	12	δ_2-CVC-NCS	1.3	350	.63	0	108	Onset
	13		1.3	300	.76	0	108	Onset
	14		1.3	825	0	0	112.5	Onset (Erratic panel response)
	15		1.3	650	.18	0	120	Onset
	16		1.3	500	.42	0	117.5	Onset
	17		1.3	400	.57	0	125	Onset
	18		1.3	450	.51	0	105	Onset
	19		1.3	250	.81	0	100	Onset
	20		1.3	250	1.13	0	110	Onset
	21		1.3	225	.96	0	100	Onset
	22		1.3	500	.49	0	110	Onset
	23		1.3	500	.61-.73	.08	120	Penetration sequence
	26		1.3	400	.60	0	110	Onset
	27		1.3	400	.70-.82	0	105-112	Penetration sequence
	35		1.3	860	0	0	125	Onset
	36		1.3	865	0	0	125	Onset
	37		1.3	995	0	.08	125	Onset
	38		1.3	700	.15	0	125	Onset
	39		1.3	700	.29-.50	0	110-130	Penetration sequence
	42		1.3	600	.29	0	120	Onset
	43		1.3	600	.43-.60	0	120	Penetration sequence
	46		1.3	400	1.69	.08	115	Onset
	47		1.3	350	1.69	.08	100	Onset
	48		1.3	300	1.69	.08	105	Onset
	49		1.3	300	.96	0	112	Onset survey (Data taken at q = 200, 250, 300 psf)
6	50	δ_2-CVC-NCS	1.3	300-850	.96	0	100-130	Deep penetration q increased from 300 to 850 psf

Panel	Log	Configuration	M	q (psf)	$\bar{N}_x$	ΔP (psi)	f (Hz)	Comment
6	51	δ_2-CVC-NCS	1.3	1000	1.69	0	102	Deep penetration, tunnel overheat

APPENDIX D

Effect of Mach Number on Panel Flutter Onset Prediction

It has become common practice in panel flutter analysis to describe the Mach effect by using the Ackeret aerodynamic theory (Reference 21) in which the local pressure coefficient is defined as

$$C_P = \frac{2}{\beta} \times (\text{local slope})$$

and

$$\beta = \sqrt{M^2 - 1}$$

While this relationship holds very well for $M > \sqrt{2}$, it has been demonstrated (see Reference 3 for example) that it does not hold in the low supersonic region ($M < \sqrt{2}$). This is readily evident since, as M approaches 1.0, β approaches zero implying that the pressure coefficients increase without limit. Experimental data do not bear this out.

A related problem is the untenable nature of the nondimensional panel flutter parameter

$$\Phi = \left\{\frac{\beta E}{q_{on}}\right\}^{1/3} \frac{t}{L}$$

in the low supersonic region. This parameter is commonly used to define panel flutter boundaries and tacitly implies that β/q_{on}, and consequently Φ, are invariant with Mach number. It is equivalent to assuming that the Mach number effect is properly accounted for by the parameter variation $\beta = \sqrt{M^2 - 1}$. The shortcoming of this assumption was pointed out in Reference 3 and an alternate panel flutter parameter f(M) was introduced to realistically account for Mach number effect. Results from the present tests further support the approach taken in Reference 3 and provide additional data on Mach number effects. Figure D.1 is a plot

of the Mach number correction factor f(M) versus Mach number for panel length-to-width ratios of 4.48, 2 and 0.5. The last two are adapted from envelopes of experimental data that are given in Reference 3. In the Mach range shown, f(M) replaces β (which is plotted for comparison) for the prediction of panel flutter onset boundaries.

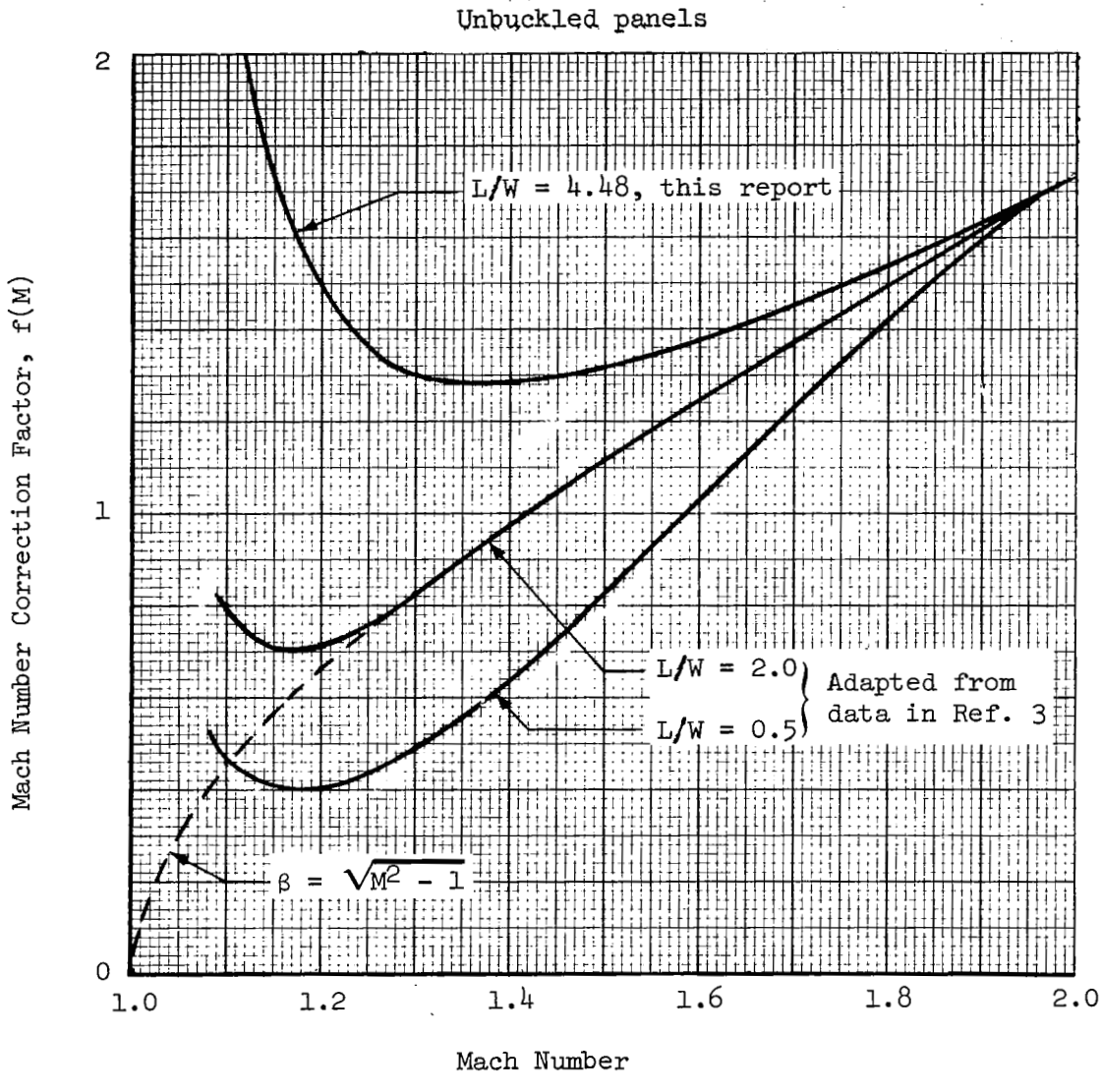

Figure D.1 Mach Number Correction Factor versus Mach Number